Title
Oxygen Loss from Venus and the Influence of Extreme Solar Wind Conditions

Author
McEnulty, Tess

Publication Date
2012

Peer reviewed|Thesis/dissertation

Oxygen Loss from Venus and the Influence of Extreme Solar Wind Conditions

by

Tess Rose McEnulty

A dissertation submitted in partial satisfaction

of the requirements for the degree of

Doctor of Philosophy

in

Earth and Planetary Science

in the

Graduate Division

of the

University of California, Berkeley

Committee in charge:

Professor Imke de Pater, Chair
Dr. Janet G. Luhmann
Professor Walter Alvarez
Professor Stuart Bale

Fall 2012

Oxygen Loss from Venus and the Influence of Extreme Solar Wind Conditions

Tess Rose McEnulty

Abstract

Oxygen Loss from Venus and the Influence of Extreme Solar Wind Conditions

by

Tess Rose McEnulty

Doctor of Philosophy in Earth and Planetary Science

University of California, Berkeley

Professor Imke de Pater, Chair

The purpose of this dissertation is to expand our understanding of oxygen ion escape to space from Venus and its dependence on extreme solar wind conditions found during interplanetary coronal mass ejections (ICMEs). This work uses in-situ measurements of ions and magnetic fields from the Venus Express (VEX) spacecraft, which has been orbiting Venus since mid-2006. VEX is in a 24 hour elliptical orbit. The ion instrument operates for ~6 hours near the planet, while the magnetometer is always on. In-situ measurements of the solar wind velocity, density, and magnetic field from Pioneer Venus Orbiter (PVO) are also used for comparison with external conditions during the VEX time period. Coronagraph images from solar monitoring spacecraft are used to identify the solar sources of the extreme solar wind measured in-situ at Venus. For interpretation of planetary ions measured by VEX, a magnetohydrodynamic (MHD) model is utilized.

The solar wind dynamic pressure outside of the Venus bow shock did not exceed ~12 nPa, during 2006-2009, while the solar wind dynamic pressure was higher than this for ~10% of the time during the PVO mission. Oxygen ions escape Venus through multiple regions near the planet. One of these regions is the magnetosheath, where high energy pick-up ions are accelerated by the solar wind convection electric field. High energy (>1 keV) O^+ pick-up ions within the Venus magnetosheath reached higher energy at lower altitude when the solar wind was disturbed by ICMEs compared to pick-up ions when the external solar wind was not disturbed, between 2006-2007. However, the count rate of O^+ was not obviously affected by the ICMEs during this time period. In addition to high energy pick-up ions, VEX also detects low energy (~10-100 eV) O^+ within the ionosphere and wake of Venus. These low energy oxygen ions are difficult to interpret, because the spacecraft's relative velocity and potential can significantly affect the measured energy. If VEX ion data is not corrected for the spacecraft's relative velocity and potential,

gravitationally bound O^+ could be misinterpreted as escaping. These gravitationally bound oxygen ions can extend on the nightside to ~-2 Venus radii and may even return to the planet after reaching high altitudes in the wake. Gravitationally bound ions will lower the total O^+ escape estimated from Venus if total escape is calculated including these ions. However, if the return flux is low compared to the total escaping outflow, this effect is not significant.

An ICME with a dynamic pressure of 17.6 nPa impacted Venus on November 11, 2011. During this ICME, the high energy pick-up O^+ and the low energy O^+ ions were affected. Oxygen ions in the magnetosheath, ionosphere, and tail had higher energies during the ICME, compared to O^+ energies when the external solar wind conditions were undisturbed. High energy ions were escaping within the dayside magnetosheath region when the ICME was passing as well as when the solar wind was undisturbed. However, during the ICME passage, these O^+ ions had three orders of magnitude higher counts. The low energy O^+ during the undisturbed days was gravitationally bound, while during the ICME a portion of the low energy ions were likely escaping. The most significant difference in O^+ during the ICME was high energy pickup ions measured in the wake on the outbound portion of the orbit. These ions had an escape flux of 2.5×10^8 $O^+cm^{-2}sec^{-1}$, which is higher than the average escape flux in all regions of the wake. In addition, the interplanetary magnetic field (IMF) was in a configuration that may have rotated an even higher escape flux O^+ away from the VEX orbit. This needs to be confirmed with sampling of other regions in the wake during large ICMEs. A lower bound on the total O^+ escape during this event could be ~2.8×10^{26} to 6.5×10^{27} O^+/sec, which is 2-3 orders of magnitude higher than the average escape flux measured by VEX. Hence, ICMEs could have played a major role in the total escape of O^+ from Venus. Considering that the Sun was likely more active (with more ICMEs) early after solar system formation.

The results presented in this dissertation can be used as a guide for future studies of O^+ escape at Venus. As we move into solar maximum, Venus will likely be impacted by more large ICMEs. The ICME from the last study of this dissertation was the largest yet measured by VEX, but its 17.6 nPa dynamic pressure is lower than the largest ICMEs during the PVO time period (~ 80 nPa). The work in this dissertation is also relevant to Mars, since Mars interacts with the solar wind in a similar manner and has analogous ion escape mechanisms. The upcoming MAVEN (Mars Atmosphere and Volatile Evolution) mission will launch at the end of 2013 to study the Martian atmosphere, escape processes, and history of volatiles. This mission will have an in-situ ion instrument and magnetometer similar to those used for the studies in this dissertation, so one could conduct similar studies of the oxygen ion escape from Mars during extreme solar wind conditions.

Dedicated to Bob Lin

Contents

Acknowledgements

Many people have helped me with the work in this dissertation. Thank you to my advisors, Janet Luhmann and Imke de Pater for all of the time you spent guiding me. I know that I was not the easiest student to advise, but you kept pushing me to become a better scientist. Thanks to all of the people that have been coauthors on my papers (which are part of this dissertation) and conference presentations: Andrei Fedorov, Yingjuan Ma, Demet Ulusen, Tielong Zhang, Lan Jian, Dave Brain, Edik Dubinin, Chris Russell, Niklas Edberg, Chris Möstl, and Yoshifumi Futaana. Thank you to Elizabeth Cappo for proofreading this whole document.

Many scientists and engineers inspired me to pursue a PhD. Thank you to my undergraduate professor at the University of Michigan, particularly to Nilton Renno and Alec Gallimore for giving me my first research experiences, and to Thomas Zurbuchen giving me advice about grad school. Thanks to the people that I worked for at JPL before grad school that taught me priceless information about space exploration and inspired me to pursue a PhD (Harold Kirkham, Lynn Baroff, Steve Fuerstenau, John Crawford, and David Atkinson).

Thank you to the people in the Earth and Planetary Science and Astronomy departments at Berkeley for giving me a broad understanding of Planetary Science outside of my specialty, especially Geoff Marcy for organizing interesting CIPS seminars and giving me the opportunity to be a GSI for his class. Thanks to Bill Dietrich for teaching an interesting Geomorphology class, and for being on my qualifying exam committee.

Thanks to all of the scientists and engineers that I interacted with at the Space Sciences Lab: Dave Brain, Rob Lillis, Christina Lee, Yan Li, Jasper Halekas, Matt Fillingham, Tim Quinn, Heidi Fuqua, Andrew Poppe, and Rebecca Samad. Special thanks to Greg Delory for giving me the opportunity to work on the MAVEN LPW instrument. I really loved getting in the lab building circuits and testing the instrument. I'm not sure if I would have made it through grad school without this break from doing data analysis on my computer.

Finally, without my family, friends, and husband I never would have made it to where I am now. I have been fascinated by space and by the planets for as long as I can remember. Thank you to my family for always encouraging me. Thank you mom for the weekly library trips, for making math fun, and for letting me decorate my room with planets and stars. Thanks dad for always reminding me to stop and smell the roses. Thanks siblings (Kendra, Cory, Kevin, and Ian). Thanks to my friends for your support throughout the past few years - especially to Natasha Chopp, Alyssa Rhoden, Kelly Wiseman, Caroline Chouinard, and Amanda Butina.

Finally, the person I credit most with helping me to finish my PhD: my husband, Ryan Falor. Words cannot describe how much you have meant to me. You are the only person that truly knows how hard I worked, and how much I struggled. You never gave up on me. You pushed me to keep going when I didn't think that I could do it anymore. You picked up the slack around the house when I was spending 16 hours a day on my computer focused on my research. Your technical support was also much appreciated. I am so lucky to have a husband that believes in me as you do.

Chapter 1

Introduction

1.1 Motivation for this dissertation research

Figure 1.1: In the foreground, the surface of Venus revealed by Magellan radar in 1996, and behind it, the planet at visible wavelengths obtained by Pioneer Venus in 1978. (Credit: NASA/JPL/RPIF/DLR)

For thousands of years people have watched the Sun, the Moon, the stars, and the objects that wander among the background stars – the planets. The brightest of these wanderers was named after goddesses of love: the Babylonian Ishtar, the Greek Aphrodite, and the Roman Venus. The planet Venus moved from a subject of myth to that of science after the invention of the telescope. In 1610 Galileo noticed that Venus exhibited phases similar to the Moon, which supported the theory that the Sun was the center of the solar system. Details of the planet were further revealed in 1761 when Mikhail Lomonosov, a Russian astronomer, discovered that Venus also has an atmosphere. This discovery was made during a transit of Venus in front of the Sun, an event that occurs in pairs separated by long gaps over 100 years. Many people thought that Venus was likely similar to Earth, and perhaps that there was even a civilization living on the planet. However, this view of an Earth-like planet and the historical associations of Venus with beauty and love were completely overturned during the space age. Close up measurements of the planet, starting with Mariner 2 in 1963, revealed that it has a hellish environment. It has a crushing CO_2 atmosphere, 100 times the surface pressure of Earth, a surface temperature of 736 K (460° C), and sulfuric acid clouds. Venus is the nearest neighbor to Earth and is similar in size and internal structure, but it ended up with a very different atmosphere. Was this always the case, or could Venus have once been much more Earth-like? A key to answering this question is the history of water on the planet.

Studying Venus can help us understand Earth and Mars, which formed in a similar location in the solar system. Although these three planets formed in a similar location (0.7 AU, 1 AU, and 1.5 AU), they are each unique. Venus and Earth are similar in radius, mass, and distance from the sun (see Table 1.1). However, Venus does not have an intrinsic dipole magnetic field as the Earth does, and (as mentioned earlier) has a very different atmosphere. Mars is smaller than both Venus and Earth, but like Venus, it does not have an intrinsic magnetic field. However, Mars does have remnant crustal magnetic fields. Another striking difference between these terrestrial planets is the amount of water. Earth's surface is covered ~70% by water, Mars has very little, and Venus is completely dry (only 200-300 ppm in the atmosphere). Although Venus currently has very little water, this may not have always been the case. As evidenced by a D/H ratio 100 times that on Earth, Venus may have actually once had an ocean's worth of water (Donahue et al., 1982, McElroy et al. 1982). Mars also has evidence of past water (e.g. Head et al., 1999;

Squyres et al., 2004). This dissertation is focused on Venus, but lessons learned can be applied to Mars.

	Venus	Earth	Mars
Radius (km)	6052	6371	3396
Mass (kg)	4.87×10^{24}	5.97×10^{24}	6.42×10^{23}
Intrinsic magnetic field	no	yes	No, but remnant
Distance from Sun (AU)	0.7	1	1.5
Surface pressure	9.3 Mpa	101 kPa	~ 0.6 kPa
Atmosphere composition	~97% CO_2, ~3.5% N_2	78% N_2, 21% O_2	95.3% CO_2, 2.7% N_2
Escape velocity (km/s)	10.5	11.2	5
Amount of water in atmosphere	200-300 ppm	1%	210 ppm

Table 1.1: Characteristics of Venus, Earth and Mars. (Amount of water from Hoffman et al., 1980; Moroz et al., 1979; Johnson and Fegley, 2000)

Water can be lost from Venus if it is photodissociated by solar UV and the hydrogen escapes to space (e.g. Lammer et al, 2006; Kasting and Pollack, 1983). However, the leftover oxygen cannot escape to space as easily due to its higher mass. A mechanism that can impart the energy needed for oxygen to escape to space is interaction with the interplanetary magnetic fields (IMF) and associated electric fields in the solar wind (if the oxygen is ionized). Oxygen could also be lost from the atmosphere due to sequestration in minerals in the crust (e.g. Fegley et al., 2004; Hashimoto et al., 2008; Smrekar et al., 2011), but this process likely cannot account for the amount of missing oxygen (Fegley et al., 2004). The study of oxygen sequestration within the crust is a separate piece of the puzzle. This dissertation focuses on escape of O^+ to space. Estimates of the current O^+ escape rate from Venus cannot account for the total amount of oxygen expected to have once been on the planet (e.g. Barabash et al., 2007; Fedorov et al., 2011). However, previous studies have suggested that the escape rate may increase during extreme conditions (Luhmann et al., 2007; Futaana et al., 2007; Edberg et al., 2011). In this dissertation, I further investigate the influence of extreme solar wind conditions on O^+ escape to space.

1.2 Atmospheric escape mechanisms

Atmospheric constituents can escape the gravitational bounds of a planet through mechanisms such as large impacts (e.g. Walker, 1986; Melosh and Vickery, 1989), Jean's escape (e.g. Chassefiere, 1996, 1997), photochemistry, or the solar wind interaction (e.g., Barabash et al., 2007; Terada et al., 2002; Luhmann, 2006, 2007). Large impacts were probably important shortly after the formation of the solar system, but the significance of these large impacts would have diminished in ~500 Myr as number and size of impacting bodies were reduced over time. Jean's escape and photochemistry at Venus are not capable of accelerating oxygen up to escape velocity because of its high mass (e.g. Nagy et al., 1981). Therefore, the solar wind interaction with ionized particles in the upper atmosphere of Venus is likely the primary mechanism for oxygen loss to space for the past 4 billion years.

The Earth has an internal dynamo magnetic field that holds the solar wind off many Earth radii, but Venus does not have an internal field. Without a magnetic shield, the solar wind gets much closer to Venus and interacts directly with its upper atmosphere and ionosphere. The solar wind carries with it frozen in magnetic fields as it propagates away from the Sun. The ionosphere of Venus responds to these magnetic fields. Since charged particles are able to move in the ionosphere they create an induced magnetic field that holds off the IMF. Outside of this region of induced magnetic field, neutral particles in the upper atmosphere of Venus can be ionized and then react with the background magnetic and electric fields. These ionized particles can be accelerated to velocities above what would be needed for escape by the pick-up process. The pick-up process is a result of the action of the solar wind convection electric field ($E = -V_{sw} \times B$), where V_{sw} is the velocity of the bulk solar wind and B is the frozen in interplanetary magnetic field. When an ionized particle is moving perpendicular to a magnetic field it rotates around the magnetic field (shown at the top of Figure 1.2). If the magnetic field that the ion is gyrating around is moving, as with the IMF in the solar wind, the particle will appear to have a cycloidal motion and be carried away with the moving magnetic field.

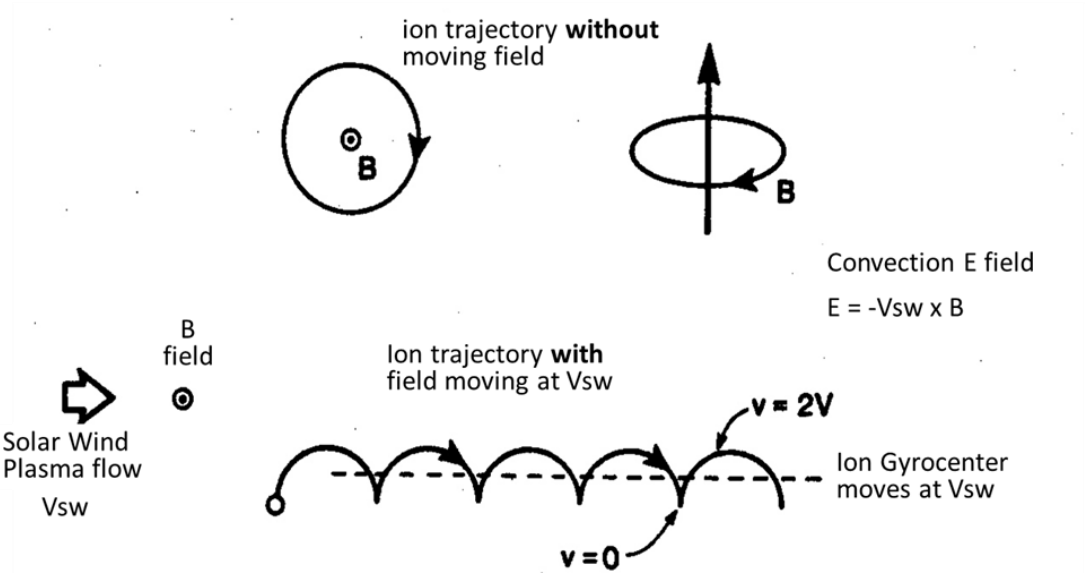

Figure 1.2: The pick-up ion process. (top) An ion moving around a stationary magnetic field (B) moves in a circle around the field. (below) The solar wind carries frozen in magnetic fields (B_{field}) with it, moving with velocity V_{sw}. As these magnetic fields move away from the Sun, ions that interact with them move in a circle around the field, but since the field is moving they appear to have a cycloidal motion (from Luhmann 2003).

1.3 Solar wind interaction with Venus

The solar wind interacts directly with the ionosphere of Venus (as opposed to the Earth where the internal dynamo magnetic field holds off the solar wind). This interaction is illustrated in Figure 1.3. The upper boundary of the ionosphere where the density quickly falls off is called the ionopause and is usually separated from the solar wind by the magnetic barrier where IMF piles up and the magnetic pressure dominates (e.g. Zhang et al., 1991, 2007). The balance between the ionosphere thermal pressure (which is sensitive to EUV) and solar wind dynamic pressure determines the location of the ionopause (e.g. Luhmann et al., 1986, 1992). The magnetosheath is the region above the ionopause where the solar wind IMF is compressed as it piles up, and where ions are picked up. The exobase is the altitude at which particles are likely to be collisionless. Above the exobase, if particles are

on outward trajectories above escape velocity they are able to escape. Below this altitude, collisions may stop particles from escaping.

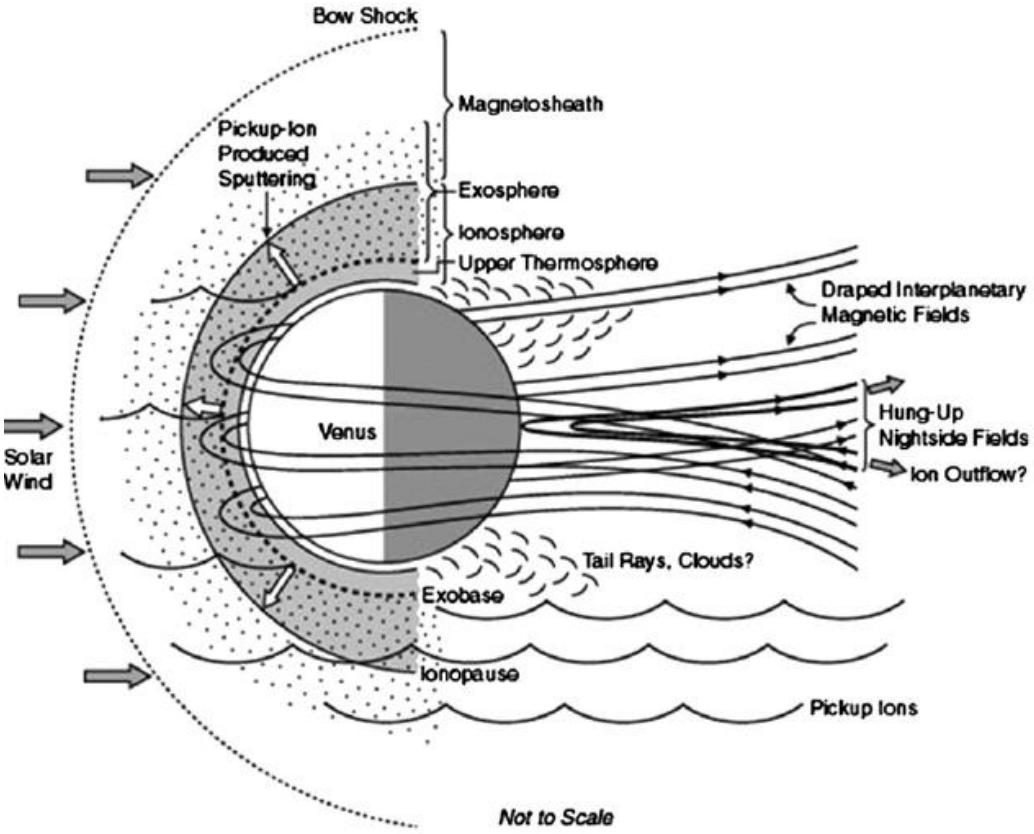

Figure 1.3: Venus interaction with the solar wind. (from Russell et al., 2007).

1.4 Previous in-situ measurements of solar wind induced O^+ escape

Instruments on Venera, a series of Russian missions in the 1960s, were the first to detect oxygen that was likely escaping from Venus. However, the majority of what we know about how Venus interacts with the solar wind came from analysis of the data obtained by instruments on the Pioneer Venus Orbiter (PVO). PVO orbited Venus from 1979-1988, and oxygen ions were detected with several of its instruments. Brace et al. (1995) gives a summary of the oxygen detections by PVO instruments. Luhmann et al. (2007) collected measurements from the PVO Orbiter

Neutral Mass Spectrometer (ONMS) and modeled features seen in the data as pick-up ions. Low energy ions were also measured flowing within the ionosphere and near the ionopause by the ONMS and Ion Mass Spectrometer (IMS) (Knudsen et al., 1982; Miller and Whitten, 1991; Grebowsky et al., 1993).

Venus Express (VEX) is an orbiter that arrived at Venus in mid-2006, which is extending the knowledge of ion escape from Venus. It is sampling a region that PVO did not sample, within -3 Venus radii in the wake behind the planet. VEX has an instrument called the Ion Mass Analyzer (IMA) which can detect ions within an energy range of 10 eV - ~25 keV. Statistical studies of the ions detected by the IMA showed a majority of ions escaping in the wake, rather than through the magnetosheath (Barabash et al., 2007; Fedorov et al., 2011) The spatial distribution of O^+ escape is shown in Figure 1.4 (from Fedorov et al., 2011). Integration of these O^+ fluxes over the plane shown in Figure 1.4 gives a total escape rate of 2.7×10^{24} O^+/second (Fedorov et al., 2011). The flow vectors in the wake from this same data source are shown in Figure 1.5.

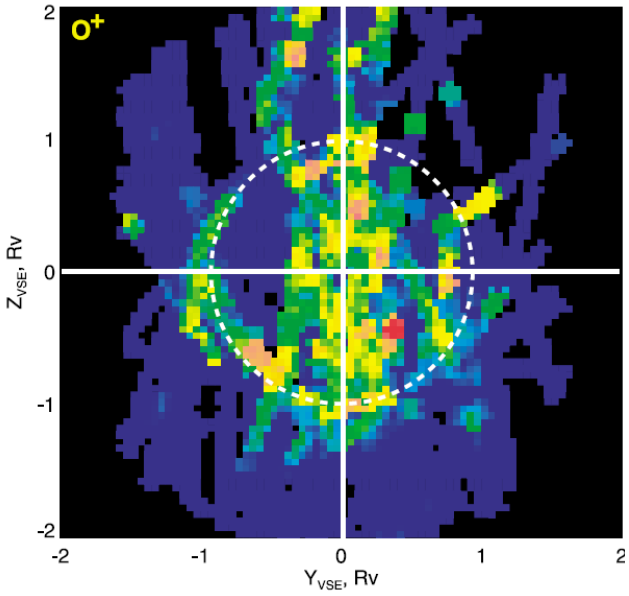

Figure 1.4: Oxygen ion measurements in the Venus wake showing the spatial distribution averaged over a region of -0.8 to -2.5 Venus radii in the wake. (from Fedorov et al., 2011)

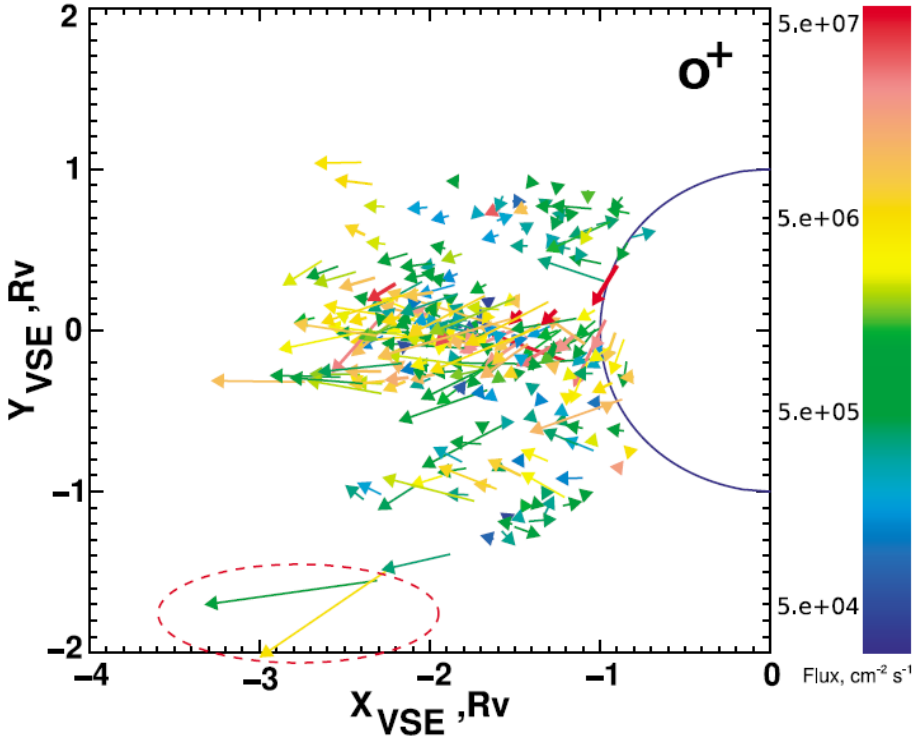

Figure 1.5: O^+ flow vectors averaged from VEX IMA measurements. (from Fedorov et al., 2011)

1.5 Characteristics of the Sun and solar wind

Conditions on the Sun and in the solar wind can control the Venus-solar wind interaction, and therefore may affect ion escape. In order to understand how representative our current measurements of O^+ escape rate are of historical values it is important to consider the Sun and solar wind conditions. In addition to average conditions on the Sun, we are interested in extreme solar wind conditions that happen in solar wind disturbances. The Sun, the solar wind, the solar cycle, and solar disturbances are described further in the following sections.

1.5.1 The Sun

The Sun is a massive ball of plasma (ionized gas), which creates the majority of energy that we use here on Earth through nuclear fusion of hydrogen to helium in its

very high temperature and pressure core. Magnetic fields are created inside the Sun, which can sometimes loop above the visible layer of the Sun and become visible due to hot plasma flowing along the magnetic fields lines (see the loop structures on the edge of the Sun in Figure 1.6). The energy created within the Sun is radiated into space by photons. These photons of different wavelengths heat the planets and create their ionospheres. The outer layer of the Sun - the corona - also influences the planets through the solar wind.

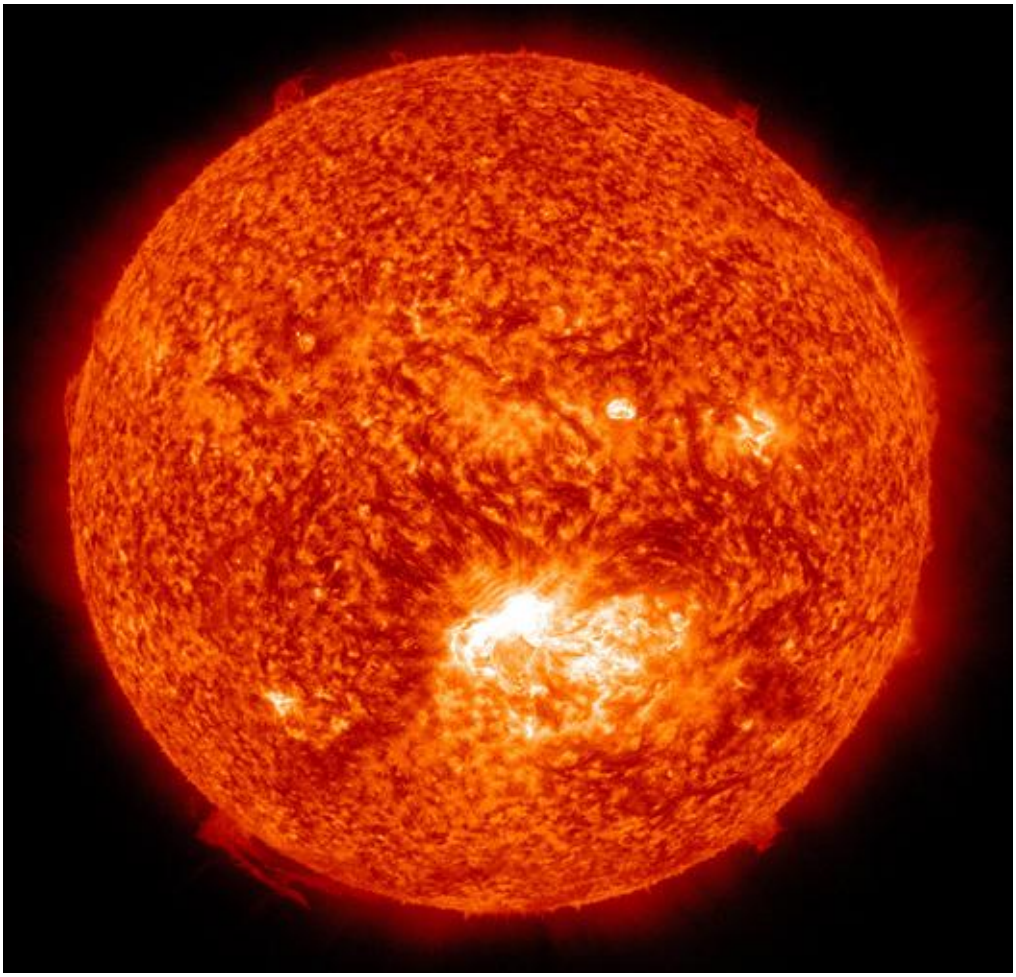

Figure 1.6: Image of the Sun from the Solar Dynamics Observatory on July 12, 2012. The image is captured in the 304 Angstrom wavelength, which is typically colorized in red. A flare is seen in near the center of the image. (Credit: NASA/SDO/AIA)

1.5.2 The solar wind

The solar wind is an outflow of plasma from the Sun, primarily ionized hydrogen and electrons. It carries with it magnetic field lines from the Sun, called interplanetary magnetic field (IMF). The solar wind propagates out in all directions in our solar system, interacting with all of the planets. The solar wind has a structure referred to as the Parker spiral due to the rotation of the Sun as solar wind particles exit the same spot on the sun (Figure 1.7). These regions of solar wind from the same place on the Sun are called sectors. Different sectors have different IMF orientations.

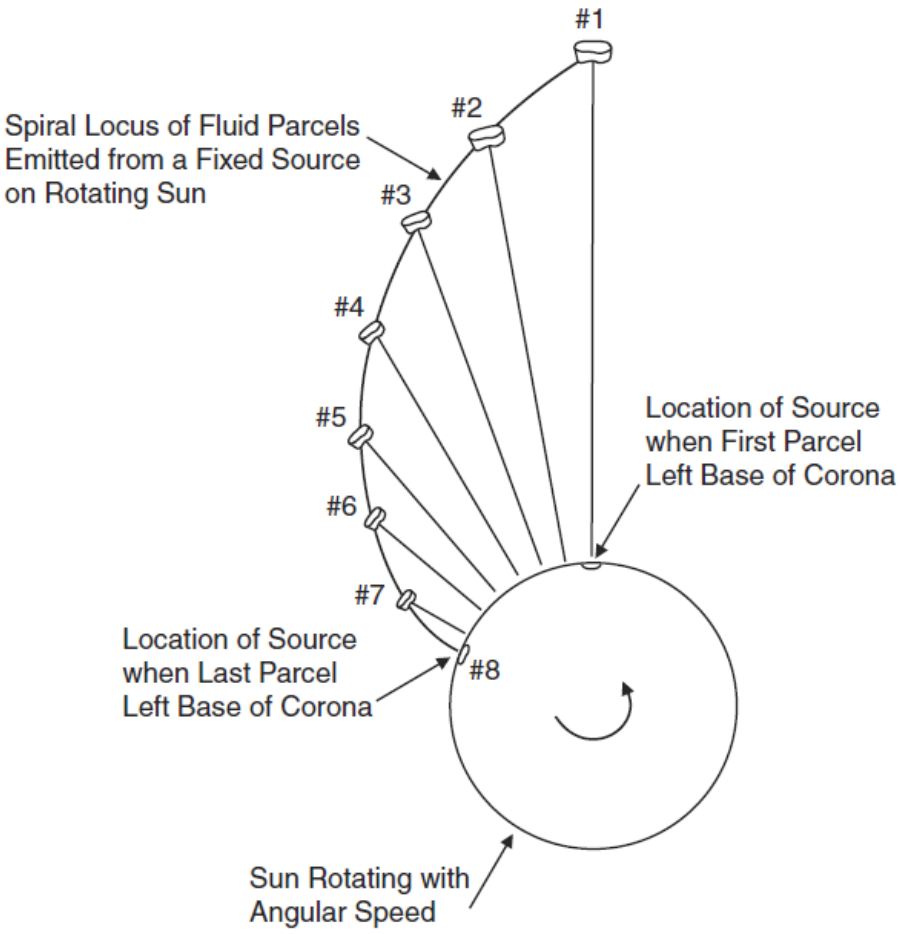

Figure 1.7: Archimedean (Parker) spiral structure (from Hundhausen 1995)

1.5.3 The solar cycle

The Sun has an 11-year cycle in which the internal magnetic field flips direction. Dark spots on the sun (called sunspots) occur where the Sun's magnetic field loops above the photosphere of the Sun. The plasma is cooler, within these loops, relative to the background solar plasma (making them dark). The change in direction of the internal magnetic field alters the number of sunspots visible on the surface of the Sun, therefore the sunspot number is a measure of the solar cycle. When the Sun is most active and has the most sunspots it is considered to be in solar maximum (and the opposite for solar minimum). The EUV flux is solar cycle dependent with higher flux at solar maximum compared to minimum by a factor of two (Brace et al., 1988; Ho et al., 1993). The sunspots are the location of solar flares and coronal mass ejections discussed in 1.5.4. These solar wind disturbances also depend on the solar cycle. More disturbances occurring during solar maximum when there are more sunspots. Figure 1.8 shows the sunspot number during the PVO mission and for the beginning of the VEX mission. PVO sampled escaping ions at Venus over a full solar cycle, while VEX has spent the majority of its mission near solar minimum.

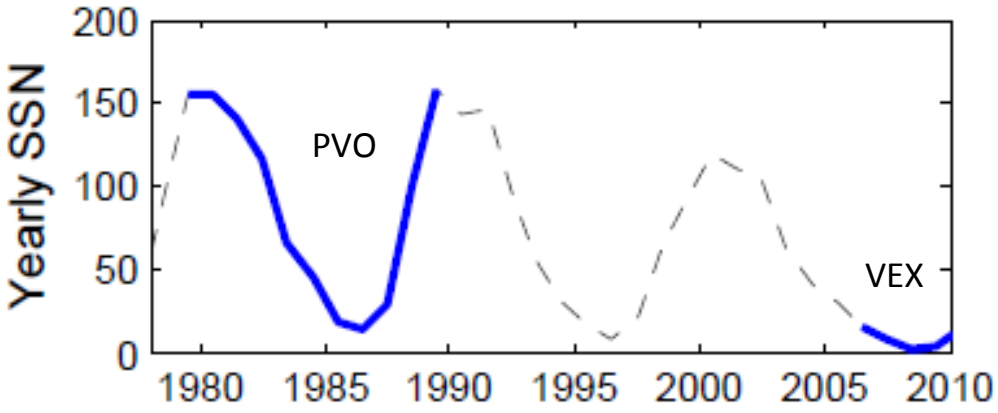

Figure 1.8: Yearly sunspot number (SSN) plotted from 1979-2010 to show the 11 year periodicity of the sunspot cycle. The time periods of PVO and VEX are marked in blue. (SSN data from http://solarscience.msfc.nasa.gov/SunspotCycle.shtml)

1.5.4 Solar wind disturbances

Coronal Mass Ejections (CMEs) are outbursts of plasma and twisted magnetic fields from sunspots (Figure 1.9). They propagate into the ambient solar wind and are then referred to as ICMES (Interplanetary CMES). ICMEs are characterized by a leading shock jump and compressed solar wind (high density and dynamic pressure) followed by a larger than average magnetic field that is smooth and rotating. Properties of ICMEs are summarized in Jian et al. (2006, 2008). The region of compression is called the 'ICME sheath' (See Figure 1.10).

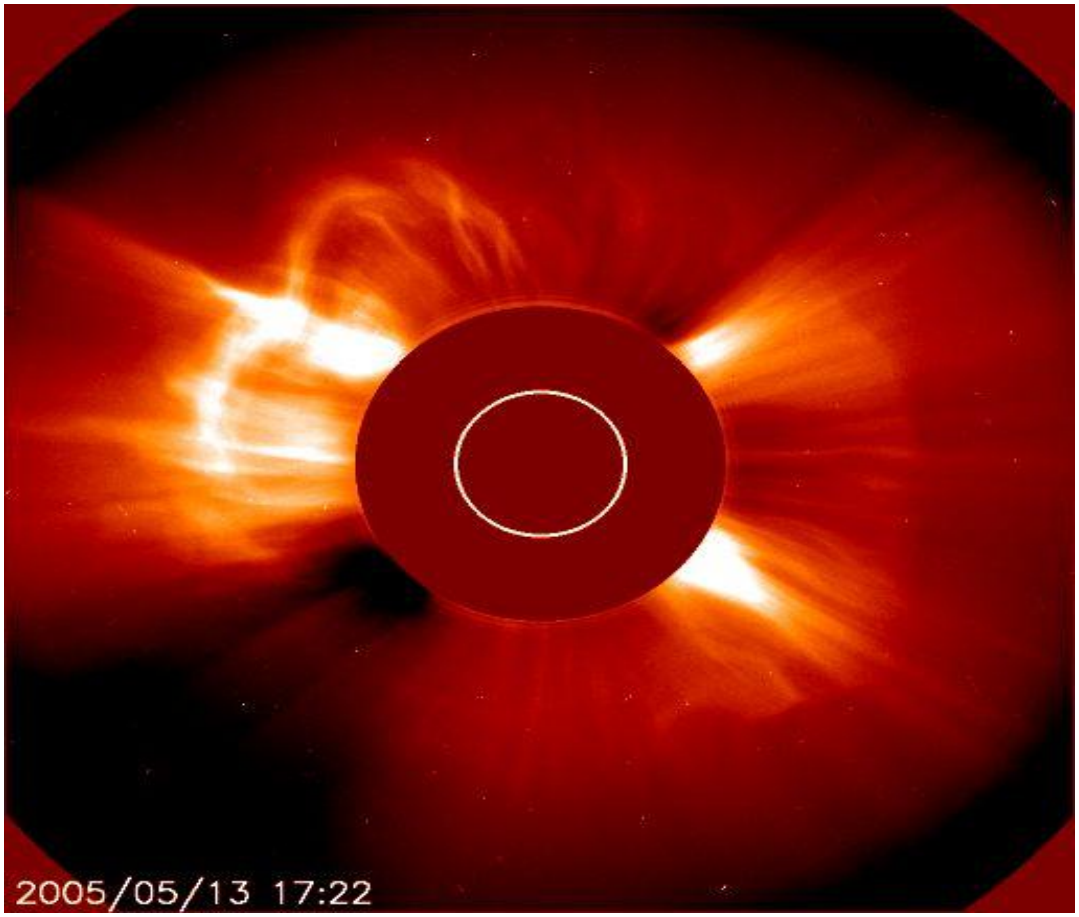

Figure 1.9: Coronal Mass Ejection (CME) imaged by SOHO LASCO white light coronagraph (http://cdaw.gsfc.nasa.gov/CME_list/)

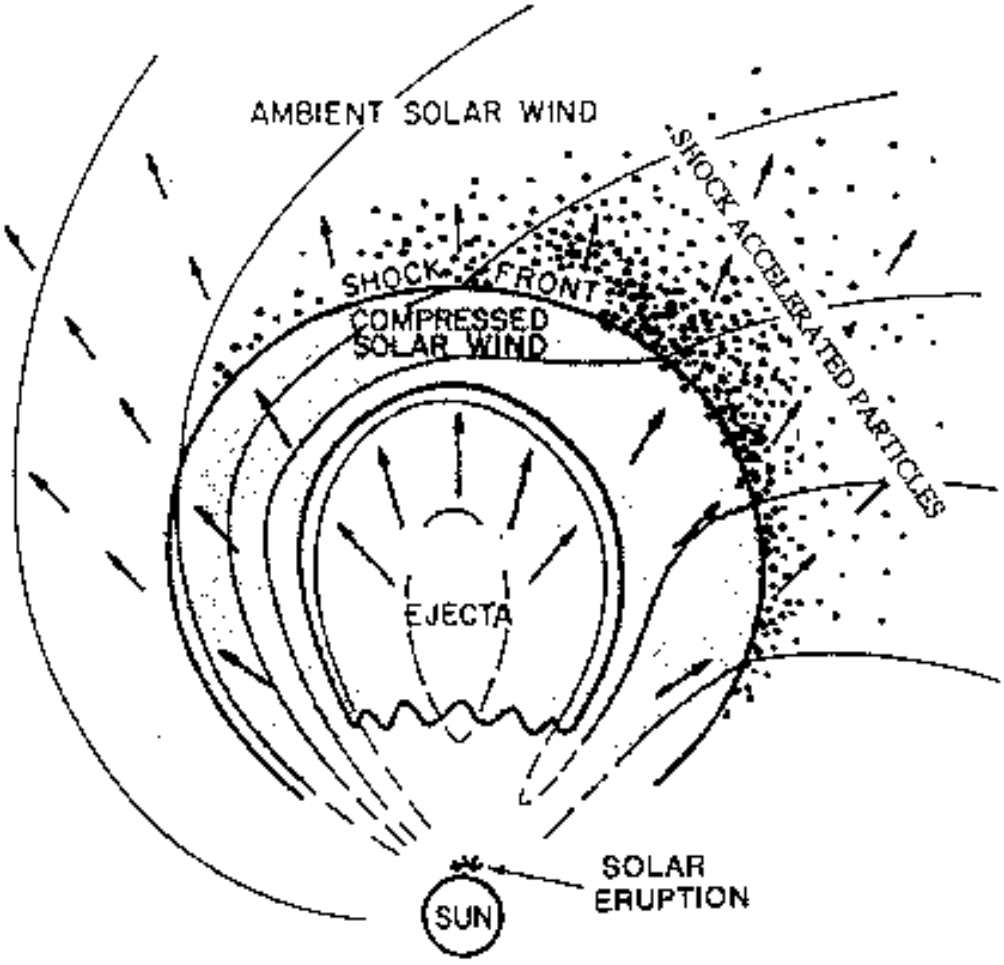

Figure 1.10: Cartoon of the CME expanding into and affecting the background solar wind and interplanetary magnetic field. (J.Luhmann, personal comm.)

Stream Interaction Regions (SIRs) occur at sector boundaries where solar wind with different velocities meet and a higher velocity stream compresses the slower moving stream ahead of it, as shown in Figure 1.11. SIRs are identified as regions of enhanced magnetic field and density followed by a high speed solar wind upstream, as in Jian et al. (2008). They are also called Corotating Interaction Regions (CIRs).

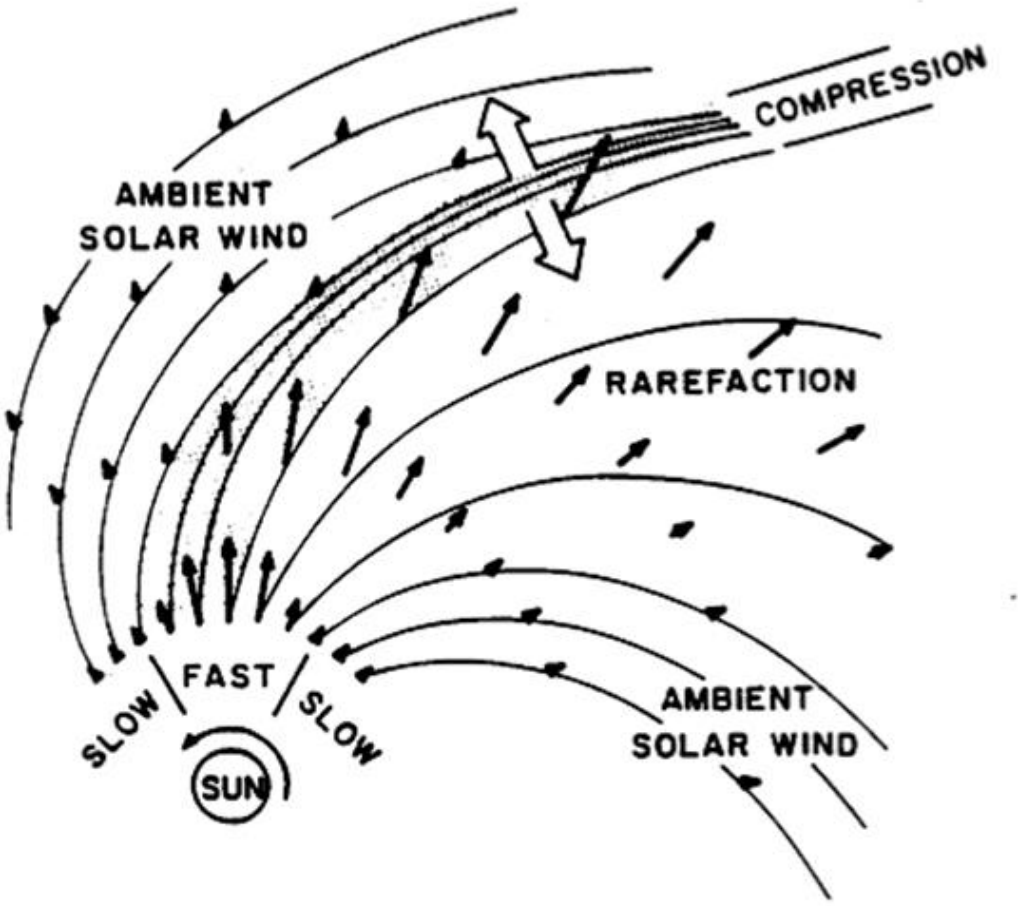

Figure 1.11: Stream Interaction Region (SIR) is a compression region where streams of different solar wind origins meet. (from Pizzo et al., 1991)

1.6 Previous studies of solar wind disturbance effect on oxygen ion escape

Enhancements of up to 10x in the O^+ escape flux were measured by PVO during periods of high dynamic pressure in ICMEs (Luhmann et al., 2007) (See Figure 1.12). Possible enhancements by 5-10x escape flux during ICMEs were also reported on VEX (Futaana et al., 2008, Luhmann et al., 2008). Enhanced O^+ escape flux during SIR/ICME passage has been found by Edberg et al. (2011), which showed a 1.9x enhancement compared to undisturbed solar wind (Figure 1.13). In

addition, SIRs with dynamic pressure above the average (1.3 nPa) had 36% more escape than the lower dynamic pressure SIRs.

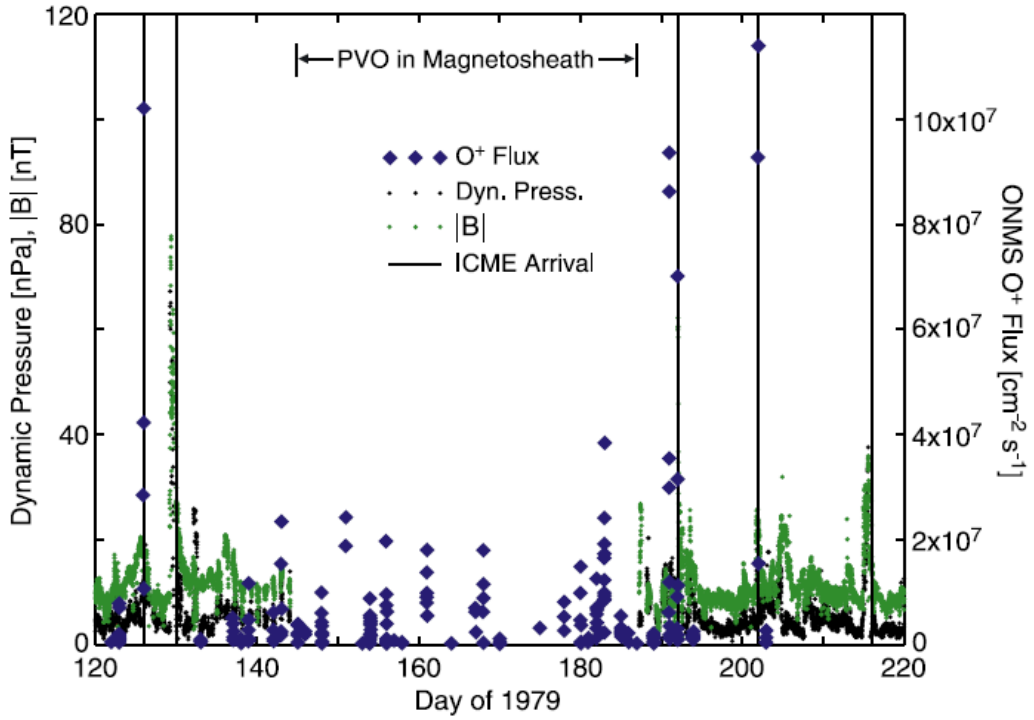

Figure 1.12: Suprathermal >36 eV O^+ flux measured by the PVO neutral mass spectrometer during 1979, compared to the magnetic field magnitude and solar wind dynamic pressure measured in the upstream solar wind. Vertical lines indicate where ICMEs were identified. (from Luhmann et al., 2007)

1.7 Dissertation Outline

This dissertation is comprised of four papers, three of which have been published or are in the review process with the journal Planetary and Space Science, while the fourth paper will be submitted to the journal Geophysical Research Letters. Chapter 2 compares the external solar wind conditions that VEX encountered from 2006-2009 to the conditions during the PVO time period. This paper is titled 'Comparing External Conditions That Influence Ion Escape at Venus during Pioneer Venus and Venus Express Missions', and was submitted to Planetary and Space Science February 2012, and resubmitted after review and revision on October 2012. The next study, in Chapter 3, was published in Planetary and Space

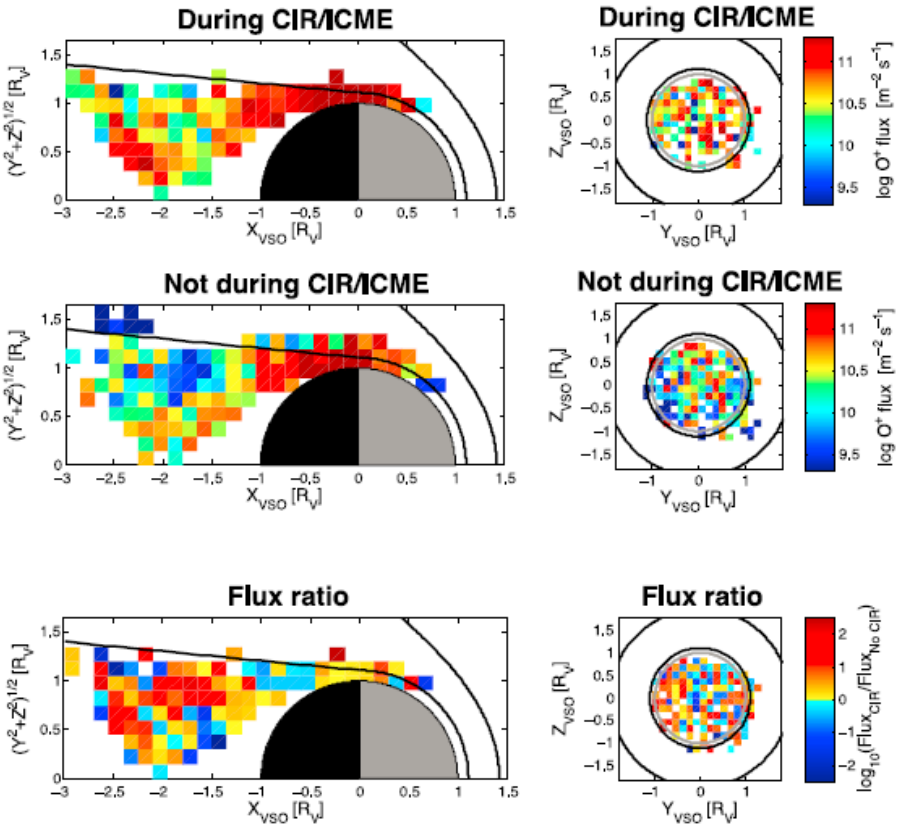

Figure 1.13: Antisunward fluxes of planetary O^+ ions as measured (top) during the impact of CIRs/ICMEs and (middle) during the time of quiet solar wind as well as (bottom) the flux ratio between disturbed solar wind times and quiet times in each bin. (from Edberg et al., 2011)

Science on July 13, 2010 titled 'Interplanetary Coronal Mass Ejection Influence on High Energy Pick-up Ions at Venus'. Chapter 4 adds to the interpretation low energy ions measured by VEX by comparison with a model. This paper was submitted to Planetary and Space Science October 2012 titled 'Comparisons of Venus Express Measurements with an MHD model of O^+ ion flows: Implications for Atmosphere Escape Measurements'. The final paper uses knowledge gained from the other three studies to investigate O^+ escape of all energies during the largest ICME that Venus Express has measured to date. This final paper will be submitted to Geophysical Research Letters.

Chapter 2

Comparing External Conditions That Influence Ion Escape at Venus during Pioneer Venus and Venus Express Missions

Abstract

Estimates of the oxygen ion escape rate from Pioneer Venus Orbiter (PVO) varied between 10^{24}-10^{26} O^+/second. The more recent estimate, from Venus Express (VEX), is ~$2.7*10^{24}$ O^+/sec. Because of the different instrument calibrations on PVO and VEX it is difficult to compare escape rates directly. However, VEX will be making measurements as we move into solar maximum allowing quantification of certain effects of the solar cycle. We can use the external conditions that PVO encountered to inform how typical the VEX conditions are compared to other solar cycles. We are interested in external conditions that influence ion escape (high dynamic pressure, small cone angles (<30°), and interplanetary magnetic field rotations). These parameters are considered to affect the ionopause altitude (above which ions are picked up), mode of ion pickup, and contribution of bulk ionosphere escape, respectively. Thus, in order to understand variations in escape rates (made with the same instrument and calibration) we must understand the solar wind setting of the measurements. In this study, we present yearly histograms of solar wind dynamic pressure, interplanetary magnetic field cone angles, and interplanetary magnetic field rotations. We show how these external conditions vary over the full solar cycle measured by PVO (1979 through 1988) and compare to the external conditions measured by VEX during the declining to minimum phase of the most recent cycle (mid 2006 through 2009). The median solar wind dynamic pressure near Venus during the VEX time period was ~0.5-1.5 nPa compared to ~4-6 nPa during the PVO time period. Also the VEX time period did not have the extreme high solar wind dynamic pressures >24 nPa that occurred during the PVO time

period. This lack of extreme solar wind dynamic pressures during the VEX time period is likely caused by the absence of large interplanetary coronal mass ejections. There was also a lower occurrence of small cone angles (15-20%) during the VEX time period versus 20-30% during the PVO time period, meaning that the cone angle was larger during the VEX time period. The VEX time period also had a higher occurrence of large (>100°) IMF spiral angle rotations than the PVO time period. The lower dynamic pressure and lower occurrence of small cone angles during the VEX time period could partially explain a low escape rate measured by VEX (if the two order of magnitude higher estimates of escape of PVO are actually representative of real escape rates). We cannot compare these rates directly, but this result opens up the possibility of higher escape during solar maximum. This will be measured by VEX over the next few years. The higher occurrence of large IMF rotations during the VEX time period could make bulk escape more important during this period compared to the PVO time period. This study illuminates the complications of interpreting ion escape rates due to the sometimes counteracting effects of numerous external variables. These do not all follow the same solar cycle trends and may differ from cycle to cycle, and can be used to inform further study of detailed ion escape on Venus Express.

2.1 Introduction

The most recent estimate of oxygen ion escape from Venus Express (VEX) is on the low-end of estimates from Pioneer Venus Orbiter (PVO) ($2.7*10^{24}$ from Fedorov et al. (2011) vs 10^{24}-10^{26} O^+/sec (from e.g., Kasprzak et al, 1991; Brace et al., 1995). The PVO measurements are from different instruments with different calibration, so they may not actually represent a real two order of magnitude difference in escape rate. It is possible that the high-end estimates are inaccurate, but they open up the possibility that Venus can have a higher escape rate than measured by Fedorov et al. (2011). It is still an open question of how the total oxygen ion escape varies with the solar cycle. It may be better answered as Venus Express continues to make measurements as we go into solar maximum. Measuring the escape rate over the full current solar cycle still may not be representative of what is possible during other, more intense, solar cycles. The observations in Fedorov et al. (2011) were from May 24, 2006 to December 12, 2007. This time period was during the declining phase of solar cycle 23, heading into the weakest solar minimum of the space age (Jian et al., 2011). It is important to consider the external conditions during the observation periods, particularly those that might modify escape rates, to put the escape rate estimates in context and guide further investigation of escape by Venus Express.

External conditions relevant to ion escape include solar extreme ultraviolet (EUV) flux and solar wind dynamic pressure nv^2, where n is density and v is velocity. The

balance between the ionosphere thermal pressure (which is sensitive to EUV) and solar wind dynamic pressure determines how much of the ionosphere will be exposed to the interplanetary magnetic fields (IMF). which can accelerate ions away from the planet (e.g. Luhmann et al., 1986, 1992). The upper boundary of the ionosphere where the density quickly falls off is called the ionopause and it is usually separated from the solar wind by the magnetic barrier where IMF piles up and the magnetic pressure dominates (e.g. Zhang et al., 1991, 2007). The configuration and magnitude of IMF can affect the mechanisms of ion escape, including ion pickup, ion outflow or bulk escape processes described below. Ion pick-up is due to the convection electric field in the solar wind $\mathbf{E} = -\mathbf{v} \times \mathbf{B}$, where **v** is the solar wind bulk velocity and **B** is the magnetic field vector (e.g. Luhmann et al., 2006). Ion pick-up occurs when there are ions created above the ionopause, which depends on the extension of the neutral exosphere. Observations have also suggested possible polar wind-like outflows (Hartle and Grebowsky, 1990). Ionosphere/solar wind boundary intrusions of ionospheric plasma referred to as "plasma clouds" which may act as a bulk ionosphere removal process from the top of the ionosphere (e.g. Brace et al., 1982). Lower energy ion outflow may also be due to the JxB force, where **J** is current density and **B** is magnetic field (e.g. Shinagawa, 1996a,b; Tanaka, 1998).

The EUV flux is solar cycle dependent with higher flux at solar maximum compared to minimum by a factor of two (Brace et al., 1988; Ho et al., 1993). This causes higher ionospheric pressure through both ion production and heating (Bauer and Taylor, 1981). When the Sun is more active, the higher ionospheric pressure holds off the solar wind plasma and prevents the draped interplanetary magnetic fields from penetrating into the ionosphere. Under these conditions, cross-terminator flows supply a nightside ionosphere. During solar minimum when the ionosphere has lower pressure the draped fields may penetrate the ionosphere, which may shut off most transterminator flows and cause the nightside ionosphere to disappear (as proposed by Luhmann and Cravens, 1991). Luhmann et al. (1993) discussed how higher EUV can lead to enhanced escape of pick-up ions through multiple mechanisms via a more extended neutral thermosphere, a denser exosphere and a higher photoionization rate. Moore et al. (1990) and Kasprzak et al. (1991) both found higher escaping O^+ flux measured by PVO during higher solar EUV periods.

The solar wind dynamic pressure (the external control of the ionopause altitude) is enhanced during the passage of Stream Interaction Regions (SIRs), which are the structures between fast and slow solar wind streams. This dynamic pressure enhancement is due to compression between streams as shown in Figure 2.1. Dynamic pressure is also high in transient events called Interplanetary Coronal Mass Ejections (ICMEs) as they compress slower solar wind in front of them as

shown in Figure 2.2 (reviewed by Crooker et al., 1997). Enhancements of up to 100x in the O^+ escape flux measured by PVO during periods of high dynamic pressure in ICMEs were reported by Luhmann et al. (2007), and possible enhancements by 5-10x escape flux during ICMEs were also reported on VEX (Futaana et al., 2008, Luhmann et al., 2008). Enhanced O^+ escape flux during SIR passage has been found by Edberg et al. (2011) which showed a 1.9 times enhancement compared to undisturbed solar wind. Edberg et al. (2011) also investigated the effect of dynamic pressure. They did this by sorting SIR cases by dynamic pressure into bins higher or lower than the median of 1.3 nPa and found that the higher dynamic pressure SIRs had 36% more escape than the lower dynamic pressure SIRs.

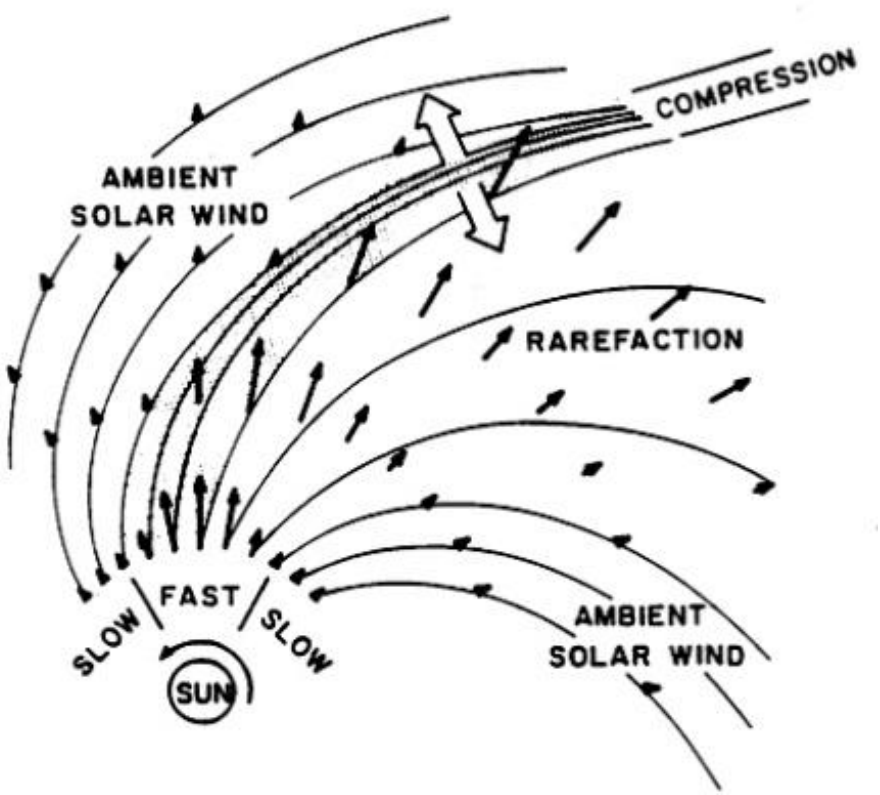

Figure 2.1: Stream Interaction Region (SIR) due to a faster solar wind stream running into a slower stream and causing a compression region in front and a rarefaction region behind it, from Pizzo (1978).

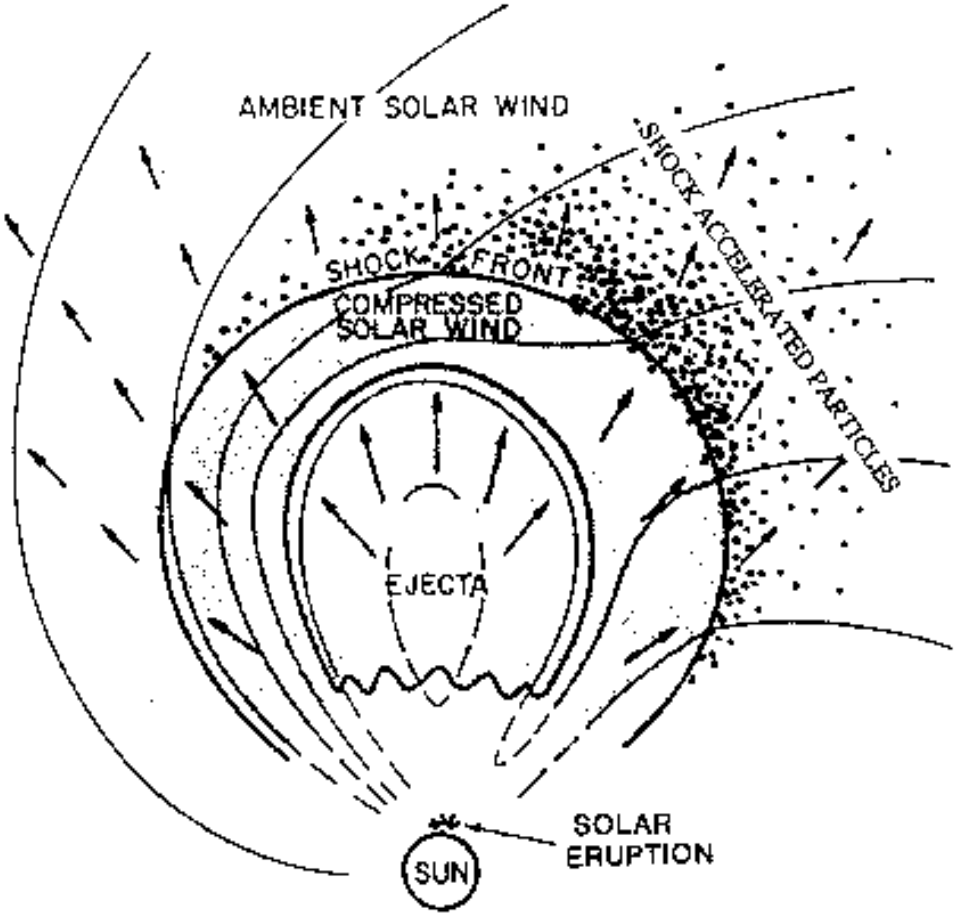

Figure 2.2: ICME expanding into the solar wind and compressing solar wind in front of it which leads to higher dynamic pressure.

Even within undisturbed solar wind, the velocity is variable due to diverse source regions on the sun, and this can lead to different orientations of the IMF based on the theory of Parker (1963), which explains the average spiral configuration of the IMF in the ecliptic, depends on solar wind velocity. The angle of the field in the ecliptic, the IMF spiral angle shown in Figure 2.3, is measured from the line radial to the sun in the orbital plane of Venus given by $\tan^{-1}(-B_Y/B_X)$. Here B_Y and B_X are IMF vector components in Venus-Solar-Orbital (VSO) coordinates (where X is toward the sun, Z is perpendicular to the ecliptic, and Y completes the right hand system). At Venus the average spiral angle is ~36°. The IMF is not always in the ecliptic and includes the B_Z component which gives the cone angle $\cos^{-1}(B_x/B_{tot})$ as shown in Figure 2.3. The cone angle has not been definitively shown to affect the ion escape rate in data analysis but was shown to possibly affect the ion escape mechanisms in VEX ion data by Masunaga et al. (2011). Low cone angle, which in

observations has a notable effect on IMF draping and fluctuations in the Venus magnetosheath, was shown to increase the escape flux in the MHD model of Zhang et al. (2009) (comparing an 11° cone angle to a 0° cone angle they found ~ 5.4 x 10^{25}/sec versus ~9.5 x 10^{25}/sec respectively), and in the hybrid model of Liu et al. (2009).

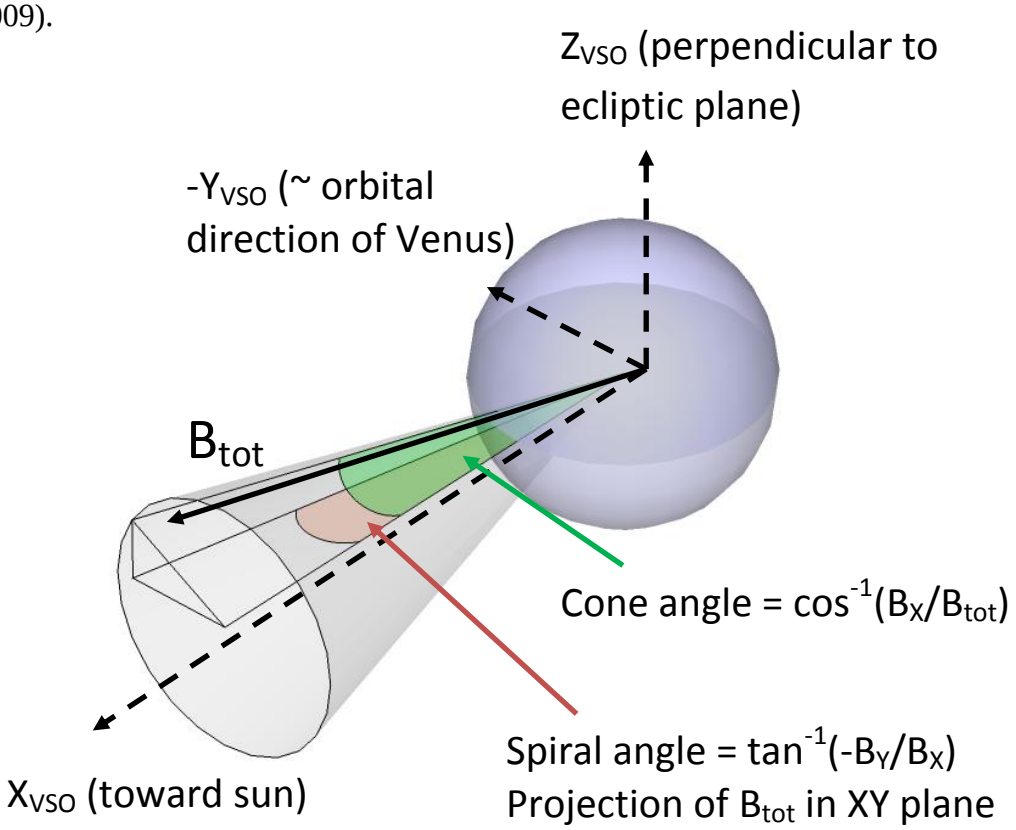

Figure 2.3: Cone angle (angle from the X axis), $\cos^{-1}(B_X/B_{tot})$ and its projection onto the XY plane the spiral angle, $\tan^{-1}(-B_Y/B_X)$, in Venus-Solar-Orbital (VSO) coordinates.

Another external control to consider is rotations of the IMF, which may lead to comet tail disconnection like behavior such as studied by Niedner and Brandt (1978a, b). Possible observational evidence of this behavior at Venus is from the density enhancements at the edge of the ionopause, the "plasma clouds" (Brace et al., 1982). Russell et al. (1982) associated the plasma clouds with rotations in magnetic fields suggesting that plasma clouds may occur at the magnetic draping poles where an anti-sunward JxB force acts. However, a follow-up study by Ong et al. (1991) showed that the plasma clouds did not organize by the orientation of the upstream IMF which would be expected if they were occurring at the magnetic

draping poles. Instead they found that the magnetic field rotations may have been external rotations in the IMF. The average clock angle rotation of the IMF inbound versus outbound on orbits that had clouds was 59°, compared to the average solar wind rotation of 29°. The average solar wind rotation in their study for comparison with the orbits containing clouds was calculated between points separated by 75 minutes, the approximate time between inbound and outbound crossings of the bow shock. If the plasma clouds are a bulk removal process, they may contribute significantly to the total escape flux with an estimated 10^{25}-10^{26} O^{+}/second (Russell et al., 1982; Brace et al., 1982). IMF rotations may also have contributed to the 1.9 times enhanced ion escape flux measured by VEX during SIRs by Edberg et al. (2011) because SIRs are often associated with heliospheric current sheet (HCS) crossings, which separate inward versus outward IMF field lines (e.g. Gosling et al., 1978; Jian et al., 2006).

In this paper we consider solar wind characteristics that may be associated with enhanced escape flux: high dynamic pressures, small cone angles, and large IMF rotations. We study the occurrence of these solar wind conditions during the full solar cycle that PVO sampled (January 1979-August 1988) and the declining to minimum phase of VEX measurements (June 2006 through 2009). The solar cycle sampling of the time periods in this study is shown in Figure 2.4. Our results provide a summary of what solar wind and IMF conditions VEX has encountered that may affect the measured escape flux. The comparisons with PVO era counterparts suggest possible reasons, other than the solar EUV flux, that might affect differences in escape rate.

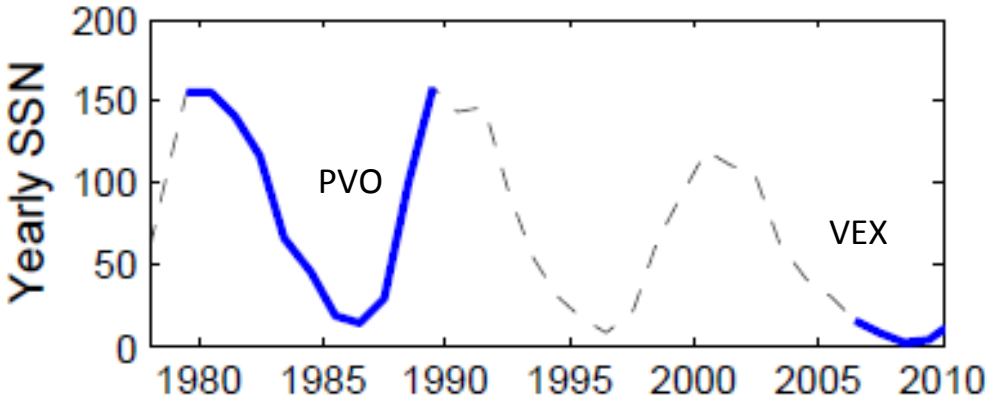

Figure 2.4: Solar cycle setting of PVO and VEX. SSN is sunspot number. (SSN data from http://solarscience.msfc.nasa.gov/SunspotCycle.shtml)

2.2 Data sets

For the VEX solar wind and interplanetary magnetic field statistics that we present in this paper, we use data from the ASPERA-4 Ion Mass Analyzer (IMA) (Barabash et al., 2007) and magnetometer (Zhang et al., 2006) during June 2006 through the end of 2009. VEX has a highly elliptical ~24 hour orbit with periapsis near the northern pole of Venus and the line joining periapsis and apoapsis nearly perpendicular to the ecliptic so that periapsis always samples near the north pole. The magnetometer makes continuous observations, while the IMA makes measurements primarily within a few hours of periapsis. We use 10 minute resolution for both datasets and restrict the available measurements to upstream of the Venus bow shock, in order to sample the solar wind rather than the planetary region. We used the bow shock equations from Zhang et al. (2008) where r is in Venus Radii: $r = 2.14/ (1+0.621*\cos(SZA))$ for $SZA<=117°$ and $r = 2.364/\sin(SZA+10.5°)$ for $SZA > 117°$. The solar wind data set is highly restricted, because the IMA instrument is normally operated for only a few hours near periapsis (out of the ~24 hour orbit) and most of this near periapsis data is not used (due to being within the bow shock). To derive the solar wind dynamic pressure we use VEX IMA density and velocity from the AMDA website (http://cdpp-amda.cesr.fr/DDHTML/index.html). The VEX IMA is not a dedicated solar wind monitor, and can become saturated in the solar wind, so we only use measurements with a high quality, and compare the calculated dynamic pressure to measurements made by the ACE spacecraft. Figure 2.5 shows a comparison of the % occurrence of dynamic pressure in 2009 measured by the VEX IMA and ACE. VEX may saturate and may underestimate dynamic pressures <5nPa, but is able to measure higher dynamic pressures similar to the ACE solar wind monitor, which are the pressures of primary interest in this paper.

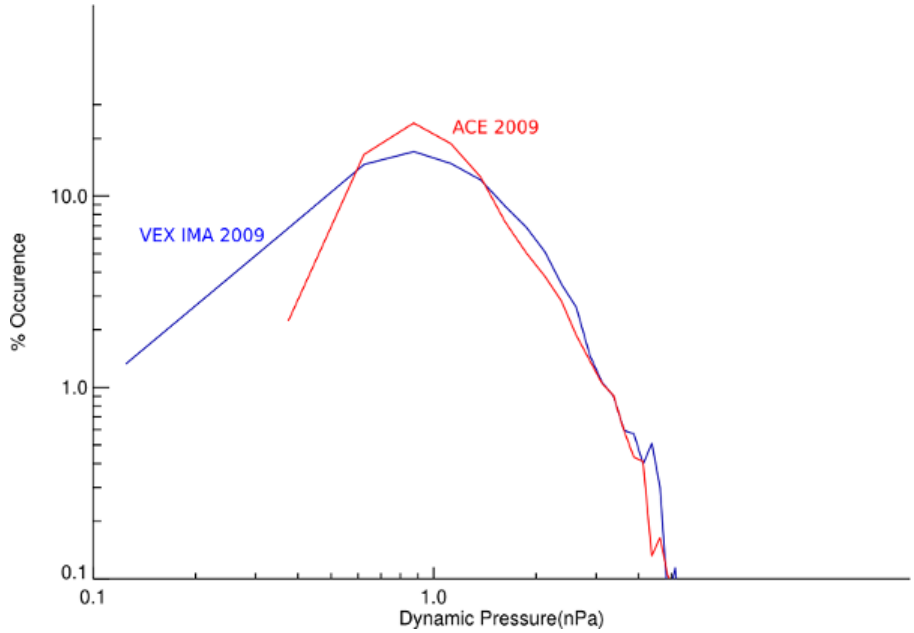

Figure 2.5: Comparing the dynamic pressure measured by VEX to ACE (scaled to the Venus orbit) during 2009. For lower dynamic pressures (<5nPa) VEX may underestimate the dynamic pressure, but for higher dynamic pressures VEX agrees with ACE.

We used data from the Pioneer Venus Orbiter (PVO) plasma analyzer (Intriligator et al., 1980) and magnetometer (Russell et al., 1980) during January 1979 to August 1988. We used 10 minute resolution for both datasets and the data available has already been restricted to upstream of the bow shock so that we only sampled the solar wind. PVO had a highly elliptical orbit with periapsis near the equator of Venus and the line joining periapsis and apoapsis near the ecliptic. The orbit spent a few months out of every year almost entirely out of the solar wind when apoapsis was in the tail. According to Jian et al. (2008), the PVO solar wind data set covers 60.3% of the 10-year period, with the amount of useable data varying by year from a maximum of 68% in 1982 to a minimum of 36% in 1988.

2.3 Statistics of solar wind dynamic pressures, IMF cone angles, and IMF rotations

This section presents histograms of dynamic pressure (3.1), cone angle (3.2), and IMF rotations (3.3) measured by instruments on PVO (1979-1988) and VEX (mid-2006 through 2009). The histograms are presented by year during these time periods in order to compare changes over a solar cycle on PVO. This yearly comparison is

useful because published escape rate estimates have used data from differing time periods on PVO and VEX. It can guide future studies of the ion escape during different time periods. For each section comparing PVO to VEX the histogram bins on the x axis are the same and the number of data points in each bin is normalized by the total number of data points, so that the distributions can be compared directly.

2.3.1 Solar wind dynamic pressure

Histograms of the solar wind dynamic pressure by year over the PVO time period are shown in Figure 2.7. The last bin of this histogram (24 nPa) includes all measurements above that value. The peak of the main solar wind dynamic pressure distribution during the PVO time period was lowest during solar maximum (~1980) and highest near solar minimum (~1985-1986). This agrees with previous statistics of the solar wind dynamic pressure on PVO showing an average of 4.5 nPa at solar maximum and 6.6 nPa at solar minimum (e.g. Luhmann et al., 1993; Russell et al., 2006). Histograms of solar wind dynamic pressure by year from VEX are shown in Figure 2.6 from the declining phase into solar minimum in 2009, which does not have the same trend. The dynamic pressure peak was highest during 2006 during the declining phase and lowest during 2009 during minimum.

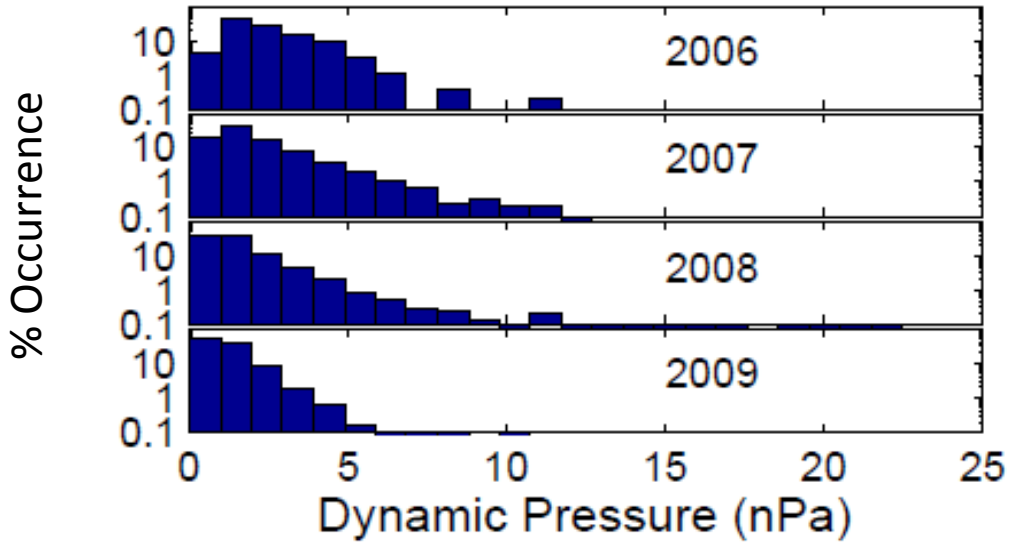

Figure 2.6: Histograms of solar wind dynamic pressure broken up by year measured by VEX.

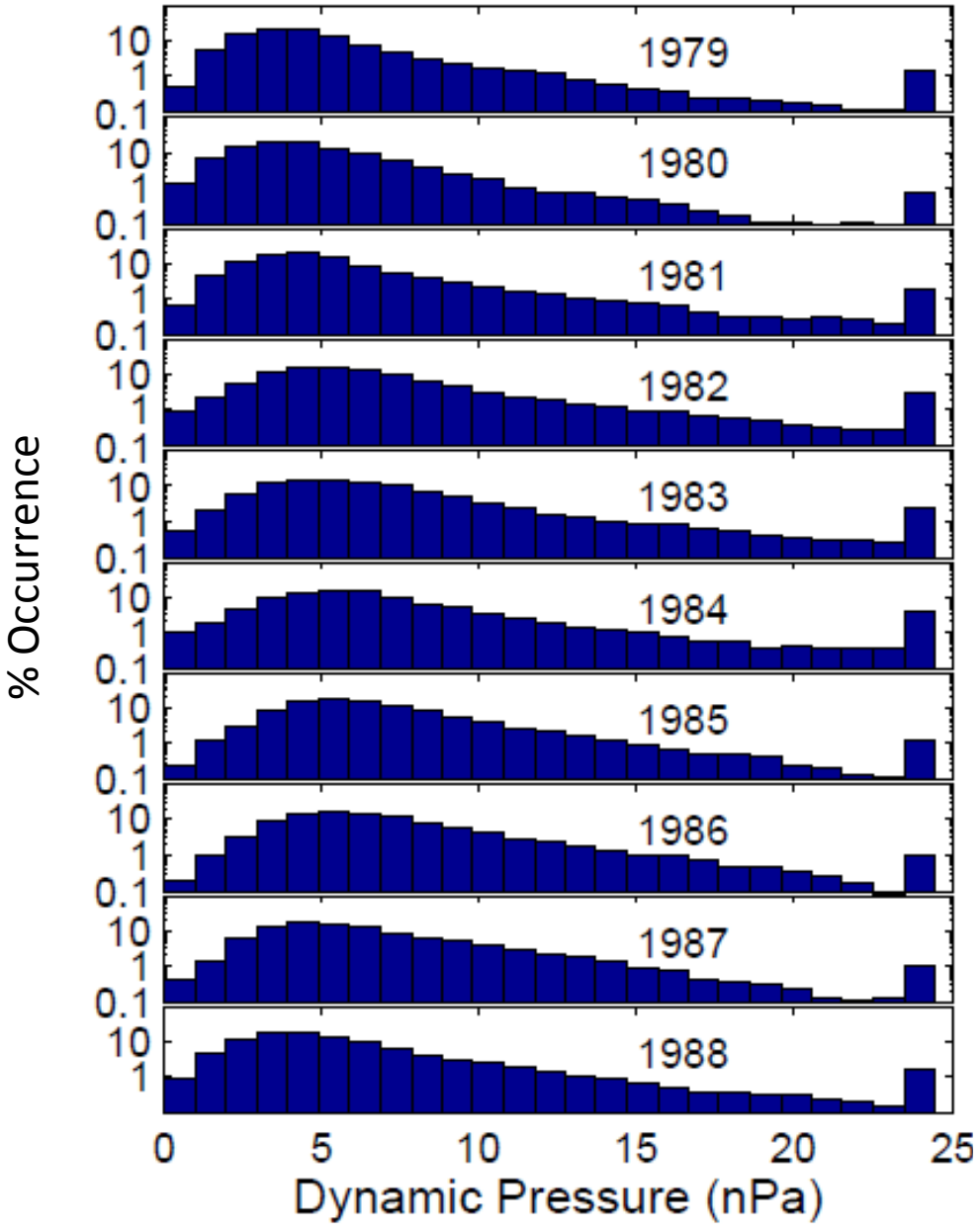

Figure 2.7: Histograms of solar wind dynamic pressure broken up by year measured by PVO (where the last bin includes all data above 24 nPa). These histograms show how the solar wind dynamic pressure distribution changed over the solar cycle on PVO and how the solar wind dynamic pressure was much higher during the PVO time period than the VEX time period (shown in Figure 2.6).

The median dynamic pressure during the PVO time period was significantly higher than during the VEX time period (~4-6 nPa compared to ~0.5-1.5 nPa). Another difference is that the PVO time period had a high dynamic pressure tail above 24 nPa that is not seen in the VEX data. The high dynamic pressure tail (>24 nPa) was likely due to ICMEs during the PVO time period as shown in the bottom panel of Figure 2.8. In this figure the red ICME distribution makes up the higher occurrence rate of dynamic pressures above 24 nPa. For more information about the characteristics of ICMEs on PVO see Jian et al. (2008).

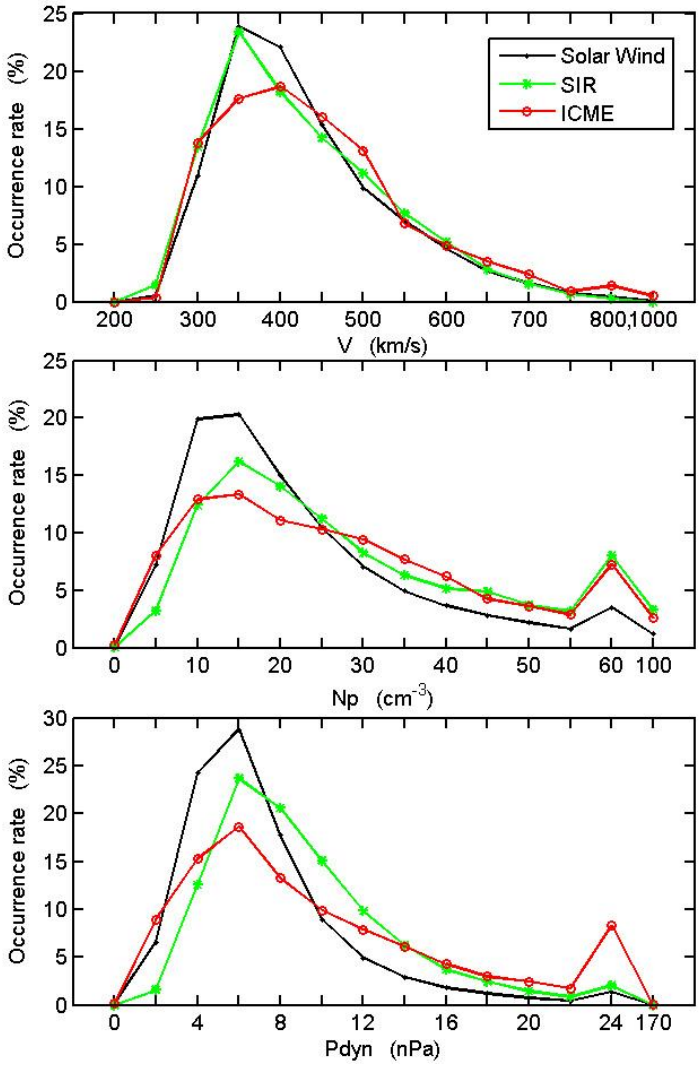

Figure 2.8: Comparing the characteristics of ICMEs and SIRs to solar wind on PVO.

2.3.2 Cone Angle

Histograms of the IMF cone angle by year from 1979-1988 from PVO are shown in Figure 2.10, and for the VEX time period (mid 2006-2009) in Figure 2.9. The background color separates small (<30° or >150°), intermediate (30°-60° or 120°-150°) and large (60°-120°) cone angles. These angle bins were chosen because they are the ranges used by Masunaga et al. (2011). These histograms show a change in the shape of the cone angle distribution by year, with the PVO distributions taking on a more saddle-like shape. This means that there are less large cone angles shown in the gray background sections. In order to better quantify the total contribution of small cone angles by year and to more easily compare PVO to VEX, we summed the % occurrence in the small, intermediate and large bins each year, with the results shown in Figure 2.11.

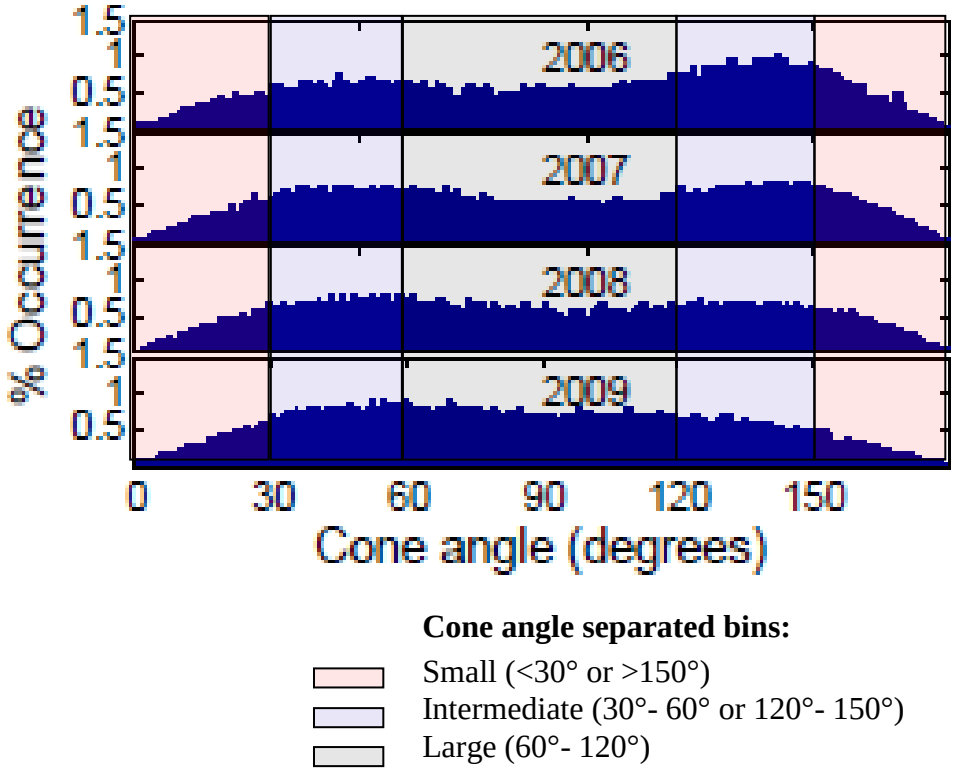

Figure 2.9: Cone angle, $\cos^{-1}(B_X/B_{tot})$, histograms of % occurrence by year during VEX (mid-2006-2009). Background color corresponds to cone angle ranges described as small (light red), intermediate (light blue), and large (gray).

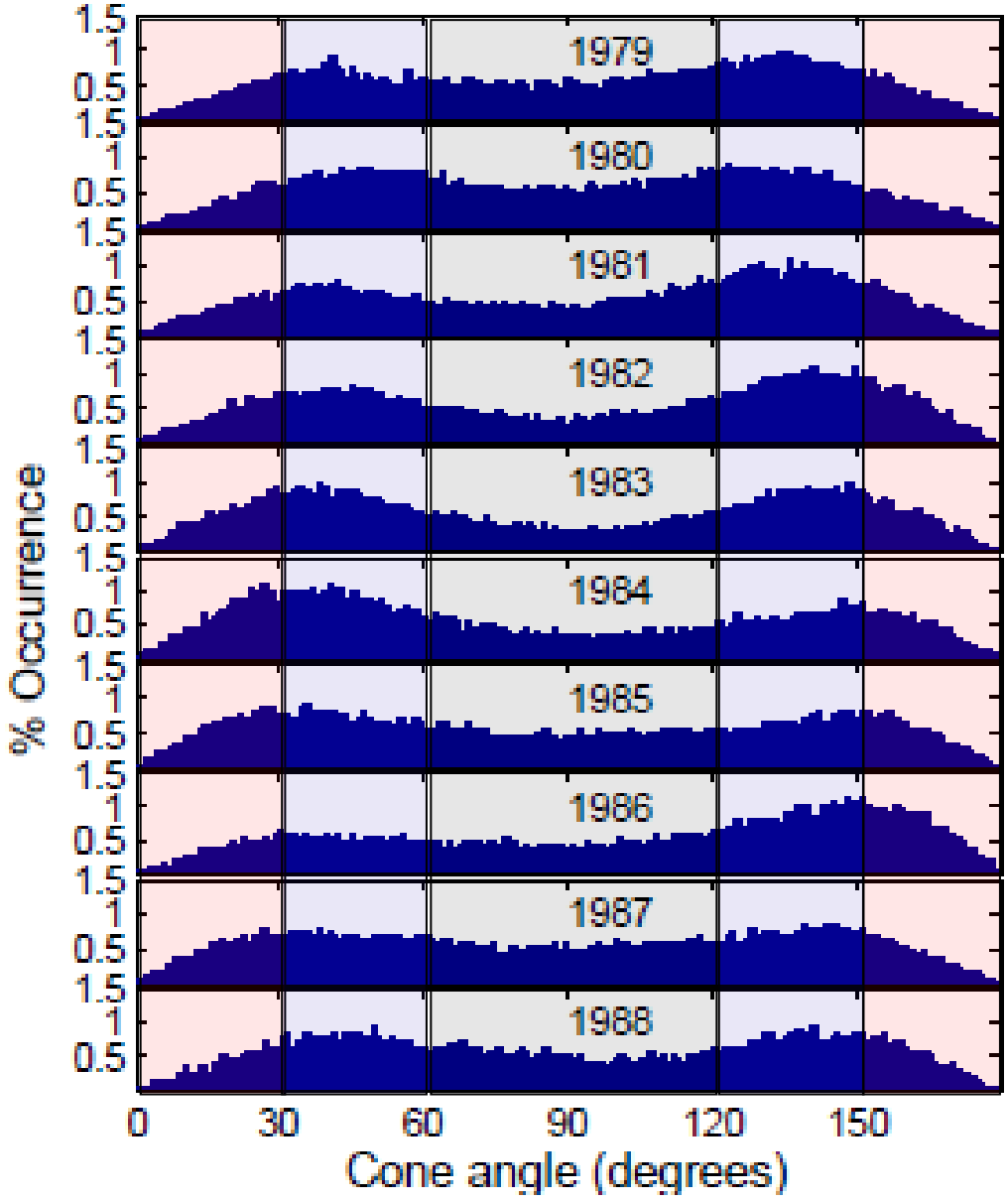

Figure 2.10: Cone angle, $\cos^{-1}(B_X/B_{tot})$, histograms of % occurrence by year during PVO 1979-1988. Background color corresponds to cone angle ranges described as small (light red), intermediate (light blue), and large (gray).

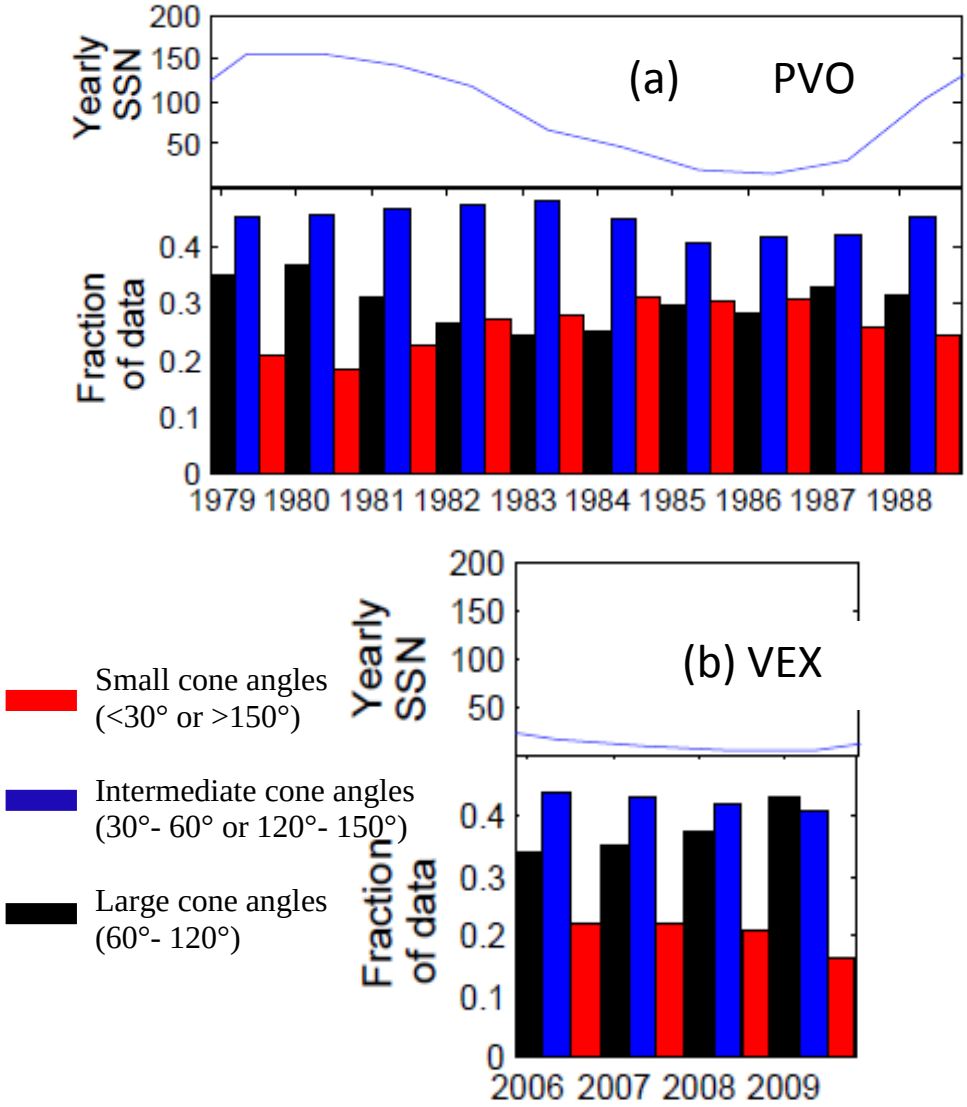

Figure 2.11: The fraction of IMF data outside of the Venus bow shock containing small, intermediate and large cone angles on (a) PVO and (b) VEX on the bottom, and the solar cycle setting of the missions as shown by the yearly sun spot number above.

The highest occurrence of small cone angles (which are shown in red in Figure 2.11) during PVO was in 1984 during the declining phase and the lowest number of small cone angles was in 1980 during solar maximum. This result agrees with Luhmann et al. (1994) statistics of cone angle at 1 AU, where the highest cone

angles occurred during solar maximum (1980) and the lowest during the declining period. For the VEX time period in Figure 2.9b the lowest number of small cone angles was in 2009 during solar minimum, which is the opposite of the PVO trend. Comparing VEX to PVO, the occurrence of small cone angles (<30°) was less during the solar minimum period of VEX during 2009 (15%) versus PVO during 1986 (30%). This would imply that the solar wind velocity was lower during the VEX period, which agrees with Jian et al. (2011) who showed that at 1 AU the average solar velocity in 1986 was 459 km/s while in July 2008-June 2009 it was 388 km/s.

2.3.3 IMF rotations

Ong et al. (1991) found that the possible bulk removal plasma clouds measured by PVO occurred more often when there was a large rotation of the IMF. Many of these rotations may have been due to crossing the heliospheric current sheet (HCS) since the current sheet separates inward versus outward spiral interplanetary magnetic field (Schulz 1973). These different sectors of magnetic field orientation can be seen in magnetic field spiral angle time series as period. The spiral angle stays near the same positive or negative value for a time period and then rotates in sign and stays at that new value, making a checkerboard-like pattern as shown in Figure 2.12. The frequency of rotations is due to the warp of the HCS which varies over the solar cycle, introducing more variations when the current sheet is everywhere near the ecliptic (e.g. Hoeksema et al., 1983).

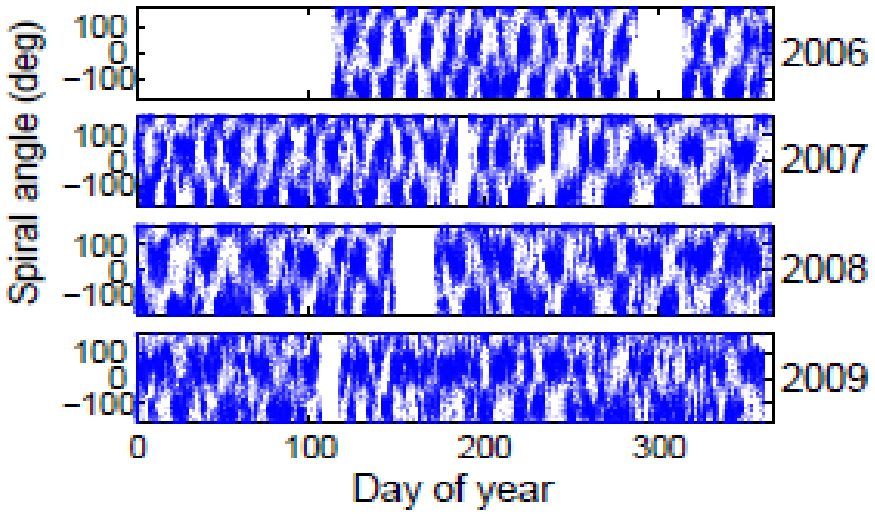

Figure 2.12: Time series of IMF spiral angle showing sector boundaries measured by VEX near Venus.

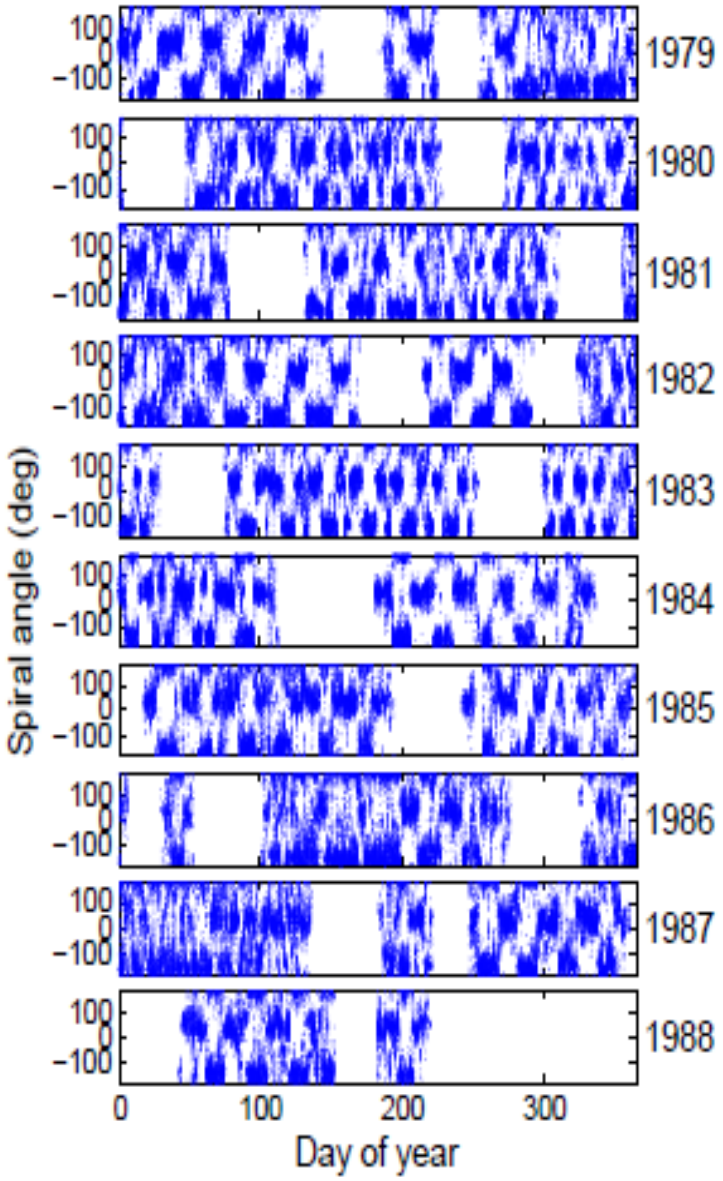

Figure 2.13: Time series of IMF spiral angle showing sector boundaries measured by PVO near Venus.

The occurrence of IMF rotations are shown as histograms of spiral angle rotation calculated between data points separated by 10 minutes in Figure 2.14b for PVO and Figure 2.14a for VEX. The majority of the IMF rotation angles during both PVO and VEX time periods changed by less than 20° every 10 minutes. Comparing PVO to VEX there are more large rotations in the VEX data as seen by the tail in

the spiral angle rotation histogram above 100°. This is absent in the PVO data except in 1985-1986 which had some high rotation occurrence (but not as high as any of the VEX years).

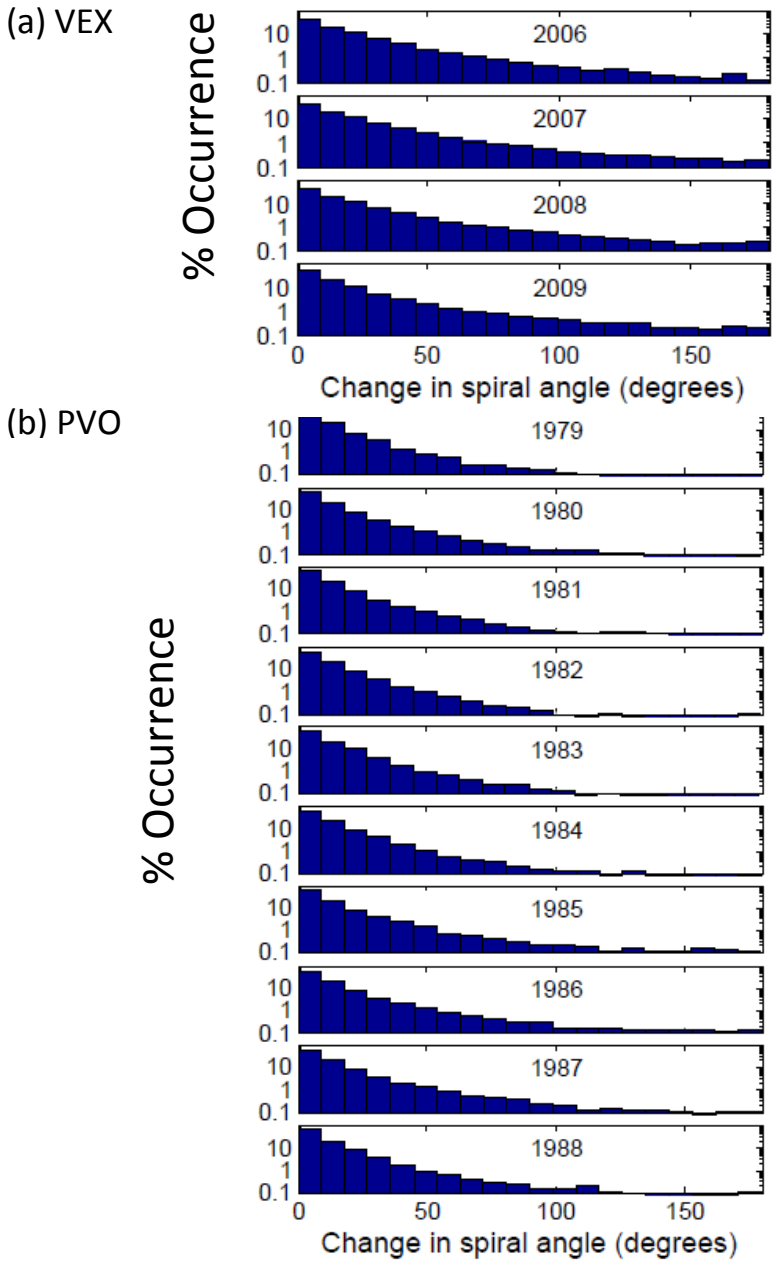

Figure 2.14: Histograms by year of spiral angle rotations on (a) VEX (2006-2009) and (b) PVO (1979-1988).

2.4 Discussion of results and comparison with other studies

The Venus Express results come from the declining phase into an unusually long and deep solar minimum (e.g. McComas et al., 2008; Lee et al. 2009; Jian et al., 2011). Lee et al. (2009) showed that this declining phase (February 4-November 4, 2007) had unusually low density at 1 AU compared to a similar solar cycle sample during the previous cycle (February 23-November 22, 1995). Jian et al. (2011) extended this result to the two previous solar minimums in 1976 and 1986, showing that the most recent minimum is the weakest of the four periods studied.

Our statistics of this most recent period show weak solar wind dynamic pressure compared to the PVO time period, which agrees with the Lee et al. (2009) results of lower density and with the Jian et al. (2011) results of lower density and lower dynamic pressure. In particular, Jian et al. (2011) point out that that at 1 AU the dynamic pressure was ~1.4 nPa in July 2008-June 2009, while it was ~2.97 nPa in 1986, which would have been during the solar minimum of our PVO analysis. Our results show a high dynamic pressure (>24 nPa) tail on the PVO dynamic pressure histograms which we attribute to stronger ICMEs during this time period. ICMEs at Venus during the PVO time period did have high dynamic pressures with a median dynamic pressure maximum of 20.7 nPa with some extending up to 82 nPa (Jian et al., 2008). Jian et al. (2011) looked at ICMEs at 1 AU during the most recent minimum versus the previous minimum in1996, and found that the most recent minimum has weaker dynamic pressure ICMEs with shorter duration, but there is not a comparison of the ICMEs during the PVO time period.

Although PVO had higher dynamic pressures, the portion of the dynamic pressure histograms presented in this study that lead to enhanced escape may depend on the EUV which is solar cycle dependent. Therefore, the EUV is also important to consider. Phillips et al. (1984) showed that during solar maximum the peak ionosphere pressure was around 6 nPa. The PVO data shows that the solar wind dynamic pressure would have often reached values higher than this, while during VEX the dynamic pressure was much lower but the EUV was also lower due to VEX measuring near solar minimum.

2.5 Possible implications for Venus ion escape rate estimates

Our study shows that during the time period we looked at (2006-2009) VEX had not yet sampled the high dynamic pressure tail of the distribution of pressures seen by PVO. The 100 times enhancement in O^+ flux seen by Luhmann et al. (2007) occurred at ICME arrivals when the dynamic pressure was above 20 nPa, and our

analysis shows that these high pressures occurred ~2-3% of the time on PVO, but have not happened on VEX (or at least have not happened with an occurrence of more than 0.1% of the time). This could significantly lower the estimated escape rate from VEX compared to PVO (although instrument differences on the missions make this direct comparison between VEX and PVO escape rates difficult to confirm).

Small cone angles (<30 degrees) occur between 15% and 30% of the time, so if the cone angle is associated with an increased (or decreased) escape flux of O^+ it is important to take into consideration when comparing escape rates from different time periods. Depending on if/how cone angle affects the flux; the large amount of time spent in this IMF configuration could significantly modify the estimates of escape. We saw less small cone angles on VEX, so it is important to consider if the cone angle is found to modify escape rates.

IMF rotations may be important drivers of escape if they are associated with the plasma clouds seen by PVO as suggested by Ong et al. (1991). It is important to consider this possible escape mechanism when estimating escape rates, particularly if orbits during which there is a rotation are screened out of the estimates (such as in Fedorov et al., 2011). Orbits with large rotations are often discarded when looking at escape because in order to put measurements in a frame considering the convection electric field. If the IMF is rotating and the spacecraft is downstream of the bow shock it is hard to estimate the external convection electric field. Therefore, further work must identify whether or not the IMF rotations are associated with bulk escape and if so consider them in the total escape flux estimate.

2.6 Summary

1. Dynamic pressure was significantly higher during the PVO time period (in general and high pressure tail due to ICMEs).
2. VEX dynamic pressure was lowest during 2009 (minimum) which doesn't agree with PVO where the lowest dynamic pressure was in 1980 (maximum).
3. VEX had less small cone angle (<30°) occurence compared to the PVO time period (15-20% versus 20-30%).
4. Small cone angles still happen in a large portion of the time (15-30%) and thus are important to consider when estimating ion escape rates.
5. VEX had more large (>100°) IMF rotations than the PVO time period.

2.7 Future work

There is still not clear consensus on how the O^+ ion escape rate from Venus varies with solar cycle and with changing external conditions. In order to understand this we must understand the mechanisms of escape and how the escape flux depends on the external conditions. In particular, additional studies on the cone angle influence on escape flux and whether plasma clouds are a bulk escape process related to IMF rotations. Also, measurements of escape during enhanced dynamic pressure by VEX should be continued as the solar activity picks up and the planet encounters ICMEs with higher dynamic pressure. All of these measurements must keep the external conditions in mind, which we have presented in this study.

Chapter 3

Interplanetary Coronal Mass Ejection Influence on High Energy Pick-up Ions at Venus

Abstract

We have used the Ion Mass Analyzer (IMA) and Magnetometer (MAG) on Venus Express (VEX) to study escaping O^+ during Interplanetary Coronal Mass Ejections (ICMEs). Data from 389 VEX orbits during 2006 and 2007 revealed 265 samples of high energy pick-up ion features in 197 separate orbits. Magnetometer data during the same time period showed 17 ICMEs. The interplanetary conditions associated with the ICMEs clearly accelerate the pickup ions to higher energies at lower altitudes compared to undisturbed solar wind. However, there is no clear dependence of the pickup ion flux on ICMEs. This may be attributed to the fact that this study used data from a period of low solar activity, when ICMEs are slow and weak relative to solar maximum. Alternatively, atmospheric escape rates may not be significantly changed during ICME events.

3.1 Introduction

There may have been an ocean's worth of water on Venus early in its history, as evidenced by a D/H ratio 100 times that on Earth (Donahue et al., 1982, McElroy et al. 1982). We must question what happened to the ocean, because Venus's atmosphere currently contains little water vapor, only 200-300 ppm (Hoffman et al., 1980; Johnson and Fegley, 2000). Water vapor can be photodissociated by solar UV when it reaches a high enough altitude in the atmosphere. After dissociation, it is possible to lose the hydrogen to space via hydrodynamic escape (Kasting and

Pollack, 1983), but getting rid of the heavier oxygen is more difficult. A portion of the oxygen may have been taken up by oxidation of the crust (e.g. Fegley et al., 1997), but this process cannot account for the amount of oxygen that is missing from the atmosphere (Lewis and Kreimendahl, 1980). Oxygen can be lost if it is ionized and stripped away by the solar wind.

The lack of an internal dipole magnetic field allows direct scavenging of ionized atmospheric constituents from the atmosphere of Venus by the solar wind (e.g., Barabash et al., 2007a; Terada et al., 2002; Luhmann, 2006, 2007). Oxygen ion escape has been observed on both Pioneer Venus Orbiter (PVO) and Venus Express (VEX), respectively described in Luhmann et al. (2006) and Barabash et al. (2007a).

Estimates of the average escape rates of oxygen on Venus range from 10^{24} s^{-1} to 10^{26} s^{-1} (cf Jarvinen et al., 2009). Atmospheric loss during the first billion years after planetary formation would have been primarily been due to large impacts. If subsequent escape (over the next 3.5 billion years) occurred at rates similar to the present day, the total escape of oxygen would be 10^{41} to 10^{43} total oxygen atoms. An Earth-like ocean contains 10^{45} water molecules or the equivalent number of oxygen atoms. Thus the currently observed average escape rates of O^+ are insufficient to account for an ocean's worth of oxygen loss. In addition, the current escape rate also includes oxygen from dissociated CO_2, so to account for the total oxygen loss from water you would need an even higher current escape rate. However, conditions in the solar system have also changed over time, including the Sun and its outputs which may have affected the total escape of oxygen. In particular, stellar analogs suggest the early Sun had both higher EUV fluxes and was more active (Newkirk, 1980; Zahnle and Walker, 1982; Lammer et al, 2003) This paper describes a further contribution to the study of solar activity effects on the escaping oxygen ions at Venus, as observed on VEX.

Understanding the solar wind induced escape at Venus is also important for understanding Mars. Since Mars is also unmagnetized it interacts with the solar wind similarly to Venus on the large scale but is more complicated because of its small size and remnant crustal magnetic fields. Escape of atmosphere on Mars is interesting because there is evidence that there was once surface water in liquid form (e.g. Head et al., 1999; Squyres et al., 2004) which would have required a thicker atmosphere to cause a greenhouse effect sufficient to warm the surface above the freezing point of water.

The solar wind induced escape of high energy O^+ from Mars has been investigated by Dubinin et al. (2006). They found a linear dependence of ion energy on altitude which was attributed to acceleration in an electric field. Dubinin et al (2006) also noticed that ions in one orbit gained energy more rapidly with altitude than for other orbits. Using data from the Mars Global Surveyor spacecraft we confirmed that this particular case where the ions gained energy closer to the planet occurred during a solar wind disturbance. This study builds on the results of Dubinin et al (2006) with a survey of more MEX ion data and a similar energy altitude analysis at Venus.

3.2 The Venus Solar Wind Interaction

The interaction of Venus with the solar wind is illustrated in Figure 3.1. Since Venus does not have a dynamo magnetic field, but has an ionosphere, it acts like a conducting sphere in this solar wind plasma (e.g. Luhmann, 1986). Around solar maximum, when PVO was at Venus sampling the ionosphere in-situ, the solar wind and interplanetary magnetic fields did not generally penetrate the ionospheric obstacle. The field lines drape around and slip over the ionospheric obstacle, frozen in the largely deflected solar wind. There is a collisionless bow shock that heats and deflects the solar wind, followed by a region where the solar wind is compressed and deflected around the ionospheric obstacle. The interplanetary magnetic fields pile up near the planet. The inner portion of this pile up region is known as the magnetic barrier or the magnetic pile-up region. The magnetic barrier interfaces with the main ionosphere at the ionopause current layer that forms between them. A comet-like tail of draped interplanetary fields is found in the solar wind wake downstream of the planet. This feature is called an induced magnetotail because it does not consist of fields of planetary origin like Earth's magnetotail. Zhang et al. (2007) refers to the regions near Venus and its wake in which magnetic pressure dominates the other pressure contributions, which includes both the magnetic barrier and the magnetotail, as the induced magnetosphere.

Proposed mechanisms for solar wind removal of O^+ ions include "ionospheric ion outflow" possibly connected to polarization electric fields (e.g., Barabash et al., 2007a) or "bulk ionospheric escape" related to macroscopic or fluid-like instabilities at the ionopause (e.g., Terada et al., 2002). However, many features of ion escape seen in PVO have been reproduced in models solely based on the pick-up ion process (e.g.Luhmann 2006, 2007). The pick-up process is a result of the action of

the solar wind convection electric field, $E = -V_B \times B$, where V_B is the bulk velocity of the solar wind plasma and B is the frozen in interplanetary magnetic field. This electric field will be greatest when the velocity and magnetic field are perpendicular, and will go to zero as V_B and B become parallel. When there is just a small angle between V_B and B there will be a small electric field, and thus a small amount of acceleration, which can produce low energy ions. According to Luhmann et al.(2006), the population of ions that is ultimately picked up may be brought into the convection electric field acceleration region by other forces such as those from pressure gradients, or they may be produced by the ionization of neutrals that were already in the region where the electric field can be effective. Pickup should work, unimpeded, on ions located everywhere above the exobase.

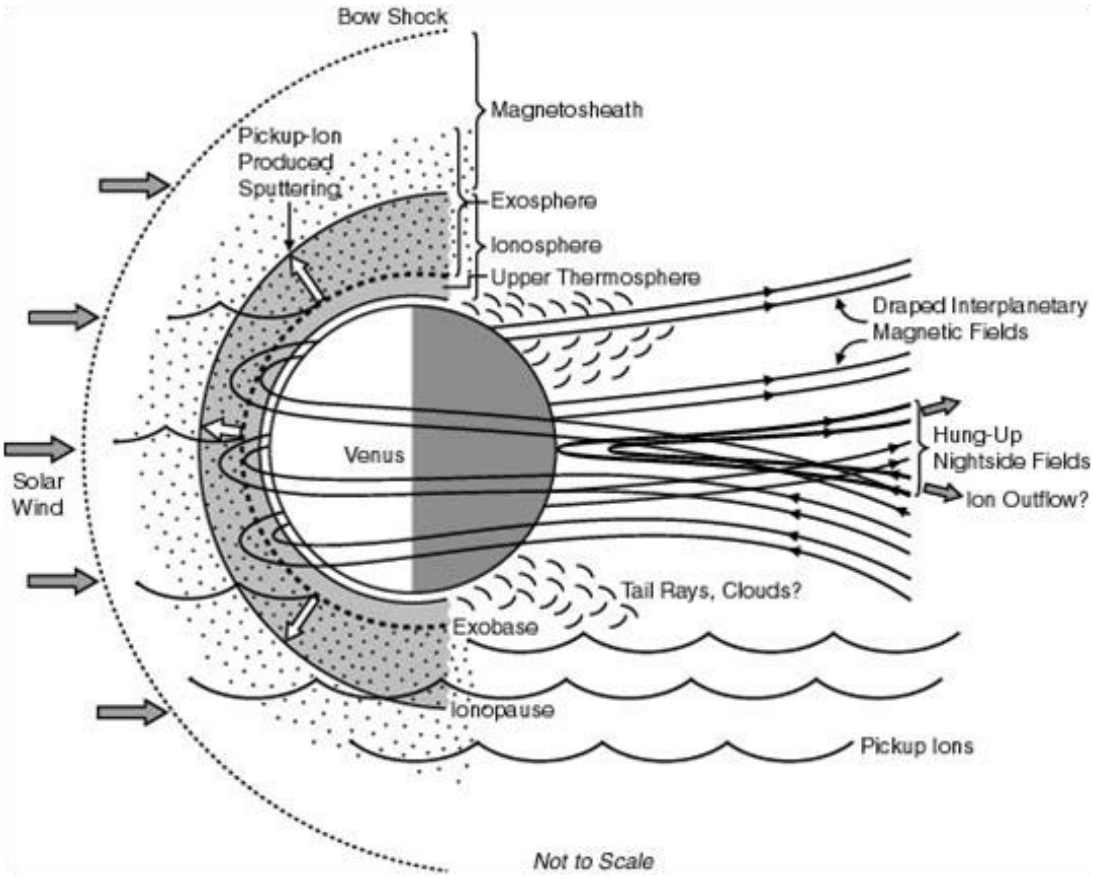

Figure 3.1: The solar wind interaction with Venus and related atmospheric escape processes. (Russell et al., 2007).

Pick-up ions will be lost mainly when they are produced on the side of the planet where the orientation of the convection electric field causes them to gyrate away from the planet. Pickup ions produced on the opposite hemisphere are more likely to impact the exobase (Wallis et al., 1972), because the planet radius (6052 km) is comparable to the O^+ gyroradius. The oxygen ion gyroradius would be 9,100 km for average solar wind conditions (velocity of 400 km and an Interplanetary Magnetic Field (IMF) of 7 nT). Therefore, one would expect to see an asymmetry in the pick-up ion population when it is organized by the convection electric field, as shown by numerical simulations of Fang et al. (2010). It has also been suggested that the pickup ions that impact the exobase may sputter or knock out additional atmospheric particles (Luhmann and Kozyra, 1991), but the contribution to atmospheric losses of this process will not be considered here.

The amount of ions that reimpact the atmosphere depends on the gyroradius of the ions, which in turn depends on the velocity and magnetic field of the solar wind. The magnetic field can be greatly enhanced during solar wind disturbances called Interplanetary Coronal Mass Ejections (ICMEs). The velocity of the events can either be slower or faster than the background solar wind.

ICMEs are the solar wind (Interplanetary) signatures of large ejections of plasma and twisted magnetic field from the sun called Coronal Mass Ejections (CMEs). The effect of ICMEs on lower energy ions at Venus has been investigated previously. Luhmann et al. (2007) used ion mode data from the PVO Neutral Mass Spectrometer, which is sensitive to >36 eV and found that three ICME passages were associated with an O^+ flux increase by a factor of 100 (out of five identified ICMEs). Luhmann et al (2008) looked at four case studies of planetary ions observed by Venus Express during ICMEs passing VEX. In three of the cases the planetary ions were either unobservable or below the limit of detectability. In the fourth case the ions were enhanced about 10 times over the typical undisturbed solar wind cases where pickup O^+ was observed. These results indicated that ICMEs or disturbed solar wind conditions may significantly increase the rate of pickup ion escape (also suggested for one VEX case by Futaana et al. (2008)). Our present study adds to these results by analyzing more data with a broader survey of pick-up O^+ features during ICMEs at Venus using data from the Venus Express Spacecraft.

3.3 Venus Express

Venus Express arrived at Venus in April, 2006 and started operations on July 4, 2006. The science mission is planned to last until the end of 2012. It has a 24 hour elliptical polar orbit with an apoapsis of 66,000 km and a periapsis of 250 km. To study the interaction of the solar wind with Venus, the spacecraft has a suite of plasma instruments called ASPERA-4 (Analyzer of Space Plasmas and Energetic Atoms) and a magnetometer. ASPERA-4 includes an electron spectrometer, two energetic neutral atom (ENA) sensors, and the ion mass analyzer (IMA) which was used in this study. The instrument design is based on ASPERA-3 on MEX (Barabash et al., 2006). IMA makes measurements between 10 eV and 30 keV for the main ion components H+, He++, He+, O+, and the group of molecular ions 20–80 amu/q. The IMA instantaneous field of view is 4.6° × 360°, but electrostatic sweeping performs elevation (±45°) coverage. ASPERA pointing generally includes the direction of the sun as part of its sampling sequence.

The IMA sweeps through the energy range over 96 steps, with sampling time for each energy step is 125 ms. The "mass image" of 16 azimuthal sectors × 32 rings (mass) is read-out once per sampling time. After each complete energy sweep the instrument changes the elevation angle of the field of view, which is broken into 16 sections. The total 3D sweep (32 rings (mass) × 16 azimuthal sectors × 96 energy steps × 16 elevation angles) takes 192 seconds. More details of the ASPERA-4 instrument are given in (Barabash et al., 2007b).

The ion mass spectrometer data can be plotted in energy time spectrograms, such as in Figure 3.2. These plots show the integrated ion counts over a specified mass range as a function of time and energy. This particular spectrogram was made over masses of 12-60 amu. The detections you see on the left are background solar wind. Then, the energy range of the detections broadens. This is due to passing through the bow shock near the planet. Gaps in detections of ions occur in the energy-time spectrograms when the instrument is looking away from the sun, because both the solar wind and planetary ions flow in the anti-solar direction.

An example of pickup ions seen in an energy-time spectrogram is shown circled Figure 3.2. These features have been referred to as "ion beams" (e.g. Carlsson et al., 2006). When the spacecraft intersects ions accelerating away from the planet it detects discrete ion features at sequences of increasing energies along the spacecraft

orbit. Similar features have also been found around Mars by Phobos-2 and Mars Express (MEX) (Carlsson et al., 2006; Dubinin et al. 2006). Carlsson et al (2006) showed the composition of the pickup ion beams, at Mars, was primarily O^+ and O_2^+.

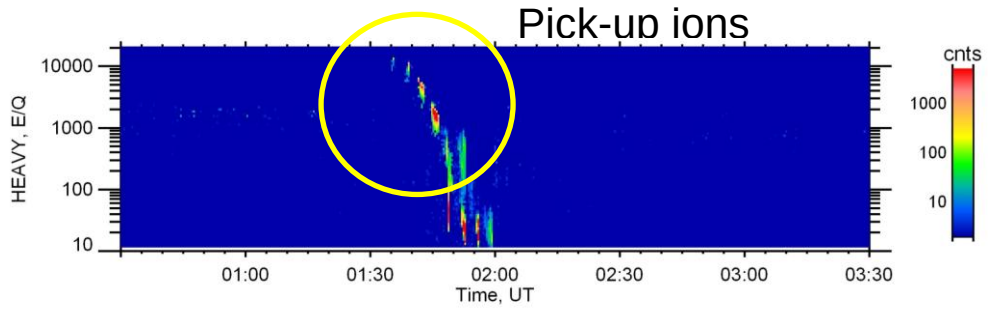

Figure 3.2: Example VEX energy-time spectrogram for high mass ions showing pick-up ion ‘‘beam’’ detections circled in yellow.

The magnetometer is a dual triaxial fluxgate magnetometer where one triad is used to correct the measurements for the spacecraft-generated magnetic fields. (Zhang et al., 2006). It has a large dynamic range between +- 32.8 and +- 8388.6 nT, and sampling is at up to 128 vectors/second.

3.4 Venus Express Data Analysis

In the present analysis, IMA data were plotted in energy time spectrograms, as in Figure 3.2, for 389 orbits between 2006-05-20 and 2007-06-13. These spectrograms were then visually scanned for high energy ion beam features. Beam features were identified in 197 of the orbits. The criteria for identifying beams were that high mass ions were seen at energies above that of the solar wind background or below but with a quasi-linear increase in energy over time. These beams were then investigated to ensure that they were O^+ by plotting mass vs. energy. The example in Figure 3.3 shows ion mass and energy of ion detections with the counts integrated over a certain time interval when a beam was seen. The increased counts at higher mass can be O^+, O_2^+ or other high mass ions. However, they are most likely O^+ because it has a lower mass and is thus escapes more easily.

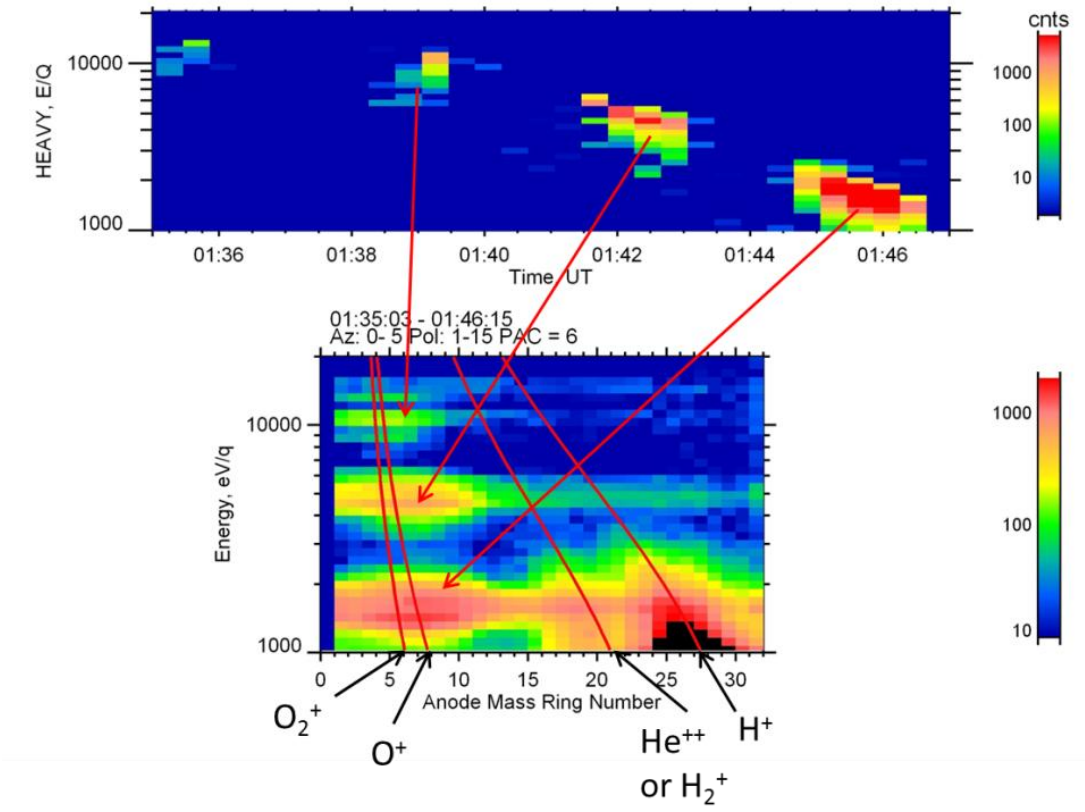

Figure 3.3: Mass ring vs energy plot used to ensure that the ion beams were composed of high mass planetary ions. The mass ring vs energy plot shows the total counts during the time interval for ions at certain instrument mass rings and energies. The red lines on the mass ring plot correspond to H^+, He^{++}, O^+, and O_2^+. The corresponding energy-time spectrogram above shows an ion beam during this time period, with red arrows pointing to where each ion detection falls on the mass ring-energy plot.

These features are also seen in the ion data at Mars, and are likely caused by a similar acceleration mechanism, therefore studies at Mars can provide insight into what may be happening at Venus and vice versa. Analyzing similar pick-up ion features at Mars, Dubinin et al. (2006) found a linear dependence of pick-up ion energy on altitude, which he attributed to acceleration in an electric field. The calculated magnitude of the required electric field was similar to that of the convection electric field, which is consistent with the assumption that these are

pick-up ions. Dubinin et al. (2006) also observed that one of the beams had decreasing energy with altitude, which was also consistent with acceleration in the convection electric field. However, in this case the ion started in the hemisphere in which the electric field was directed toward the planet. Dubinin et al (2006) also noticed that beams in one of the orbits ions gained energy more rapidly with altitude than for other orbit than the rest which he thought was due to an enhanced solar wind period, we confirmed this using MGS data.

For our study, looking at the ion beams at Venus we were able to use magnetometer data to determine when the solar wind was disturbed for all of our ion beams. Example magnetometer data from September 10-12, 2006 is shown in Figure 3.4, which shows higher magnetic field near Venus periapsis, because of the pile-up of the interplanetary magnetic field lines around the planet and what the undisturbed IMF looks like. This also shows what an ICME looks like. The data were visually scanned for these standard ICME signatures, including a leading shock jump and compressed solar wind followed by larger than average 'ejecta' magnetic field that is smooth and rotating (e.g. Luhmann et al., 2008). Most of the ICMEs were around 1-2 days in duration. In addition, IMA moment data, obtained by integrating over all angles and energies, show high densities and temperatures in the post-shock sheath due to compression and shock heating. The velocity usually declines during passage of the ICME. The temperature can be abnormally low after the sheath. ICMEs are identified according to the characteristics from Jian et al. (2006) and Jian et al. (2008). The dates of the identified ICMEs are shown in Table 3.1.

3.5 Results

The energies of the detected ion beams are plotted in Figure 3.5 as a function of altitude, showing a quasi-linear relationship. As Dubinin et al. (2006) pointed out for the counterpart Mars observations; this behavior likely corresponds to acceleration of the planetary ions due to the solar wind convection electric field. Dubinin et al (2006) stated that the highest slope sequence of beam detections in their Mars cases were likely due to enhanced ion energization from the passage of a solar wind disturbance and our results confirm this assertion. In Figure 3.5, the ICME cases are enclosed in diamonds. The ICME cases show higher slopes, meaning that the ions gain energy faster as the altitude increases. This is not surprising because the magnetic field in ICMEs is higher than under normal solar

wind conditions, which results in a larger convection electric field. Assuming that the solar wind velocity is the same between the two cases the ions would reach their maximum pickup energy ($2V_B$) at a smaller radius, and thus lower altitude.

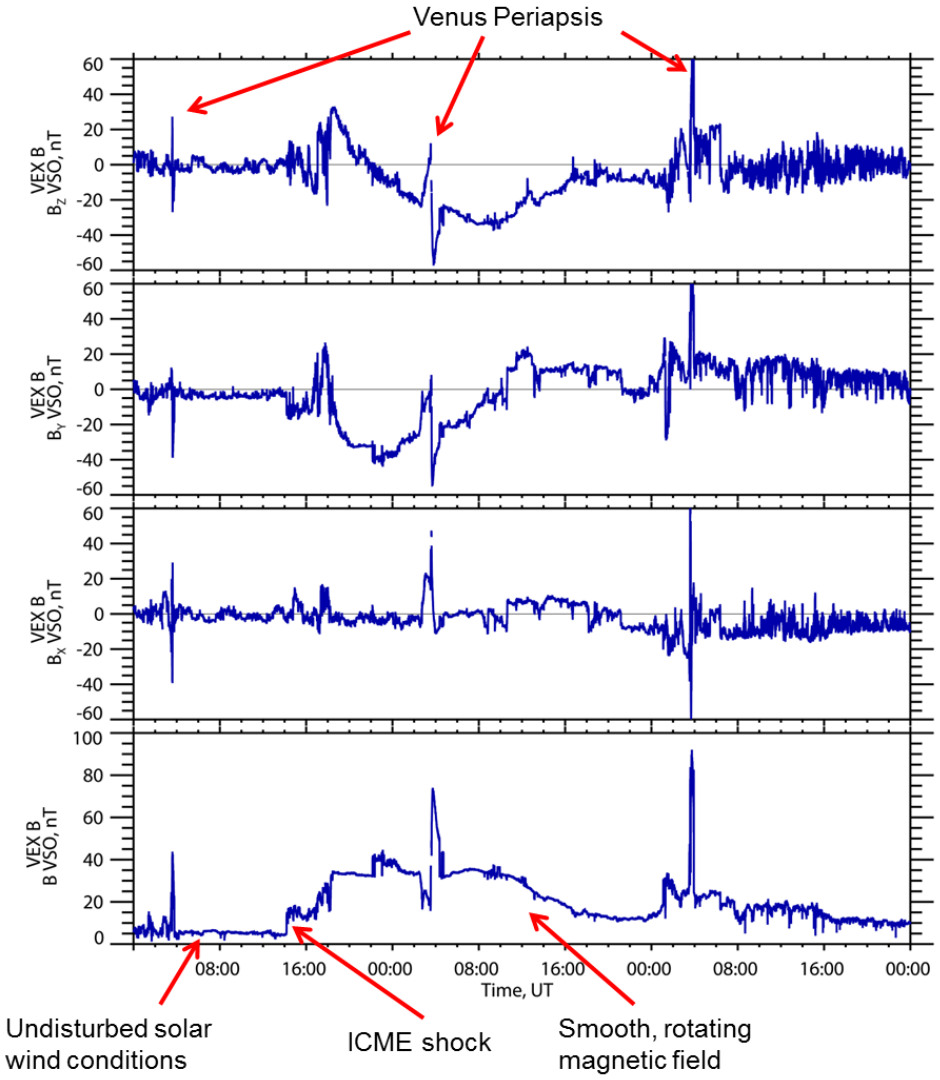

Figure 3.4: Example ICME in VEX magnetometer, September 10–12, 2006. The periapsis pass near Venus causes a higher magnetic field because of the pile-up of field lines around the planet. The undisturbed solar wind, the ICME shock and the smoothly rotating field are identified.

Start Date/Time	Stop Date/Time
2006-06-19 / 12:00	2006-06-21 / 5:00
2006-07-04 / 12:00	2006-07-06 / 1:30
2006-07-16 / 22:00	2006-07-19 / 18:00
2006-08-08 / 11:00	2006-08-09 / 22:00
2006-08-14 / 21:00	2006-08-15 / 23:00
2006-08-28 / 22:00	2006-09-01 / 8:00
2006-09-06 / 11:00	2006-09-08 / 4:00
2006-09-10 / 14:00	2006-09-12 / 16:00
2006-11-23 / 8:00	2006-11-25 / 2:00
2006-12-06 / 16:00	2006-12-09 / 04:00
2006-12-19 / 12:00	2006-12-21 / 20:00
2006-12-22 / 20:00	2006-12-24 / 12:00
2007-01-18 / 20:00	2006-01-19 / 16:00
2007-01-26 / 22:00	2007-01-28 / 20:00
2007-02-13 / 12:00	2007-02-15 / 2:00
2007-05-18 / 12:00	2007-05-19 / 20:00
2007-05-24 / 20:00	2007-05-26 / 2:00

Table 3.1: ICMEs identified during this study (June 2006–July 2007).

We examined the count rates for each event integrated over the detection interval in the disturbed and the non-disturbed cases. Since we are interested in the relative differences between disturbed and non-disturbed cases, the absolute magnitude of flux in physical units was not necessary to plot. As shown in Figure 3.5, the count rate does not clearly differ between the ICME cases and the others. The main organization of the count rate appears to be by altitude of the detections.

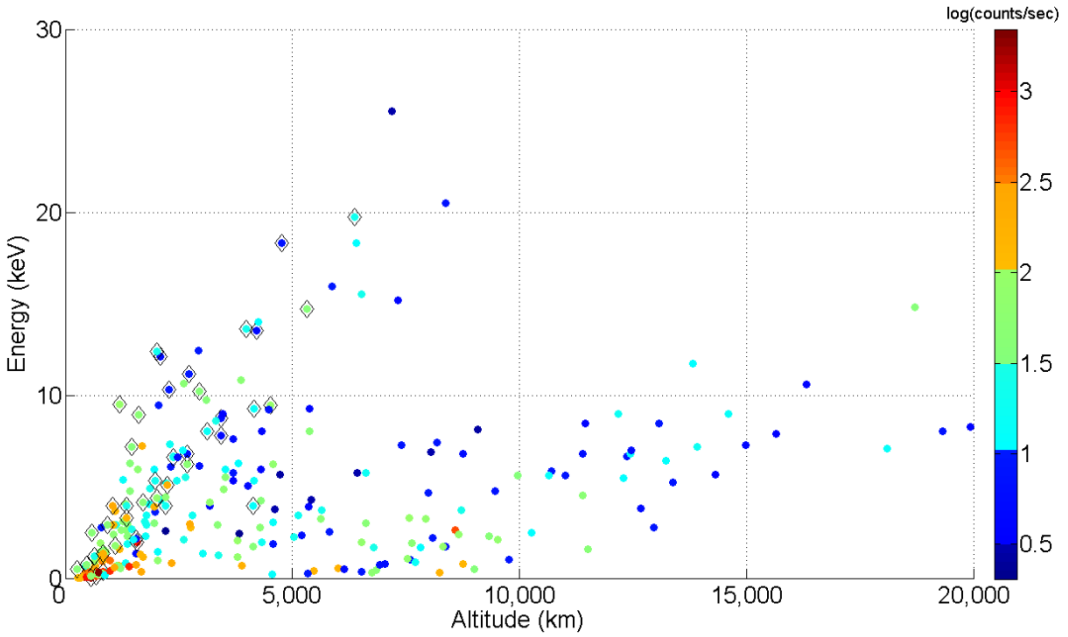

Figure 3.5: Pick-up ion detections plotted with color corresponding to log(counts/sec). ICME cases have diamonds around them. The colors are not significantly different for ICME cases, which means there is no clear correlation between count rate and ICMEs.

The orbital locations of each of the beam detections are shown in Figure 3.6. The x-axis points toward the sun, the y-axis is along the planets orbit in the opposite direction to planetary motion and the z-axis points northward to complete the right handed set. In general, the shape of the orbit plots is due to the orbital sampling. The lack of detections in the $+Z_{VSO}$ hemisphere is due to the orbital sampling. The energy coded plots show that the ions are gaining energy as they move away from Venus. The count rate plots show that the highest count rates are close to the planet. Some of these ions close to the planet may still reimpact the atmosphere so the count rates measurements aren't necessarily measuring the escape flux.

Previous analysis by Luhmann et al. (2006) on PVO data and Barabash et al. (2007a) on Venus Express data has shown that high energy (> 4 keV) planetary ions are organized by the convection electric field, consistent with a pick-up ion interpretation. This convection electric field control is established by rotating the orbital locations of the ion detections according to where the convection electric

field was pointing during the detection. This rotated frame is called the VSE coordinate system in which +X is toward the sun, and the convection electric field ($-V_B$ x B) in the + Z direction. The orientation of the IMF was determined from the magnetic field sampled closest to the beam detection outside of the bow shock. Cases where the IMF changed by>40 degrees, were not considered, because the IMF measured outside the bow shock may not be reliable during the times that the beams were detected if it was rapidly changing. Figure 3.7 shows the asymmetry expected for pick-up ions, and is consistent with the earlier results (e.g. Fang et al, 2010).

3.6 Discussion and Conclusions

This analysis showed that, for the period analyzed, ICMEs clearly influence the energization of pick-up ion beams at Venus, their effects on the total escape rate is not clear. This may be due to the strength of the ICMEs encountered during this study. The period of the VEX measurements in relation to the solar activity (sunspot) cycle is shown in Figure 8, while the dates of the identified ICMEs are shown in Table 1. All of the ICMEs for which the solar source has been identified have been slow (~250 km/s), as is typical for events occurring in the declining and minimum phase of the solar cycle (Figure 3.8). For comparison, large events during solar maximum which can range from 800 km/s up to ~2500 km/s (Cane and Richardson, 2003).

A possible cause for the ICME events that did not result in larger pickup ion fluxes may be that the observed particles for the ICMEs and the undisturbed solar wind conditions came from different source regions. Also, an important parameter for evaluating the flux dependence, for total ion escape rate, may be the ion gyroradius which is proportional to V_B/B. When the magnetic field is higher the gyroradius is smaller, so more ions may reimpact the atmosphere and not escape. However, when the velocity is higher the opposite is true. Large values of V_B are necessary for enhancing the ion gyroradius and thus the fraction of total pickup ion escape. An increased solar wind velocity creates a larger gyroradius so more ions may be able to be picked up without reimpacting the atmosphere. We do not yet have a good sample of major solar events in the VEX observations.

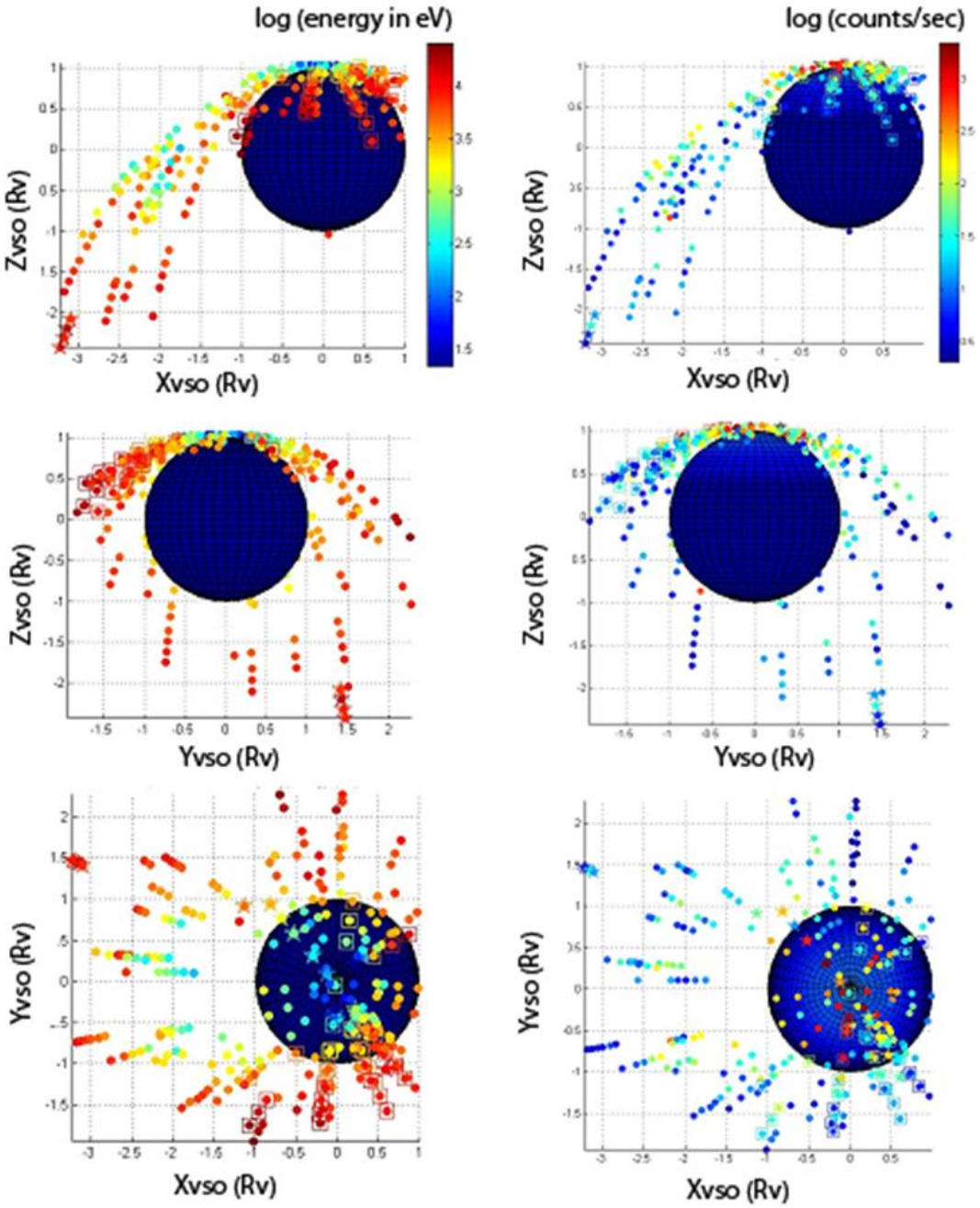

Figure 3.6: (left) VEX VSO orbit plots color coded according to log(energy), (right) VEX VSO orbit plots color coded according to log(counts/sec) showing ICME cases in diamonds. Going from top to bottom the orbital views are from the side of the planet(X–Z plane), from the sun (Y–Z plane) and from the top (X–Y plane).

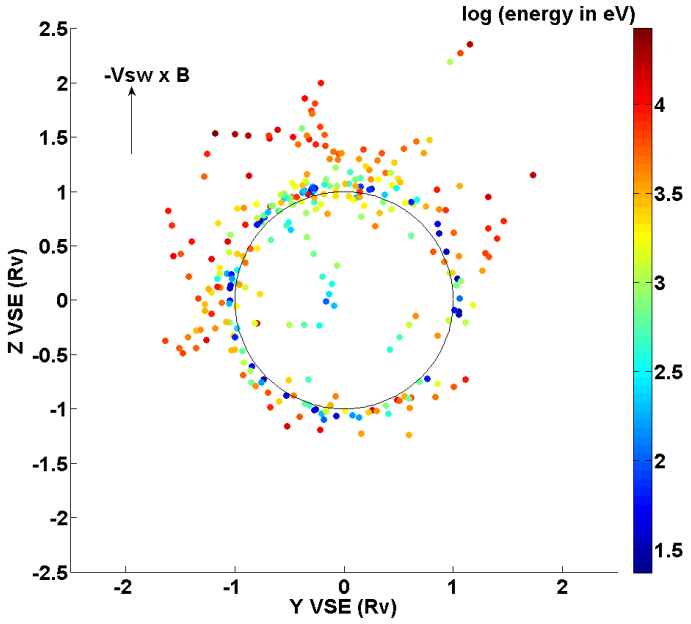

Figure 3.7: Beam detections in VSE frame (where +Z is in the direction of the $-V_B$ X B convection electric field, +X is toward the sun and +Y completes the right hand frame).

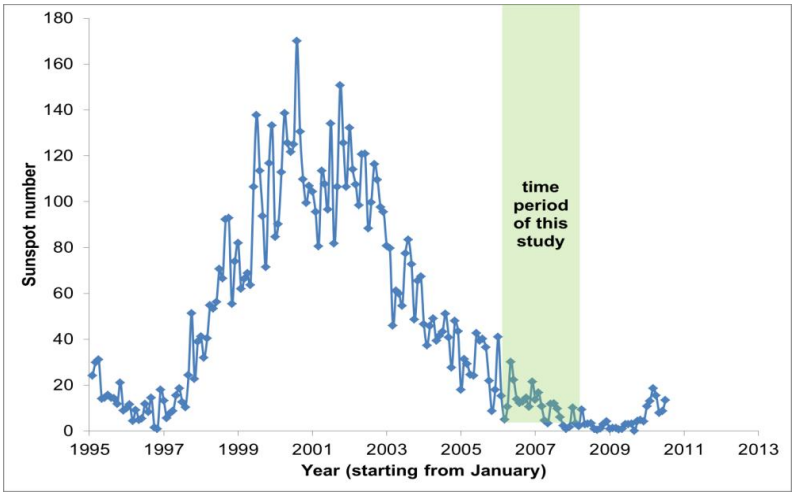

Figure 3.8: Sunspot number graph with the time period of this study shaded in green (from NOAA/SEC Boulder, Colorado). The VEX observations available so far occurred during the declining-to-minimum phase of solar cycle 23.

As mentioned in the introduction, Venus also acts as a study test bed for Mars, because Mars also does not have a significant intrinsic magnetic field. Mars is smaller, and thus has a lower escape velocity of ~5 km/s which allows photochemical processes to make a significant contribution to oxygen escape (Nagy et al., 1981), which is not as important at Venus. Also, Mars has remnant crustal magnetic fields that modify its interaction with the solar wind (Fang et al, 2010). Understanding the simpler case at Venus will help us interpret the pieces of the puzzle at Mars. As a taste of the possible future comparisons we show comparable beam detections at Mars. Figure 3.9 shows similar beam features that were seen with Mars Express data plotted in energy vs altitude and color coded for log(counts/sec). Disturbed solar wind conditions are not easily identified because MEX does not have a magnetometer.

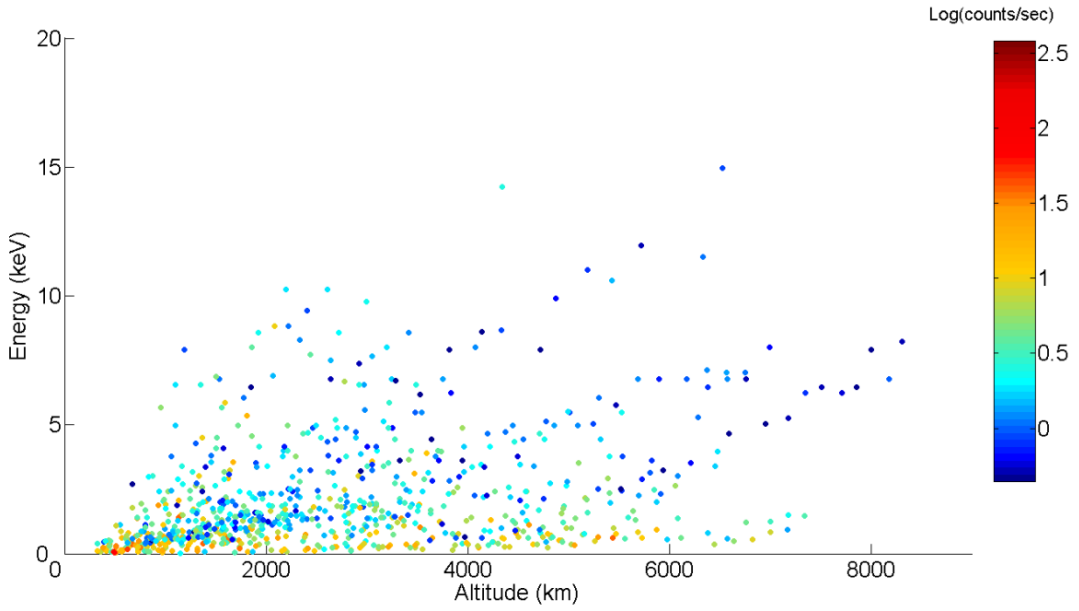

Figure 3.9: Mars ion analysis. Each point corresponds to a pick-up oxygen ‘‘beam’’ detection by the Mars Express spacecraft plotted at the energy of the detection and the altitude that the spacecraft sampled it at. This plot shows that at Mars there is linear acceleration away from the planet due to the convection electric field. The color code is log(counts/sec).

The main conclusion of this study is that ICMEs affect pick-up ions, but whether they change atmospheric escape rates as suggested by the earlier PVO based study

is still to be determined. This will influence how we think about early Venus and early Mars, because the early active sun possibly produced more ICMEs as well as higher EUV (Lammer et al, 2003). Further characterization of the escape rate of oxygen with modeling and data analysis of ICMEs during the upcoming solar maximum will help us answer this question. In addition, a new mission to Mars called MAVEN will investigate planetary pick-up ion escape further and will include a solar wind plasma analyzer and a magnetometer. (Jakosky et al., 2008)

Chapter 4

Comparisons of Venus Express Measurements with an MHD Model of O^+ ion flows: Implications for Atmosphere Escape Measurements

Abstract

Low energy (< 100 eV) oxygen ions flowing into the Venusian wake have been detected by the Venus Express Ion Mass Analyzer, but the spacecraft potential and relative velocity complicate the interpretation of these ions. We use a magnetohydrodynamic model to illustrate how Venus Express ion measurements can be affected by these complications. We simulate Venus Express energy-time spectrograms with the model by including the spacecraft relative velocity and potential. Our results illustrate that the shape of the simulated spectrograms depends on orbit geometry and interplanetary magnetic field direction. Our results facilitate better orbit-to-orbit comparisons of Venus Express ion data than can be done with the current ion data. We also address the question of whether the Venus Express orbit biases statistics of total oxygen escape. We show the global picture of the wake in the model, and calculate the oxygen ion escape rate that would be inferred. This is based on averaging the oxygen ion flux measured along the Venus Express 2006-2007 orbits, which were used for published Venus Express escape estimates. In the model, a region on the nightside contains ions turning back toward the planet out to 3000 km in the wake. Despite this flow geometry, the escape rate estimates calculated by averaging along the Venus Express orbit are still within 25% of the actual total escape from the model. We then look at the escape in the model calculated along the 2009 and 2010 Venus Express orbits (when the periapsis was lowered), and find that the estimated escape rate is still within ~20% of the actual escape from the model. Therefore, return ion flows like those in the MHD model wake would not significantly affect Venus Express escape rate estimates.

4.1 Introduction

Venus does not have an intrinsic magnetic field, thus the solar wind interacts directly with the planet's upper atmosphere (e.g. Luhmann and Bauer, 1992). The solar wind carries with it the magnetic field of the sun and sets up electric fields that can accelerate ionized atmospheric particles to velocities above that needed to escape from the gravitational field of the planet (e.g., Luhmann, 1986; Russell et al., 2006). Instruments on Venera, Pioneer Venus Orbiter (PVO), and Venus Express (VEX) detected ionized hydrogen and oxygen at distances and with energies high enough to indicate that they were escaping (e.g., Vaisberg et al., 1995; Brace et al., 1995; Barabash et al., 2007a; Fedorov et al., 2011). Understanding escape processes, quantifying the current escape rates of H^+ and O^+, and determining how escape depends on external conditions are crucial to ascertain how much water may have once been on Venus. In order to estimate the escape rate using in-situ measurements from spacecraft, ion measurements made at one location and time have to be statistically assembled into a global picture. This step can be facilitated by using models to provide the context of single orbit measurements. In this paper, we use a magnetohydrodynamic (MHD) model as a tool to interpret VEX ion measurements within the ionosphere and wake. MHD models cannot represent high-energy pick-up ion beams, such as those presented in McEnulty et al. (2010), but Venus Express investigators claim that the majority of escape is happening at low energies and within the regions that we explore with the model in this paper (e.g. Barabash et al., 2007a; Fedorov et al., 2011; Lundin et al., 2011).

Instruments on PVO also measured ions flowing within the ionosphere and into the wake (e.g., Brace et al., 1995). The Retarding Potential Analyzer (RPA) measured ionospheric flows across the terminator between 200 and 1000 km altitude at velocities between 2-5 km/sec, with transient velocities up to 8 km/sec (Knudsen et al., 1981; Miller and Whitten 1991). Above the ionopause - the boundary between the ionosphere and solar wind – the Ion Mass Spectrometer (IMS) and the Neutral Mass Spectrometer (NMS) detected ions with velocity above what would be needed to escape (Grebowsky et al., 1993; Kasprzak et al., 1991). Brace et al. (1995) suggested that the RPA flows were higher than needed to maintain the nightside ionosphere with the implication that some of it may have also escaped. Indeed the Orbiter Neutral Mass Spectrometer (ONMS) detected O^+ ions with >36 eV energies and antisunward velocities in the low altitude wake (Kasprzak et al., 1991; Luhmann et al., 2007) even though details of the ion population from this instrument are limited. Measurements made by the Ion Mass Analyzer (IMA) on VEX are within the energy range needed to investigate the transition to escape velocity and better understand the processes controlling escape in these regions. However, the spacecraft's relative velocity and potential make these measurements

difficult to interpret. In order to shed light on these complications, we use an MHD model to illustrate how the spacecraft relative velocity and potential can affect the energy of ions measured within VEX orbits.

Models are also useful for exploring the global picture and how the orbital bias of measurements can affect the amount of escape inferred. The latest estimate of ion escape using VEX ion statistics by Fedorov et al. (2011) motivates our investigation of the orbital bias; in particular, measurements as close to the center of the planet as 1.2 Venus Radii ($R_{v)}$ were used in the statistics. Fedorov et al. (2011) said that past 1.2 R_v in the wake the flow is laminar and the total outflow from the planet is conserved and does not depend on the distance. However, this laminar conserved flow is called into question by the results of Lundin et al. (2011) who presented ion statistics within the wake and said that oxygen ions are gravitationally bound out to 6000 km altitude (2 R_v) in the wake. In this paper, we use an MHD model to interpret VEX IMA measurements. Section 2 describes some details of the MHD model used here and its input conditions and section 3 discusses the VEX orbit and IMA sampling. Case studies and applications to escape measurements are respectively presented in sections 4 and 5 to illustrate the interpretive value of the model and its implications.

4.2 Description of the MHD model

In order to create a general picture of the solar wind interaction with the Venus ionosphere, and in particular the outflowing ions measured by VEX, we use an MHD model. This model is similar to those described for Mars (Ma et al., 2004a, 2007) and Titan (Ma et al., 2004b). The model has a spherical grid with an inner boundary at 100 km altitude and a graduated radial grid resolution of 5 km (at the lower boundary, in the ionosphere) to 600 km. It is single-fluid, multi-species MHD model utilizing the BATS-R-US (Block Adaptive Tree Solar Wind Roe-Type Upwind Scheme) code described in Powell et al. (1999). A self-consistent ionosphere is included with four major ion species (H^+, O^+, O_2^+ and CO_2^+). Atmospheric neutral profiles and ionization rates are based on Fox et al. (2001). Solar minimum EUV conditions were assumed, which are appropriate for most of the VEX observations up to late 2009. The model also includes self-consistent mass loading and ion-neutral collision effects. Many details about the model development and numerical treatments of the Venus ionospheric obstacle can be found in the paper by Ma et al (2012).

The external solar wind description used in the model version for solar minimum is based on Pioneer Venus Orbiter (PVO) measurements of average solar minimum

solar plasma and field conditions at Venus from Luhmann et al. (1993): solar wind density = 22/cc, solar wind velocity = 420 km/s, total magnetic field = 9.6nT, solar wind temperature = 3.0E5 K. The solar wind flow is in the -X direction, and the interplanetary magnetic field (IMF) is in the XY plane with a spiral angle, $\tan^{-1}(-B_Y/B_X)$, of 36°. The convection electric field ($E = -\mathbf{V} \times \mathbf{B}$ where **V** is the bulk velocity and **B** is the IMF vector) is in the +Z direction. This model frame of reference is similar to the VSE (Venus Solar Electric) frame, which is used to organize Venus Express data, in that Z_{VSE} is parallel to the convection electric field and X_{VSE} is antiparallel to the solar wind bulk velocity vector. Our VEX orbit data are in VSO coordinates where Xvso also points sunward, and the +Yvso axis is in the direction opposite from planetary orbital motion. For our purposes, we assume that the model coordinate system is equivalent to VSO coordinates. We also point out that because the model assumes a single fluid velocity even though it has multiple species it does not contain convection electric field related asymmetries related to ion mass except in an averaged sense. We assume this is adequate for our analysis because we are focusing on the low energy ions whose gyroradii are generally small compared to the overall solar wind interaction.

The basic model results that we use to study the O^+ flows are illustrated by the contour plots and vectors in Figures 4.1 and 4.2. These show the model O^+ and H^+ densities and velocity magnitude as contours with normalized velocity vector overlays in the terminator plane (Figure 4.1) and the noon-midnight meridian plane (Figure 4.2). The H^+ panels (Figures 4.1b and 4.2b) are dominated by the solar wind external flows in the magnetosheath and shown for context, while the O^+ represents the ionosphere contribution. The velocity vectors are the same in all plots because the model is calculated from single fluid MHD. One can see from these two model cuts that the appearance of the ion fluxes sampled along simulated VEX fly-throughs will be different depending on the VEX orbit phase with respect to the Sun and IMF direction. For example, the O^+ extends to higher altitudes in the noon-midnight plane (which intersects the nominal tail plasma sheet region) than in the terminator plane. In the terminator plan, the magnetic field draping geometry limits the altitude of the ionopause.

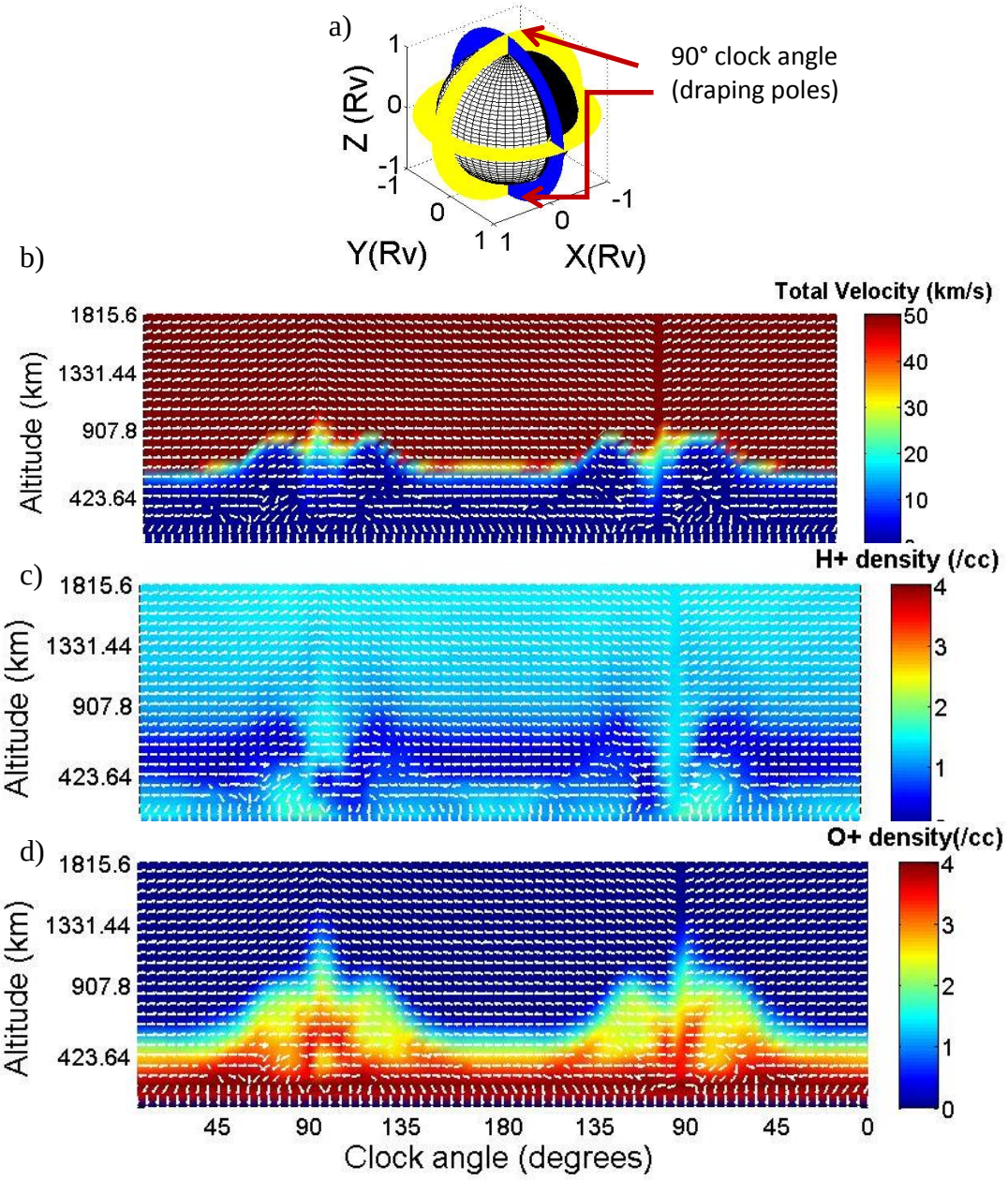

Figure 4.1: Contours of (b) total velocity, (c) H^+ density, and (d) O^+ density from the MHD model as a function of altitude and clock angle on (a) the terminator (YZ) plane colored blue. Near the draping poles (~ 90°) the O^+ density is higher, but the velocity lower at altitudes between 500 and 1000 km compared to the magnetic equators (0° and 180°).White arrows correspond to normalized flow vectors

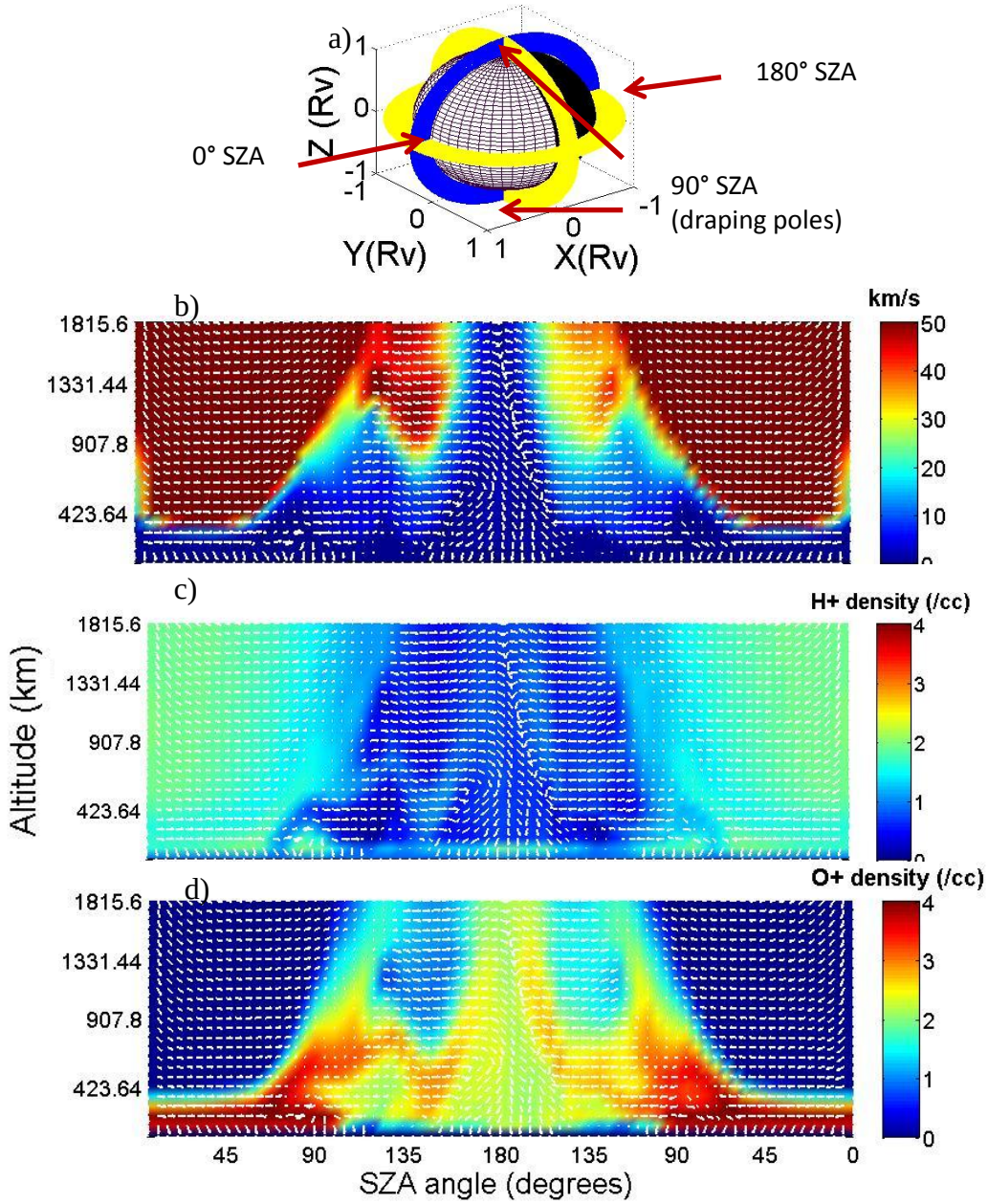

Figure 4.2: Contours of (b) total velocity, (c) H^+ density, and (d) O^+ density from the MHD model as a function of altitude and solar zenith angle on (a) the noon-midnight (XZ) plane colored blue. 180° SZA is midnight, so the middle of the plots corresponds to the wake. White arrows correspond to normalized flow vectors, which turn back toward the planet near midnight.

4.3 Details of VEX IMA, Ion Measurement Complications, and Orbit

The Venus Express in-situ Ion Mass Analyzer is part of the suite of instruments called ASPERA-4 (Analyzer of Space Plasmas and Energetic Atoms) detailed in Barabash et al. (2007b). The IMA separates ions by mass allowing investigators to distinguish between hydrogen and heavier ions, such as O^+ and O_2^+, with an energy range of 10 eV – 20 keV and energy resolution of 8% within the instantaneous field of view 4.6° × 360°. The instrument sweeps electrostatically to ±45° in elevation. The spacecraft body partially blocks this field of view, and the amount of the ion distribution that is blocked depends on the orientation of the spacecraft.

IMA measurements of ion energy are affected by the relative velocity of the spacecraft and by the spacecraft potential. These issues are particularly important to consider when analyzing data at the low end of the energy range. The spacecraft velocity at periapsis is ~10 km/s (which corresponds to a possible increase of ~10 eV to the measured ions) and the negative (mostly in the night side of Venus) spacecraft potential may upshift the ion energies by nearly the same magnitude (~5-10 eV). In order to determine the actual velocity of the measured ions, the spacecraft relative velocity must be subtracted vectorially and the measured energy shifted down by the spacecraft potential (the negative potential measured in volts shifts positive ions up in energy by that magnitude in eV). The potential is not always well characterized, making some orbits unusable for escape flux statistics. This type of correction for the spacecraft relative velocity and potential is described in detail by Fraenz et al. (2010) using a similar instrument on Mars Express.

The orbit of VEX is highly elliptical and polar with a period of 24 hours. Until August 2008, the periapsis altitude was ~300 km and was then lowered to ~185 km, and the apoapsis is ~12,000 km. IMA is operated for ~4.5 hours near periapsis, sampling the solar wind for ~1-2 hours inbound and outbound and sampling within the induced magnetosphere for 0.5-1.5 hours depending on orbit geometry. The periapsis stays near the geographical northern pole, while the orbit rotates and samples different solar zenith angles. It sometimes passes along the terminator and at other times in a noon-midnight direction. In the next section, we explore how orbit geometry and IMF direction may affect what IMA measures.

4.4 Case Studies – validating model, and investigating orbit geometry and IMF influence

VEX ion data are often plotted in energy-time (ET) spectrograms. These plots display measured ion energy as a function of time along the spacecraft orbit, color-coded by the counts measured in each energy bin (see Figure 4.4a for an example). ET spectrograms are not usually corrected for the spacecraft relative velocity or potential, which vary as a function of time within an orbit and between orbits. Therefore, it is important to understand how ion measurements are dependent on these spacecraft characteristics as well as the VEX orbit sampling geometry. We present two case studies used by Lundin et al. (2011), a terminator orbit and a midnight-noon orbit (shown in Figure 4.3) as examples to illustrate how the MHD model can approximate the observed oxygen ion energy and flux variation.

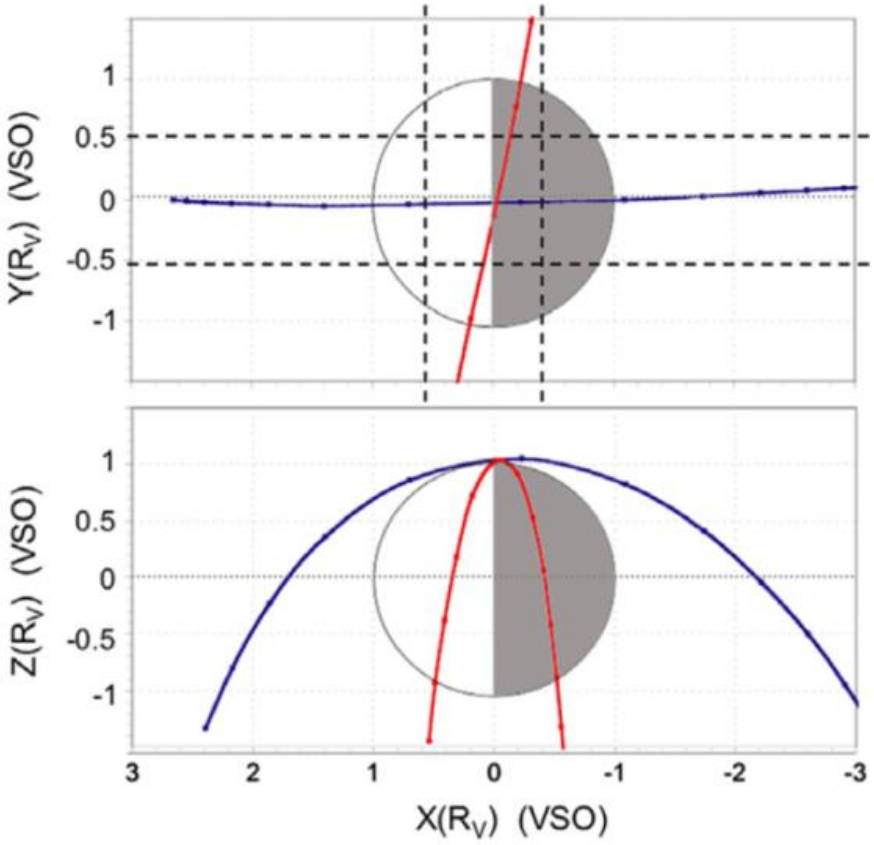

Figure 4.3: The VEX terminator orbit in red is from May 24, 2007 and the blue midnight-noon orbit is from August 24, 2006 (from Lundin et al., 2011).

4.4.1 Validating the model and investigating orbit geometry effect on VEX ion measurements

To simulate ET spectrograms by "flying through" the model, we calculate the energy that thermal or fluid ions would have if VEX was orbiting in the MHD model. We use the model density multiplied by the velocity as a counterpart of the fluxes or 'counts' registered by the IMA. This does not directly correspond to counts because of the instrument sampling and calibration factors, but can give an idea of relative differences in the counts of ions. The H^+ and O^+ velocities cannot be separated since the MHD model is single-fluid, but we assume that the total velocity would approximately correspond to the O^+ velocity in the region in the ionosphere and wake where the O^+ density dominates. The model simulated ET spectrograms do not completely capture the information in the observed ET spectrograms at each time step, because the data contains ions at different energies at each time step. While in this model each time step corresponds to one bin and therefore only one velocity/energy. The model temperature could simulate this spread of energies, but the temperature is not of concern for this study, therefore we did not include it in the simulated spectrograms. As an approximation, the model results can be compared to the measured energy value with the highest counts at each time step.

We first study an example based on the near-terminator VEX orbit (red in Figure 4.3). The VEX ion ET spectrograms for this pass are shown in Figure 4.4 (a). The O^+ ion velocity in the model for this orbit would correspond to H^+ and O^+ energies less than 1 eV between ~ - 8 and +6 minutes from periapsis in the model spectrogram Figure 4.4 (b). Comparing Figure 4.4 (b) to the actual IMA data in Figure 4.4 (a), there were O^+ ions detected by the VEX IMA in this portion of the orbit (near periapsis) that are not obtained with the model. When the model velocity is modified to include the spacecraft relative velocity and potential, the model energy is shifted up into the range measured by the IMA. The final simulated ET spectrogram with the spacecraft relative velocity and potential included (Fig.4d) is similar to the peak count energies measured by the IMA. For this orbit, the model is able to approximate the ion energy and the width of the ionosphere between the Induced Magnetosphere Boundaries (IMB). The fact that we needed to include the spacecraft relative velocity and potential illustrates that the ions measured by the IMA during this orbit, in Figure 4.4 (a), that appear to have energy above 10 eV would not have this energy when these corrections are made to the data. This is important to keep in mind when looking at uncorrected IMA data that appear to show ions slightly above the energy needed to escape.

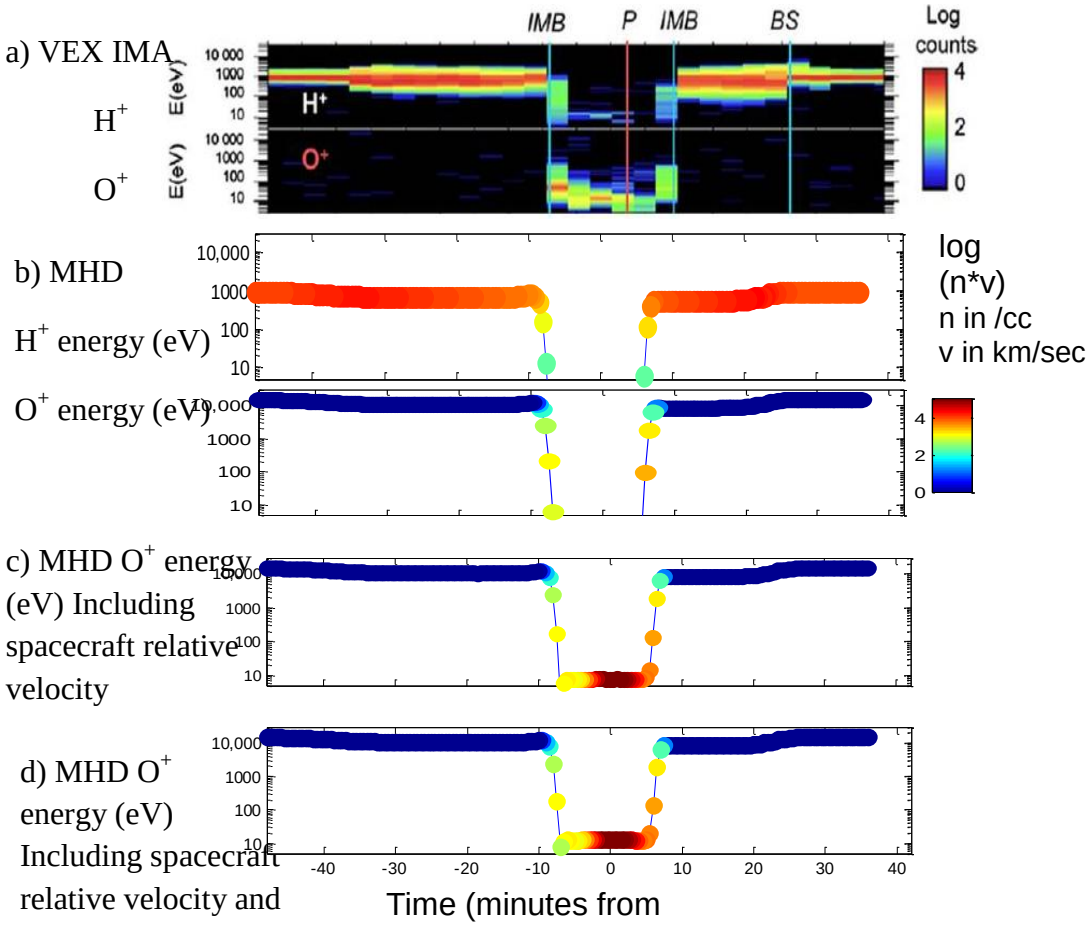

Figure 4.4: (a) VEX IMA energy-time spectrograms for H^+ and O^+ from May 24, 2007 - a terminator orbit. IMB = Induced Magnetosphere boundary, P = periapsis, BS = bow shock. (b) Simulated H^+ and O^+ spectrograms with energy calculated from the MHD single-fluid velocity, color-coded by model density*velocity. (c) Simulated O^+ spectrogram from the MHD model modifying the model velocity with the spacecraft relative velocity. (d) Simulated O^+ spectrogram from the MHD model including the spacecraft potential in addition to the spacecraft relative velocity.

In contrast to the terminator orbit where O^+ was only detected by the VEX IMA within ~ - 8 and +6 minutes from periapsis, the instrument detected O^+ for nearly 50 minutes before periapsis for the midnight-noon orbit in Figure 4.5 (a). These ion detections by the IMA included O^+ with energies between 10 eV and 1 keV near periapsis in the ionosphere and in the wake behind the planet. The MHD model is

able to reproduce the general energy versus time profile in the wake shown in Figure 4.5 (b), but there is no O^+ above 1 eV within +-5 minutes of periapsis. Similar to the terminator orbit, adding the spacecraft relative velocity and potential to the model velocity adjusts the simulated ET spectrogram (Figure 4.5d) and better represents the IMA measurements at periapsis in Figure 4.5 (a).

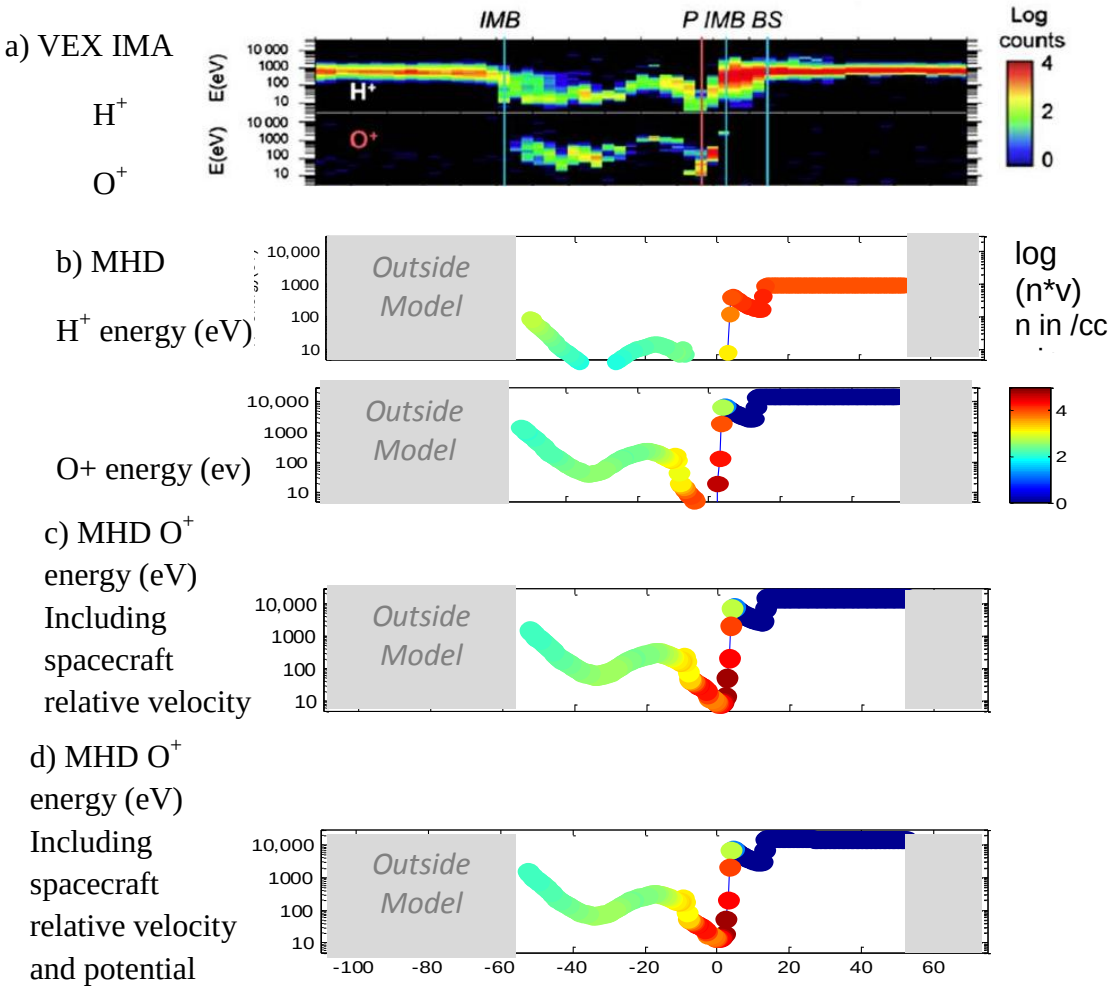

Figure 4.5: (a) VEX IMA energy-time spectrograms for H^+ and O^+ from August 24, 2006 - a midnight-noon orbit. IMB = Induced Magnetosphere boundary, P = periapsis, BS = bow shock. (b) Simulated H^+ and O^+ spectrograms with energy calculated from the MHD single-fluid velocity, color-coded by model density*velocity. (c) Simulated O^+ spectrogram from the MHD model taking the spacecraft relative velocity into account. (d) Simulated O^+ spectrogram from the

MHD model including the spacecraft potential correction in addition to the spacecraft relative velocity.

4.4.2 IMF direction effect on ion energy-time spectrograms

VEX IMA ET spectrograms have varying shapes, even in cases with similar orbit geometry. Dissimilar IMF direction is one possible explanation for the change in ET spectrogram shape when the orbit geometry is similar. In order to illustrate how the IMF direction might affect the shape of ET spectrograms, we rotated the orbits presented in section 4.1 by angles between 0° and 315° (see Figs 6a and 7a) within the YZ plane. We then created simulated spectrograms from the new positions within the model. This approximates a change in the IMF clock angle.

There were slight variations in the shape of the simulated spectrograms depending on rotation of the orbit as shown by the varying panels in Figures 4.6 (b) and 4.7 (b), which are labeled with the angle rotation of the orbit. Corresponding magnetic field from the model is plotted in Figures 4.6 (c) and 4.7 (c) to show which rotated orbits pass through the magnetic draping pole (where B_x changes sign inbound versus outbound). For the terminator orbit (Figure 4.6c) this B_x rotation appears in the magnetic field time series of the 0° orbit (not rotated, with periapsis passing through the northern draping pole) and the orbit rotated 180° (periapsis passing through the southern draping pole). The spectrograms for the terminator orbit show only modest variations in appearance for all IMF rotation angles, while the magnetic fields show considerable change.

The actual IMF vector most often has a low B_z component, which would correspond to a rotation of the orbit of 0° or 180° (since the model has the IMF in the XY plane). However, the different simulated ET spectrogram shapes show that a rotation of the IMF may change what regions (in a VSE frame) the VEX spacecraft samples, and therefore the shape of the ET spectrogram. This is helpful for investigators to keep in mind when comparing IMA data between different VEX orbits because the IMF can rotate to large inclinations (especially during solar wind disturbances). The model's ability to simulate the general shape of the VEX IMA ET spectrograms in the ionosphere and in the wake, for the individual VEX passes presented in section 4.1, provides confidence it can be applied to a more global context.

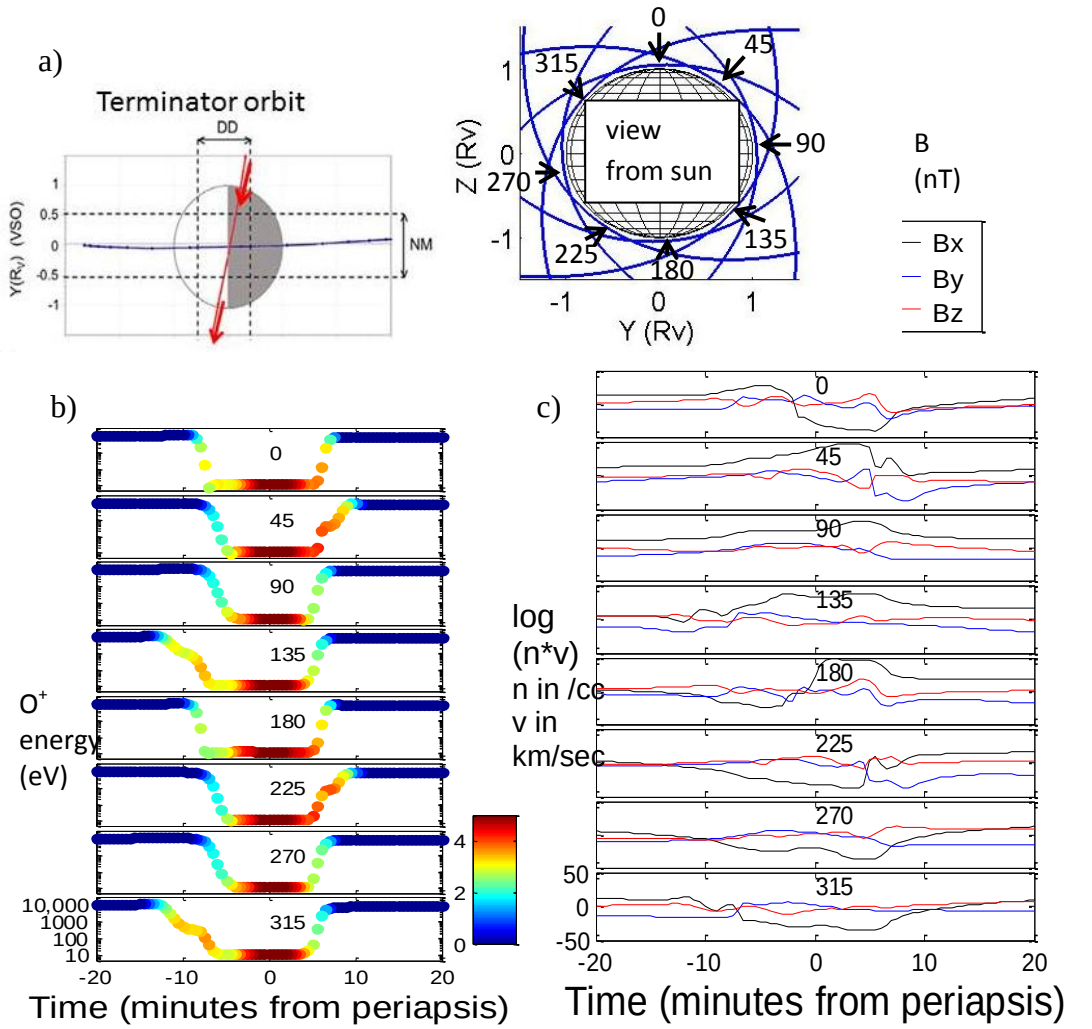

Figure 4.6: (a) XY plane view of the May 24, 2007 terminator orbit on the left and on the right YZ plane view of this orbit segment rotated by the angles labeled with black arrows pointing to the periapsis of the corresponding orbit. (b) Simulated O^+ energy-time spectrograms calculated from MHD velocity (with the spacecraft relative velocity included) for the rotated orbit segments (0-315°) as indicated. (c) Corresponding magnetic field from the model for each rotated orbit segment in which the 0° and 180° rotated orbits pass through a magnetic draping pole evident by a rotation in the B_x component near periapsis. Note that the spectrograms show only modest variations in appearance for all IMF rotation angles, while the magnetic fields show considerable change.

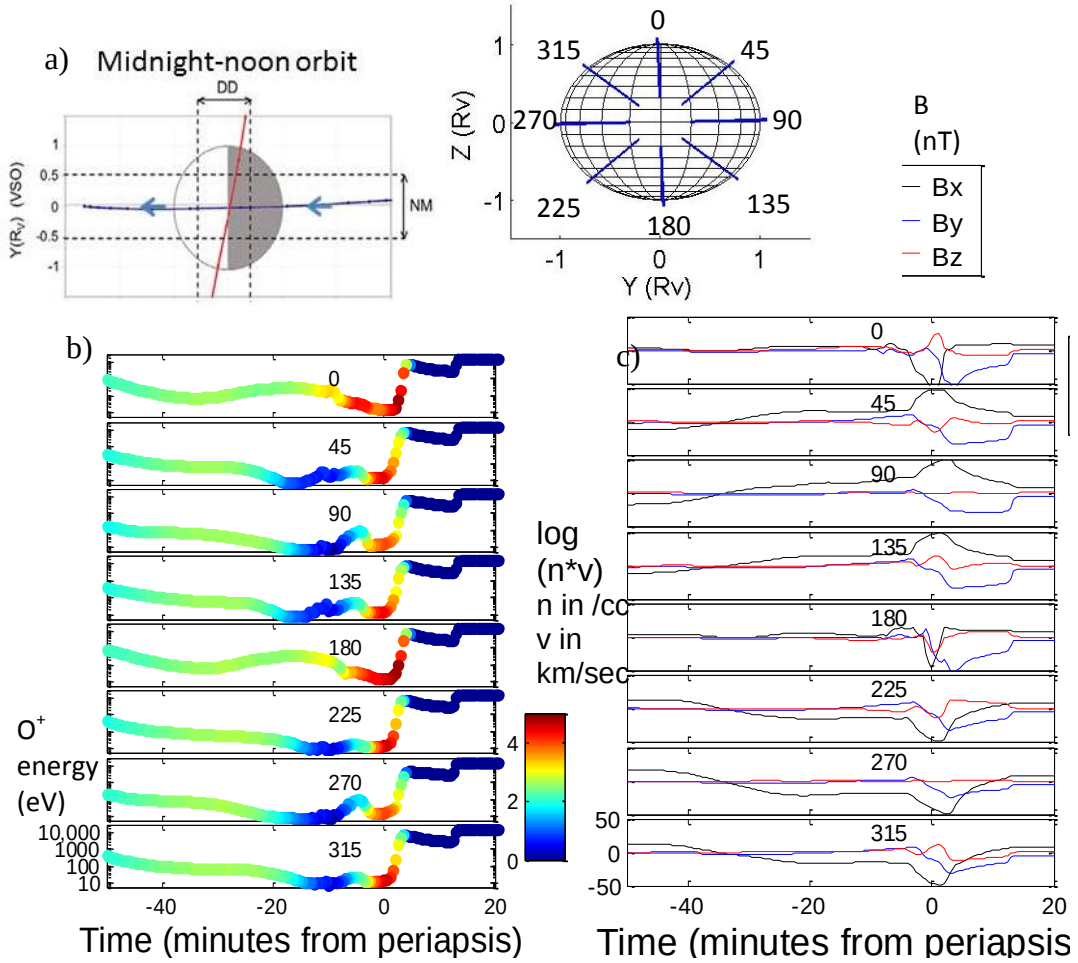

Figure 4.7: (a) XY plane view of the August 24, 2006 midnight-noon orbit on the left and on the right YZ plane view of this orbit segment rotated by different angles. (b) Simulated O^+ energy-time spectrograms calculated from MHD velocity (with the spacecraft relative velocity included) for the rotated orbit segments. (c) Corresponding magnetic field from the model for each rotated orbit segment. The 0° and 180° rotated orbits show higher flux between –20 and -5 minutes from periapsis.

4.5 MHD wake geometry, return flows, and escape rate

The global picture provided by the model in Figures 4.1 and 4.2 can help to relate single orbit case studies to statistical results such as escape rates. In this model, on the terminator plane, the total velocity is lower near the draping poles ~900 km

altitude, but the O^+ density is higher there. This is shown in the altitude versus clock angle contour plots in Figure 4.1 (b) and (d). Here the clock angle refers to the angle in the YZ plane where 90° is at the magnetic draping poles (+ and –Z), see Fig 1 (a). The H^+ density in Fig 1 (c) indicates that the O^+ density in Fig 1 (d) dominates at altitudes below ~500 km near the equator and up to altitudes of ~900 km at the draping poles. The vectors, discussed later, are normalized flow vectors in this plane, which are the same for all species in this model.

Comparisons to model behavior in a meridian plane (Figure 4.2a) bring out the significant differences in the 3D model behaviors at different locations. In the model wake, along the noon-midnight plane the high O^+ density from the ionosphere extends to higher altitudes (Figure 4.2d). Here altitude versus Solar Zenith Angle (SZA) is used - where 0° is subsolar and 180° is in the wake. Again the arrows show the geometry of ion flow along this plane. The model O^+ density dominates the H^+ in the wake (Figure 4.2c versus Figure 4.2d).

The simulated spectrograms that we presented as case studies looked different because of how they were sampling the 3D space of the model. The example terminator orbit dipped into the ionosphere down to ~300 km, but the high O^+ densities only occur from below ~400 km at the equator to ~900 km at the draping poles. Therefore, the VEX orbit would not spend much time (only ~ 10 minutes) sampling these ions in the model. The slight differences in the simulated rotated terminator orbit spectrograms were due to different sampling of the draping poles versus the magnetic equator. In contrast to the terminator orbit, the midnight-noon example VEX orbit spent ~50 minutes in the wake, where the model has O^+ ions with density ~100/cc flowing to high altitudes. These showed up in the simulated spectrograms as an extended higher density portion in the orbit. The shape of the energy time series in the model wake is due to the asymmetric flow of ions. Higher density ions flow into the wake from the draping poles gaining velocity as they move into the wake, while at the equator there is lower density O^+ flowing that does not have these high velocities. We attempted to determine if draping pole asymmetries are evident in VEX IMA data, but because the VEX orbit primarily samples the draping poles, there were not enough non-draping pole samples (e.g. from occasional high inclination IMF cases) for adequate comparison. In addition, as shown by the simulated spectrograms rotated by IMF angle in the YZ plane (Figures 4.6b and 4.7b), the asymmetry seen in the global model would not be obvious in ET spectrograms.

4.5.1 Return Ion Flows in the Model Wake

Since Lundin et al. (2011) analyzed IMA data and found oxygen ions gravitationally

Since Lundin et al. (2011) analyzed IMA data and found oxygen ions gravitationally bound at large distances, we explored return flows in the model. Sunward return ion flows are not apparent in the simulated energy-time spectrograms, because the spectrogram energy is calculated using the total velocity (i.e., the direction is not considered). Depending on the orbit and the IMF direction, the energy-time spectrogram may contain return flows. An example of VEX observations with possible return flows (from June 6, 2009) is shown in Figure 4.8 by the +X O^+ velocity from ~1:25 to 2:05. The return flows are confirmed by looking at the direction that the ion detections came from (Figure 4.10), which is a plot of the Azimuth and Polar angles where (0,0) corresponds to tailward flow. The simulated ET spectrogram from flying this VEX orbit through the model also contains return ion flow marked by the shaded blue area in Figure 4.9.

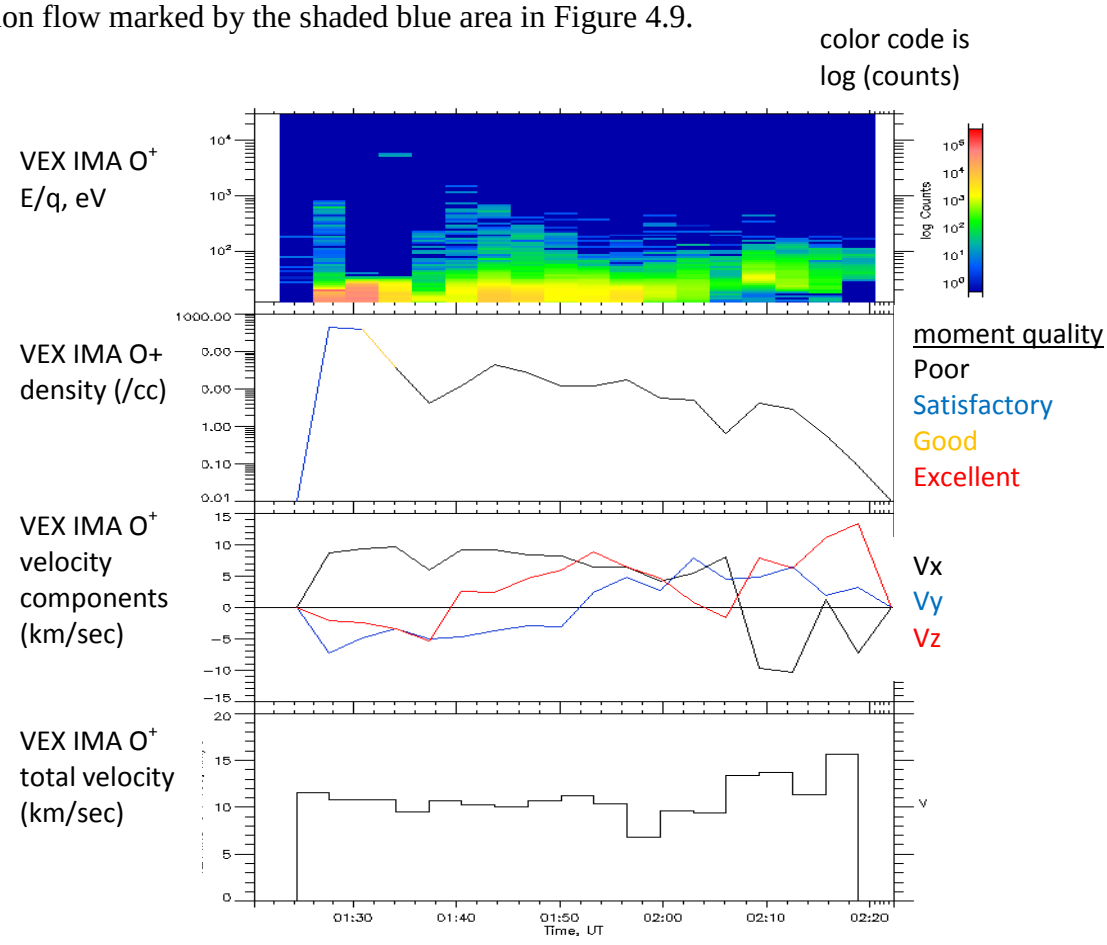

Figure 4.8: VEX energy time spectrogram from June 6, 2009 on the top, with calculated O^+ density, velocity components, and total velocity below. The color code on the VEX density denotes the quality of the moments.

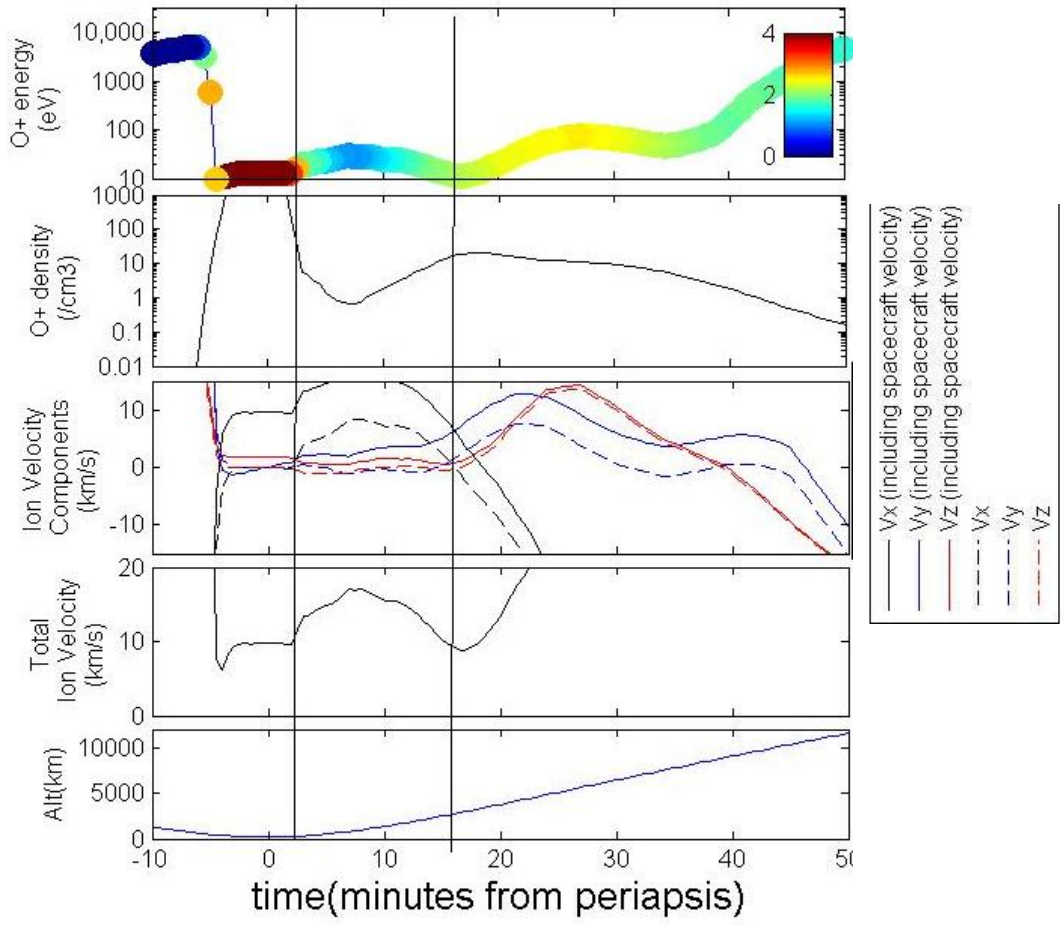

Figure 4.9: Model simulated O^+ spectrogram, O^+ density, velocity components (solid lines include the spacecraft relative velocity and dashed lines are just ion velocity) and total velocity (including spacecraft velocity). Blue shaded area on simulated time series plots bounds the ~15 minute period within the VEX orbit where return flows are sampled in the model. Both the model and the data show sunward (+X) flowing ions in the wake, but these sunward flows in the data are even further back in the wake than in the model.

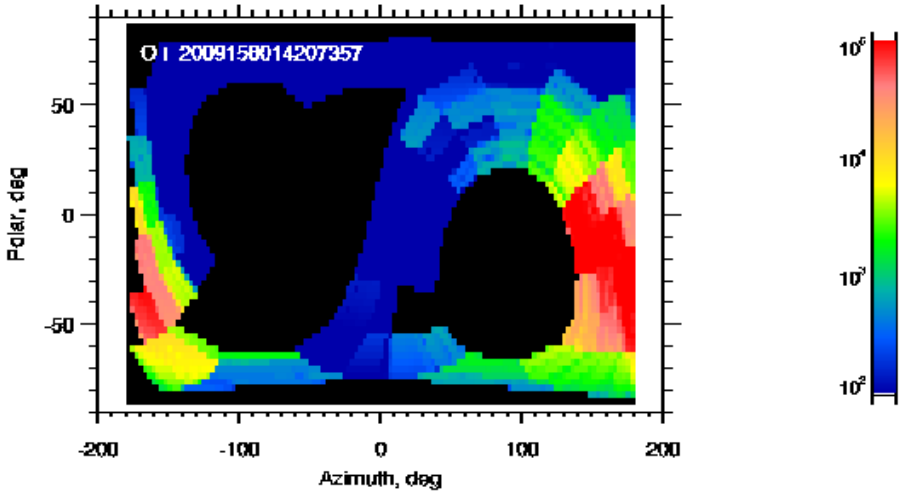

Figure 4.10: Ion detections plotted in Azimuth and Polar angle, where (0,0) corresponds to tailward flow. For this case, the ions are flowing sunward.

The model has ion flows turning back toward the planet in the wake as far out as ~3000 km (an X of - 1.5 R_v), as shown by yellow, orange and red shades representing sunward O^+ fluxes in Figure 4.11, where contours of model O^+ flux in two planes (XY-the equator and XZ-the meridian plane) are displayed. These return ion flows start near the terminator, and occur throughout a large portion of the equator (XY plane). The ions that eventually do escape into the wake originate from the draping poles (shown in blue at 90 degrees SZA in Figure 4.11b). These returning flowing ions, which occur out to -1.5 R_v in the X direction in the model, are shown in YZ plane cuts in the tail to illustrate how they affect the escape spatial distribution in Figure 4.12. Similar to Figure 4.11, the yellow and red portions of the figure correspond to ions turning back toward the planet. The extent to which observations support this picture of extensive return flows seen in the model has potential implications for global ion escape.

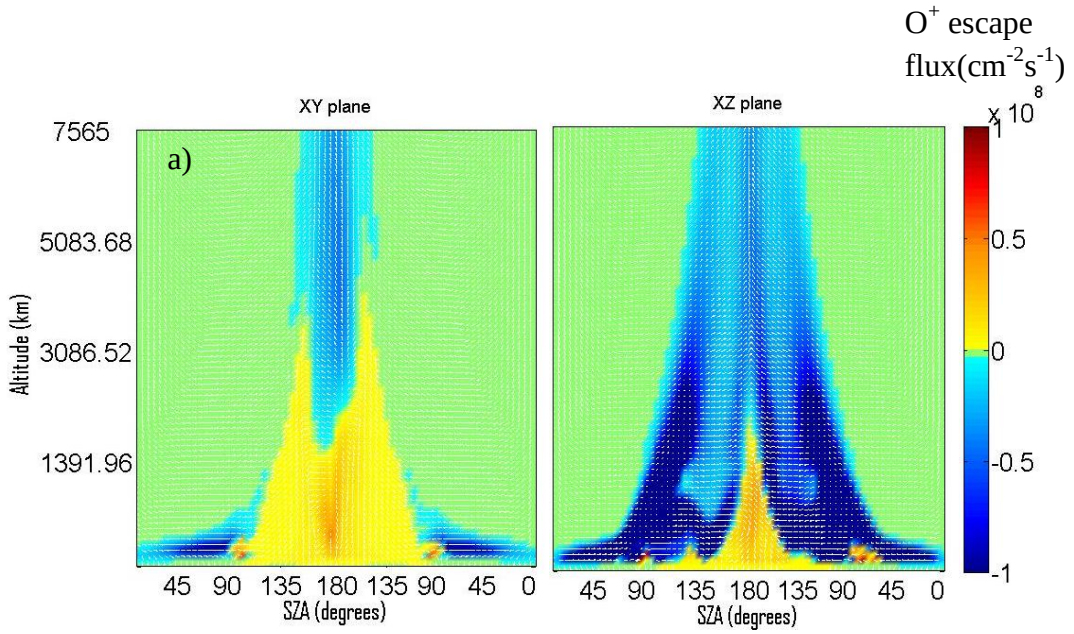

Figure 4.11: (a) MHD O^+ flux along on the XY (equator) plane, (b) MHD O^+ flux along on the XZ (noon-midnight) plane. Warm colors are sunward (+X) flowing ions, while cool colors are flowing away from the planet (-X) into the wake. The sunward flows occur in the wake out to ~3500 km on the equator and ~2000 km on the noon-midnight plane. The ion flows that pass over the terminator (90° SZA) on the XZ plane continue into the wake at higher altitudes, while the flows that pass over the terminator on the equator (XY plane) end up turning back toward the planet.

4.5.3 Escape flux in model depending on integration region

Since the geometry of the volume containing outflowing ions changes with distance, we can use the model to investigate how flow geometry could affect the escape inferred from the VEX orbit sampling. We are interested in the effect of the orbit bias on the reported VEX escape rate estimates, specifically the escape rates using the integration region applied by Fedorov et al. (2011). Fedorov et al. (2011) calculated the total oxygen ion escape rate with a superposed-epoch technique, "where the ion distribution is obtained by accumulating and averaging measurements on individual orbits in the spatial and velocity bins". These statistics were done within the VSE reference frame. Average ion distributions within the $Y_{VSE}Z_{VSE}$ plane were obtained in the wake with the following orbital constraints: the

spacecraft had to be further away from the center of the planet than 1.2 Venus radii (R_v), the X_{VSE} was between -0.8 to -3 R_v.

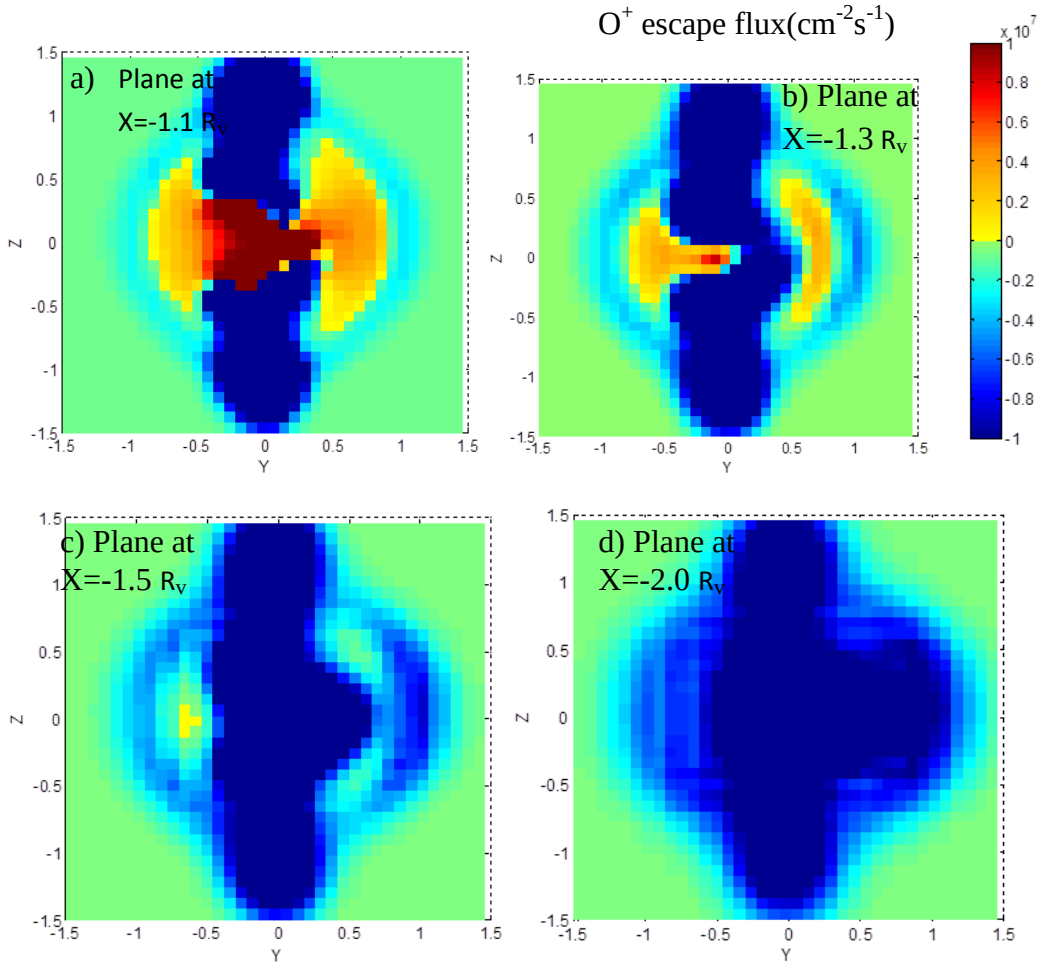

Figure 4.12: O^+ escape flux ($cm^{-2}s^{-1}$) on YZ planar cuts in the tail at X values in the wake of (a) -1.1 R_v, (b) -1.3 R_v, (c) -1.5 R_v, (d) -2.0 R_v.Yellow-red shades correspond to ion flows headed back toward the planet. The pattern of escaping ions changes with distance from the planet in the model.

Figures 4.13 (a) and (b) show the escape flux calculated from the model if the integration region was started from different X positions behind the terminator (-0.8 and -1.6 R_V). Planet-ward (return) ion flows were not included. Because the orbit passes over the northern pole, these figures show a high flux at near Z = +1 R_v for X = -0.8 R_v. If the integration region is started at -1.6 X_{VSE} the orbit is no longer sampling the region near the northern pole at altitudes where there are high ion fluxes. A similar plot is shown for the escape flux through an YZ plane at -2 R_v

X_{VSE} in Figure 4.13 (d). By this distance into the wake, there are no longer return flows. Therefore, all of the flow is escaping and represents the total escape through the wake in the model.

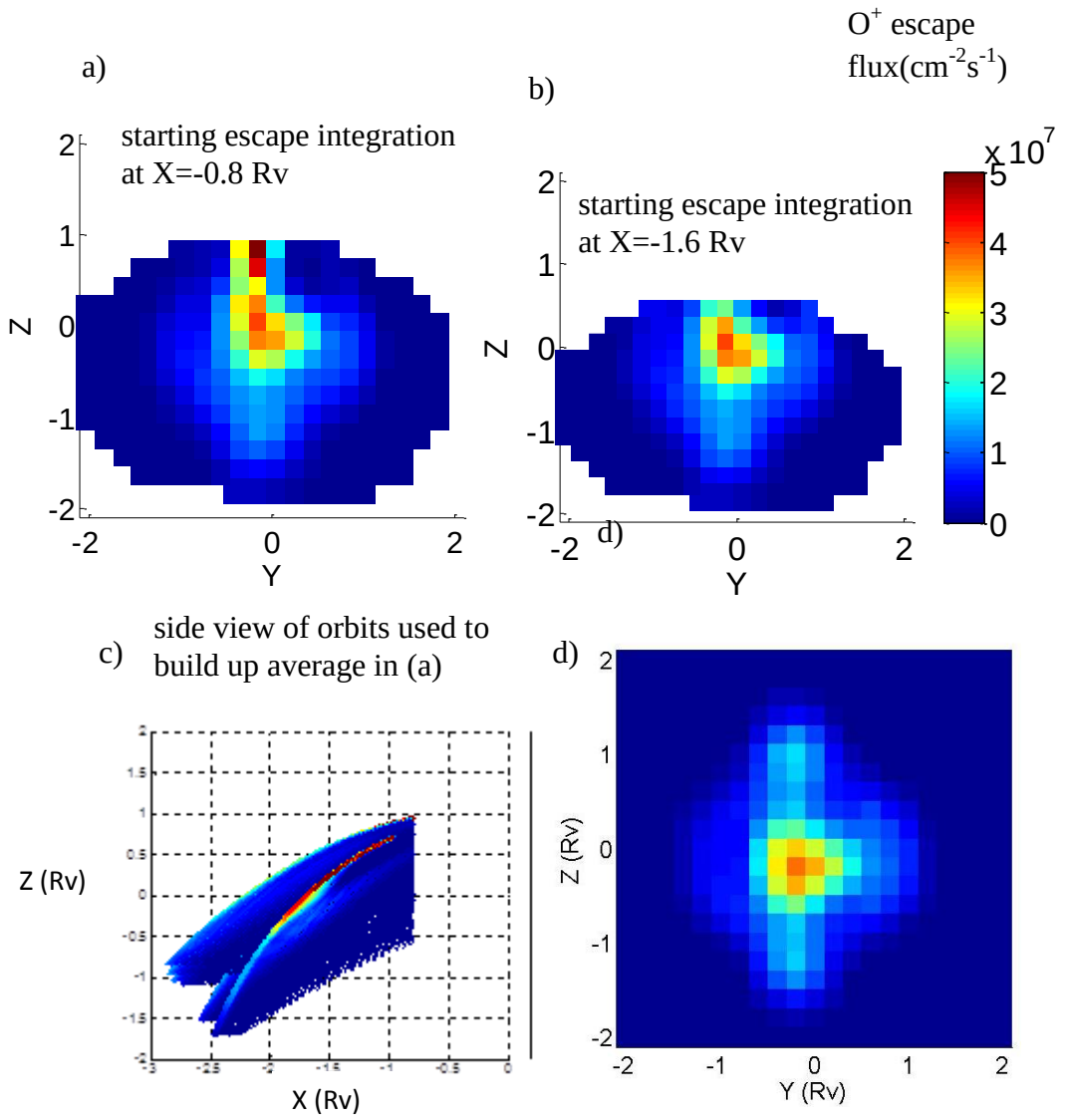

Figure 4.13: Plots of the escape flux ($cm^{-2}s^{-1}$) calculated using the VEX orbit starting at difference distances in the wake (a) -0.8 Rv and (b) -1.6 Rv - only including ions flowing in the -X direction. White areas are due to no orbit sampling. (c) XZ view of the orbits used to calculate the average escape flux in (a). (d) Escape flux on a YZ plane at X = -2 R_v (not averaging along the X direction).

Since the average ion flux in the YZ plane depends on the orbit, we also investigated what ion flux geometry would be measured and averaged within the region used by Fedorov et al. (2011) for the 2009 and 2010 orbits, when the periapsis was lowered. This lowered periapsis would mean more time spent near the northern draping pole. We found that the escape flux modeled using the orbits from 2009 and 2010 was not significantly different than the 2006-2007 orbit. Consequently, this change in periapsis altitude does not significantly bias the inferred YZ plane ion flux.

In addition to the inferred geometry of ion escape flux, we are also interested in the total rate of O^+ outflow in each of these cases. This is important to consider because a comparison of the total escape rate between solar minimum and maximum is one of the goals of Venus Express. We calculated the total escape rate (O^+/sec) within the model for each of these cases, and they were all within 25% of the actual escape flux (see Table 1). If there are return flows in the VEX ion data the estimated total escape flux calculated by averaging along the VEX orbit would thus not be too far off of the actual global escape rate.

Geometry of integration region	**X_{VSE} constraint (Rv)**	**Escape estimate (O^+/sec)**
2006-2007 VEX orbit	-0.8	2.16×10^{25}
2006-2007 VEX orbit	-1	2.09×10^{25}
2006-2007 VEX orbit	-1.6	1.84×10^{25}
2006-2007 VEX orbit	-1.5	1.84×10^{25}
2009 VEX orbit	-0.8	2.23×10^{25}
2010 VEX orbit	-0.8	2.24×10^{25}
-2 Rv X_{VSE} YZ plane in wake		2.27×10^{25}

Table 4.1: Total escape calculation flying through the model and averaging in different regions. The escape estimates are all within 25% of the actual escape from the model.

The model total escape estimate of 2.27×10^{25} O^+/sec is an order of magnitude larger than the estimate from Venus Express data by Fedorov et al. (2011) of 2.7 X 10^{24}. This may be because the model solar min description was based on Pioneer Venus conditions, while the VEX measurements have been made during a particularly weak solar minimum. The model escape estimate of 2.27×10^{25} O+/sec does fall within the range of escape estimates from PVO, which were between 10^{24} – 10^{27} O^+/second (e.g., Mihalov et al., 1981; Brace et al., 1982; Hartle and Grebowsky, 1990; Moore et al, 1991). Since we are looking at relative escape

estimates in the model, the uncertainty in the accuracy of the total escape rate in the model does not affect our conclusions.

4.6 Conclusions

Low energy ion measurements are complicated by the spacecraft's relative velocity and potential. These spacecraft characteristics can upshift ion energies in the data to make ions seem to have enough energy to escape from the planet, when in reality they may not. Orbit geometry and IMF direction can also affect the shape of energy-time spectrograms. When undertaking case studies of Venus Express orbits it is important to consider that the time series of ion energies are generally not corrected for the spacecraft's relative velocity or potential, and that the orbit geometry and IMF direction must be considered on a case-by-case basis. We were able to reproduce the general shape of VEX ion energy-time spectrograms at low energies (< 1 keV) in the ionosphere and wake using an MHD model.

We also considered the consequences for escape of both these energy corrections and the VEX orbit sampling. The inferred escape flux spatial distribution averaged in the YZ plane in the model along the VEX orbit looked different depending on the region in the wake used to integrate the measurements. The MHD model has ion flows turning back toward the planet out to -1.5 Rv in the wake, and Lundin et al. (2011) suggested that extended return flows may also exist in the VEX IMA data. These return flows can change that total escape flux inferred by averaging along the VEX orbit, but only by ~20%, thus these are not a major concern considering the other sources of error in the measurements. Nevertheless, it is important for users of low energy ion measurements to use caution in interpreting such observations. Indeed, the errors can be a major source of differences obtained in different studies. Separating such measurement complications from natural variations is a particular challenge, and should moderate arguments regarding accuracy of these fluxes. Perhaps reported results should be viewed as order of magnitude in accuracy at best with only exceptional changes meriting debate.

Chapter 5

Effects of a Large ICME on Oxygen Ion Escape at Venus

Abstract

Understanding the effects of large solar wind disturbances on O^+ ion escape is critical for characterizing the history of water on Venus. Previous studies suggested that disturbances can enhance the ion escape rate, but did not specifically study how escape is affected during the passage of the sheath region of a fast interplanetary coronal mass ejection (ICME). During ICME sheaths, the highest dynamic pressures in the solar wind occur. We present a case study of a large ICME that impacted Venus on November 5, 2011, and had the highest magnetic field yet encountered by Venus Express (VEX) (>250 nT). This event is unique because VEX was near Venus right at the time the ICME sheath was present. This is a circumstance that has occurred only a small fraction of the time VEX has been sampling ions near its periapsis. Oxygen ion escape was enhanced during this event compared to the days before and after the event when no ions were observed escaping into the wake

5.1 Introduction

Quantifying the present oxygen ion escape rate and its variation with external conditions is crucial to reconstructing the history of water on Venus (in addition to measurements of isotope ratios, estimates of the past solar activity, and escape models) as discussed by Chassefiere et al. (2012). Ion escape rates were estimated using instruments on Pioneer Venus Orbiter (PVO) (e.g., Brace et al., 1995), but none of these instruments were capable of fully characterizing the ion escape by species and at all energies expected for escaping ions. Venus Express (VEX) has an ion instrument, the ASPERA-4 (Analyzer of Space Plasmas and Energetic Atoms)

Ion Mass Analyzer (IMA) detailed in Barabash et al. (2007a), that can determine the composition of the escaping species over a broad energy range ~10eV-25keV. However, VEX launched just prior to the recent solar minimum. As a result, VEX ASPERA-4 ion escape statistics have only been published for low solar activity conditions when the largest variations in solar wind conditions, caused by major ICMEs, are generally absent (Barabash et al., 2007b and Fedorov et al., 2011). Hence, previous studies suggesting that O^+ escape may be enhanced at disturbed times (Luhmann et al, 2007; Futaana et al., 2008; Luhmann et al., 2008; Edberg et al., 2011) could not be verified. In addition, Luhmann et al. (2008) found that in three out of four case studies of moderately disturbed conditions in the earlier part of the mission, ICME passage did not produce apparent enhancements in the inferred ion escape. McEnulty et al. (2010) similarly did not find an increase in the escape flux during ICMEs, specifically at the highest-energies. The question has then been left open as to whether there is indeed a 'space weather' effect on Venus ion escape and if so, is solar wind dynamic pressure the main factor in its importance?

The highest dynamic pressures in the solar wind are within large ICMEs. As an ICME propagates away from the Sun it interacts with the background undisturbed solar wind. At the leading edge of the ICME, the interplanetary magnetic field (IMF) and solar wind is compressed (see Figure 5.1). This compression results in high total magnetic field and high dynamic pressure and is called the ICME sheath. This compressed sheath region lasts for a few hours (as measured at Venus). The main body (ejecta) of the ICME then follows the sheath region. This ejecta portion is often associated with a magnetic cloud, which has a rotating IMF and is smoother (less variance) than the sheath region. This magnetic cloud signature can last for 1-4 days at Venus. (For more details of ICME time series see Jian et al., 2006, 2008).

Since the earlier studies were published, solar activity has increased and ICMEs observed in the solar wind near Venus have become faster and larger, with associated greater solar wind plasma and field modifications. In the present study, we look closely at escape during the highest dynamic pressures seen in the solar wind so far on VEX – in the sheath region of a large ICME. The average dynamic pressure during the VEX mission from 2006-2009 was 1.5 nPa (McEnulty et al., 2012a) and the dynamic pressures in the study of Edberg et al. (2011) did not exceed 4 nPa. However, the dynamic pressure in the ICME sheath region at Venus,

based on PVO statistics which spanned a solar cycle, can often exceed 20 nPa even reaching 80 nPa (e.g., Jian et al., 2006, 2008; McEnulty et al, 2012a). When the dynamic pressure is high, the altitude of the boundary between the Venus ionosphere and the solar wind (the ionopause) is lowered (e.g., Phillips et al, 1985). A lower ionopause altitude can expose more ionospheric particles to the solar wind convection electric field, possibly enhancing their escape (Luhmann et al., 2006).

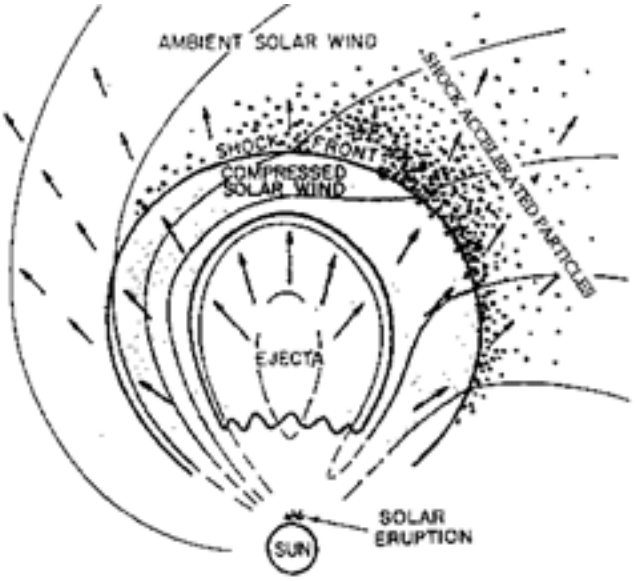

Figure 5.1: Cartoon of an ICME propagating into the ambient solar wind. Fast ICMEs compress the solar wind in front of them causing a region of high density and dynamic pressure. (from J. Luhmann, personal comm.)

In order to measure the ion escape during the time of most interest, the spacecraft must be near the planet when the ICME sheath passes. This does not occur often because VEX has a 24 hour orbital period, and is only near the planet measuring ion escape for ~2 hours of the orbit. The typical fast ICME passes an observer at Venus' heliocentric distance in ~a day, but the ICME sheath passage only lasts for a few hours. Thus most ICME sheaths pass the planet when VEX is away from its periapsis and not measuring planetary ions. There was fortunate timing on November 5, 2011, when a large (fast and high magnetic field) ICME hit Venus just as the spacecraft was nearing the planet. Figure 5.2 shows the location of Venus together with the locations of the STEREO (Solar TErrestrial RElations Observatory) twin spacecraft, which were observing solar activity from widespread

multiple perspectives at this time. In this paper, we show this ICME as imaged by STEREO A and B and the response of Venus to this event as seen on VEX in both magnetic field and ion measurements during the ICME sheath passage. The general properties of the VEX ASPERA-4 IMA and Magnetometer (MAG) measurements used in this study are described in Barabash et al. (2007a) and Zhang et al. (2006), respectively, and will not be repeated here.

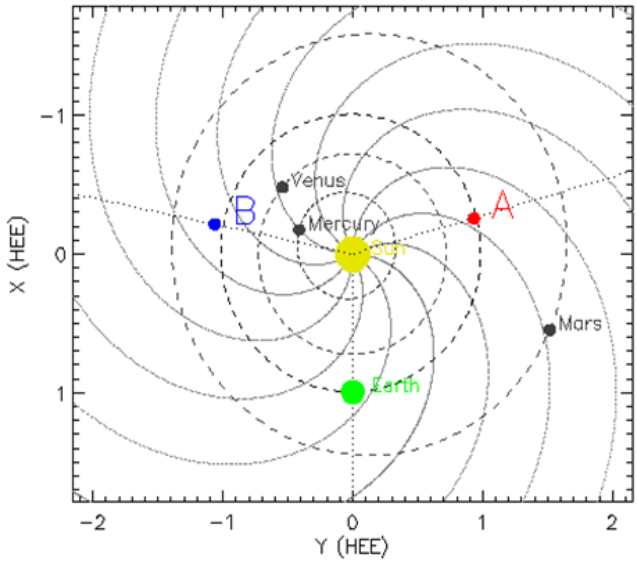

Figure 5.2: Locations of Venus, STEREO A, and STEREO B on November 5, 2011.

5.2 November 3, 2011 Coronal Mass Ejection

The Coronal Mass Ejection (CME) of interest occurred at the end of the day on November 3, 2011 on the far side of the Sun as seen from Earth. The location of the STEREO A and B spacecraft allowed imaging of this event from multiple viewpoints. This event produced a partial halo in the STEREO B white-light coronagraph COR2 image shown in Figure 5.3. The COR2 detectors observe within a region from 2-15 solar radii, as described in Howard et al. (2008). The location of Venus and the STEREO twin spacecraft (Figure 5.2) were thus useful in understanding both the origins and characteristics of the event that impacted the planet. The CME speed estimated from STEREO A was 1038 km/sec (http://spaceweather.gmu.edu/seeds/). To put this CME speed into context, the average speed of CMEs that impacted Venus in 2006-2007 from McEnulty et al.

(2010) was only 250 km/sec. Also, from 10 years of PVO observations, the average speed of ICMEs was 476 km/sec. (See Table 2 of Jian et al., 2008.)

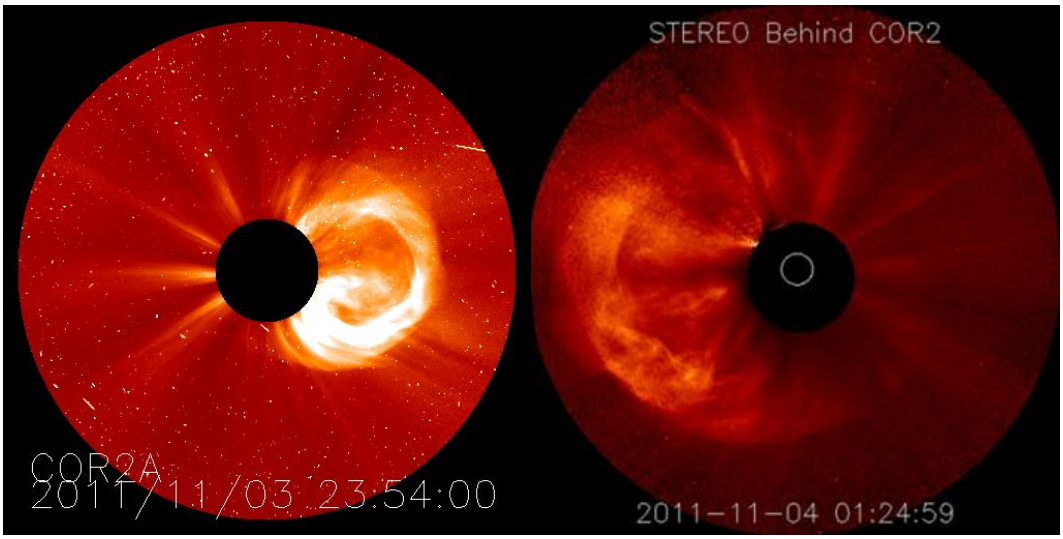

Figure 5.3: White-light coronagraph images from STEREO A (left) and B (right) showing a partial halo toward STEREO B at the beginning of the day on November 4, 2011. This event started at the end of the day on Nov 3rd, shown on the left

5.3 ICME at Venus

An ICME was measured in the VEX magnetic field and plasma data on November 5, 2012 03:00 UT. This ICME arrived at Venus within a few hours of the time calculated from the speed of the Nov 3 CME discussed in the previous section. Figure 5.4(b-e) displays the IMF near Venus measured by the Venus Express magnetometer in VSO (Venus-solar-orbital) coordinates (where X is toward the sun, Y is opposite the orbital direction, and Z completes the right hand system). The sheath region lasted for ~ 6 hours, and the ejecta portion for ~18 hours. This disturbance was also observed in the solar wind plasma. Before the ICME arrived at Venus, the H^+ measured within the solar wind by the VEX IMA had an energy of ~1.5 keV. After the ICME arrived, the solar wind H^+ had energies above 10 keV, even up to 20 keV in the ICME sheath. This increase in the background H^+ energy is illustrated with an energy-time (ET) spectrogram created from the VEX IMA data in Figure 5.4a. This ET spectrogram is a plot of the measured H^+ ion energy (at time steps averaged every 3 minutes). The color code is log(counts) of the measured H^+.

Gaps on this plot occur during time periods when the IMA instrument is not operating. H^+ measured near Venus has energies below ~ 1 keV, which appears on the ET spectrogram every day for ~ 2 hours as the VEX spacecraft nears the planet in its 24 hour orbit. The solar wind dynamic pressure calculated from IMA density and velocity (downloaded from http://cdpp-amda.cesr.fr/) for this event was 17.6 nPa (density 13/cc, velocity 900 km/sec). For comparison, before the event the dynamic pressure was 0.72 nPa (density 3/cc, velocity 345 km/sec). The VEX spacecraft was near periapsis and sampled planetary ions near Venus during the ICME sheath (the Btot increase up to 260 nT, and the H^+ detections on low energies on Nov 5th were in the green shaded region on Figure 5.4).

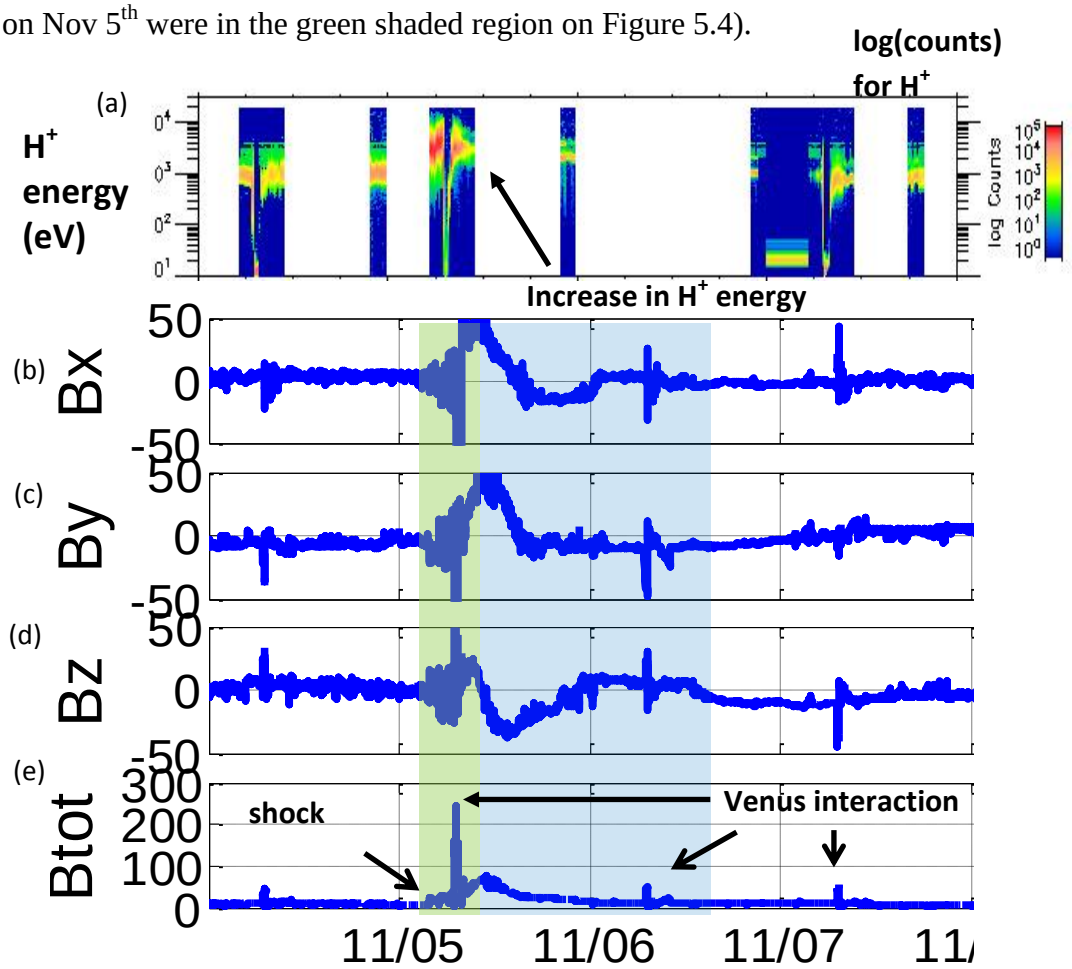

Figure 5.4: (a) VEX IMA H^+ detections plotted as a function of time and energy and color-coded for H^+ log (counts). (b-d) VEX magnetic field vector components and (e) total magnetic field strength. An ICME solar wind disturbance was detected on November 5, 2011 in both the magnetic field and solar wind H^+. The ICME sheath

is shaded in green, and the blue shaded time period is the ICME ejecta. Daily spikes are due to the interaction of the IMF with the Venus ionosphere.

5.4 O^+ detections during the ICME and comparison to an undisturbed orbit

As the VEX spacecraft moves closer to Venus it begins to measure heavier mass ions in addition to the solar wind H^+. These ions can be detected within the magnetosheath where the IMF piles up above the ionosphere obstacle (see Figure 5.5). This obstacle occurs at the ionopause, where the solar wind dynamic pressure on the outside balances the thermal pressure from the ionospheric plasma on the inside. The VEX IMA also detects O^+ beneath the ionopause (in the ionosphere) and in the wake (e.g., Barabash et al, 2007b; Fedorov et al., 2011).

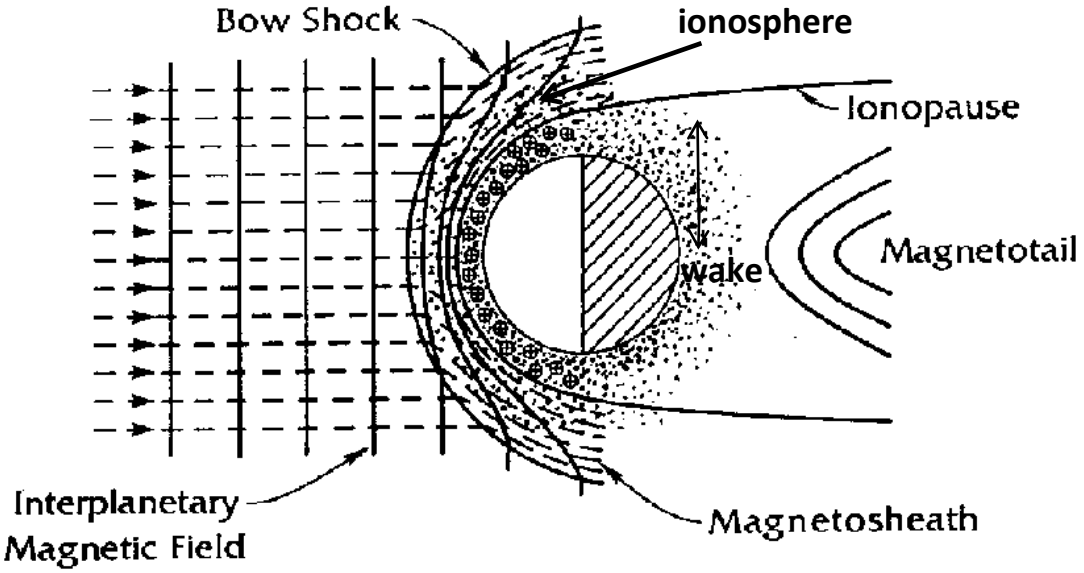

Figure 5.5: Cartoon of the Venus-solar wind interaction. The dashed lines on the left with arrows represent the flowing solar wind particles carrying with them the interplanetary magnetic field lines (vertical and perpendicular to the flow in this case). These field lines pile up near the ionosphere in the magnetosheath and drape around the planet. The ionopause is the boundary between the region of solar wind particles and the ionosphere. In this figure ions are represented by circles on the dayside with pluses and minuses. In the wake (the region on the nightside where there is little solar wind), the field lines that have slipped over the planet form a magnetotail. (from Luhmann and Russell 1997)

We are interested in details of the O^+ measured within the magnetosheath, ionosphere, and wake of Venus when the large ICME impacted Venus. We also want to know how the O^+ behavior during the large ICME compares to O^+ measured during undisturbed solar wind conditions. To determine the influence of ICMEs it is important to control for other aspects that can affect the O^+ measurements, such as the orbit and IMF direction. The measured O^+ will depend on the spacecraft's orbit due to sampling different spatial regions and is affected by the spacecraft's relative velocity as described in McEnulty et al. (2012b).

The most straightforward comparison is of the O^+ detected on November 5, 2011 to measurements of O^+ within a few days of Nov 5, but before the ICME arrived at Venus. The VEX orbit does not change significantly within 2 days, so we compare to November 3, 2011. During this time period (Nov 3-5), VEX was in an orbit moving from the sunward side to the night side, referred to as noon-midnight (see Figure 5.6a and b). On Nov 3, O^+ was detected within the magnetosheath near the ionopause, and at low energies (<40 eV) within the ionosphere. On Nov 5, the ionopause was at a lower altitude, and the magnetosheath was compressed (as would be expected from high dynamic pressure in the solar wind). There was also O^+ detected in the magnetosheath near the ionopause, but it was of higher energy and counts than on Nov 3. The O^+ detected within the ionosphere and wake was of much higher energy than on Nov 3, but not necessarily higher counts, and even lower counts within the wake. In addition, high energy O^+ was detected up to 20 keV, which was not detected on Nov 3. Comparisons of IMA O^+ ions (along with the H^+ ions to show the solar wind background) periapsis are plotted in ET spectrograms in Figure 5.7 and 5.8. These plots show the counts color-coded at each time step (which is averaged every 3 minutes) as a function of energy. The ionopause is marked with the white line closest to periapsis (marked with the yellow dotted line). The color along the orbit plots of Figure 5.6a and b corresponds to the rectangles at the bottom of the energy-time spectrograms showing where the ions were detected within the orbits.

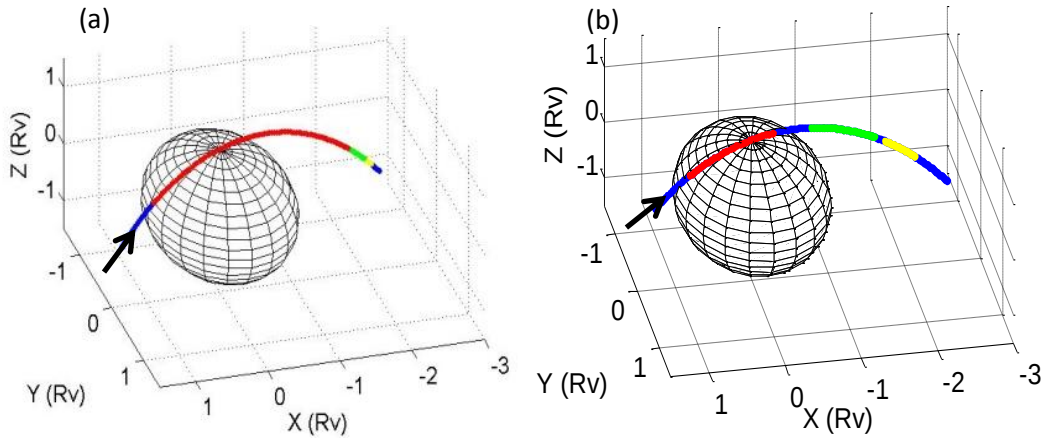

Figure 5.6: (a,b) VEX noon-midnight orbits color coded red, green, and yellow in the regions that planetary ions were detected on Nov 3 and Nov 5, respectively. These colored orbit segments correspond to the time periods of ion detections marked by rectangles at the bottom of Figure 5. a and b.

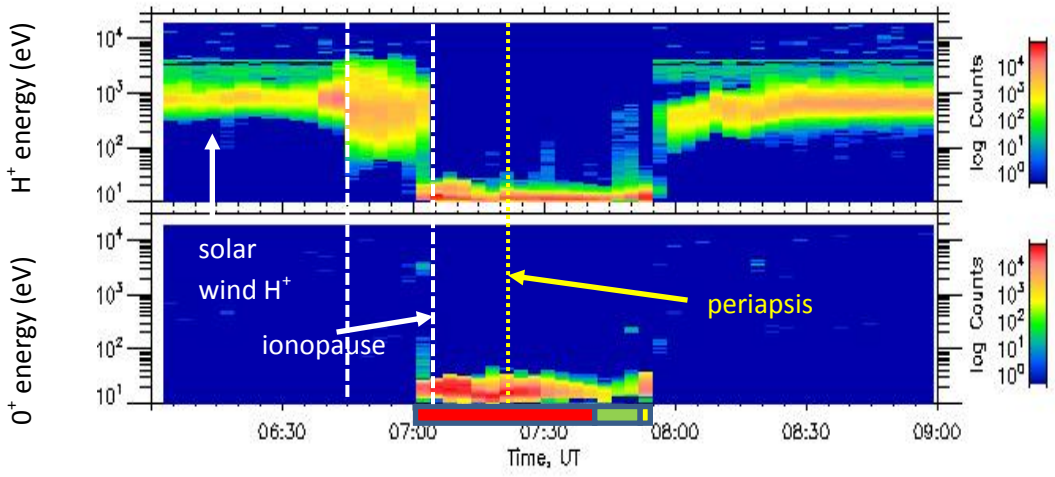

Figure 5.7: VEX IMA H^+ (top) and O^+ (bottom) detections plotted as a function of time and energy and color coded for counts for November 3, 2011 (during undisturbed solar wind). Colored rectangles at the bottom of the plots (red, green, and yellow) correspond to the orbit segments in Figure 5.6.

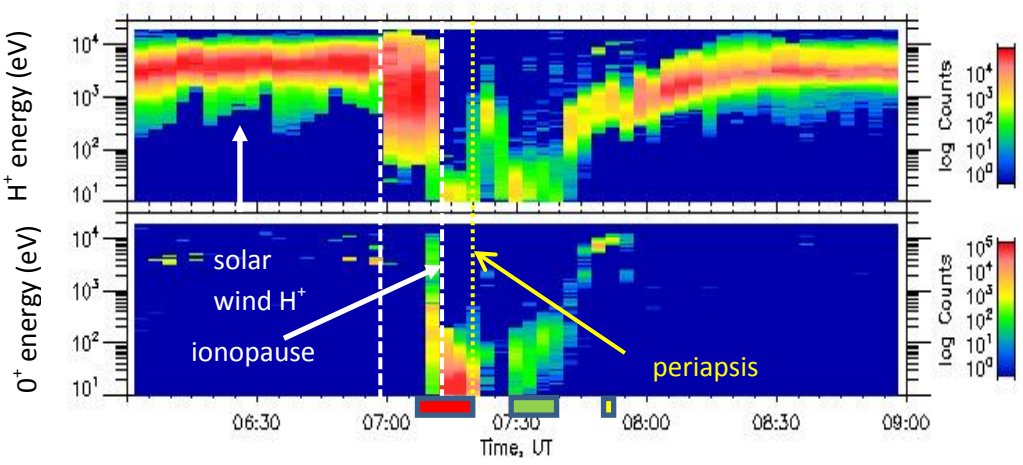

Figure 5.8: VEX IMA H^+ (top) and O^+ (bottom) detections plotted as a function of time and energy and color coded for counts on November 5, 2011 (when an ICME was passing Venus). Colored rectangles at the bottom of the plots (red, green, and yellow) correspond to the orbit segments in Figure 5.6. There was increased energy of the H^+ and O^+ ions near the planet during the ICME.

5.5 O^+ escape during ICME compared to undisturbed orbits

In the previous section, we discussed O^+ detections during the Nov 5 ICME compared to detections during undisturbed solar wind conditions on Nov 3. The O^+ during the ICME had higher energy, but the difference in counts (which relates to flux) was not as clear. During the ICME, the counts were higher in the magnetosheath and there were high energy ions (>1 keV) detected on the outbound section of the orbit that weren't detected on the undisturbed day. However, within the ionosphere the counts were similar during the ICME and the undisturbed day. In the wake (~7:30-7:40), the ICME had lower counts than the undisturbed day. In order to understand the total difference in O^+ escape flux measured during these orbits, we must make sure that all of these ions are actually escaping. The flow direction of O^+ is a major concern when determining if the ions are actually escaping, because O^+ ions have been detected gravitationally bound and perhaps flowing back toward the planet out to ~1.5-2 Venus Radii in the wake (Lundin et al., 2011; McEnulty et al., 2012b). For additional comparison, we added another example of undisturbed ion flow on November 4, 2011 to our analysis, which had low energy detections similar to Nov 3 (see Figure 5.9. Labels and arrows on Figure 5.9 correspond to times of interest for studying detailed O^+ flow direction.

During the ICME, O^+ was escaping in the magnetosheath near the ionopause, within the ionosphere, and at high energies outbound in the tail. During the undisturbed orbits (Nov 3 and 4), ions were also escaping within the magnetosheath close to the ionopause, but the counts at each energy were 1-3 orders of magnitude less than the escape in this region during the Nov 5 ICME. All other O^+ detected during the undisturbed orbits were coming from the direction of the tail, as shown by plots of the angle that O^+ entered the instrument (Figure 5.10). The axes are azimuth and polar angles, where (0, 0) corresponds to ions that are were detected as coming from the direction of the Sun. Furthermore, (180, 0) corresponds to ions which entered the instrument from the opposite direction. The color code is O^+ counts averaged over 3 minutes (black signifies no detections, which occurs at angles where the spacecraft is blocking incoming ions). Ions detected at (180,0) are either returning to the planet, or are static/moving at very low velocity, but the spacecraft ram made them appear to be coming from the tail direction. Uncertainties in the spacecraft potential make it difficult to separate these two possibilities, but these ions are either returning to the planet or are gravitationally bound and not escaping.

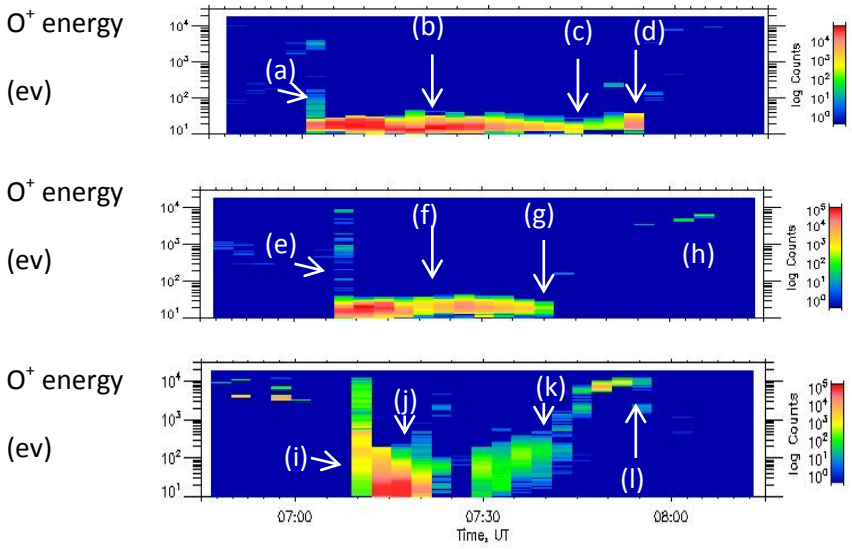

Figure 5.9: VEX IMA O^+ ET spectrograms for (top) Nov 3, (middle) Nov 4, (bottom) Nov 5. The white letters and arrows mark times of interest for investigating the O^+ flow direction. (These letters correspond to labeled plots in Figure 5.).

To get an approximate estimate of the O^+ escape flux during the Nov 5 ICME, we then used density and velocity moments from http://cdpp-amda.cesr.fr/. Since the O^+ detected in the ionosphere and wake region was not all escaping, we focused on the O^+ detected in the dayside magnetosheath and on the outbound high energy ions in the tail (labeled (i) and (l) on Figure 5.9). The O^+ in the dayside magnetosheath had a density of 10 O^+/cc and a velocity in the $-X_{VSO}$ direction of 35 km/sec. This corresponds to an escape flux of $3.5x10^7$ $O^+cm^{-2}sec^{-1}$. For the outbound high energy ions, the density was 10 O^+/cc and velocity in the $-X_{VSO}$ direction was 250 km/sec. This corresponds to an escape flux of $2.5x10^8$ $O^+cm^{-2}sec^{-1}$ within this outbound wake/magnetosheath region during the ICME.

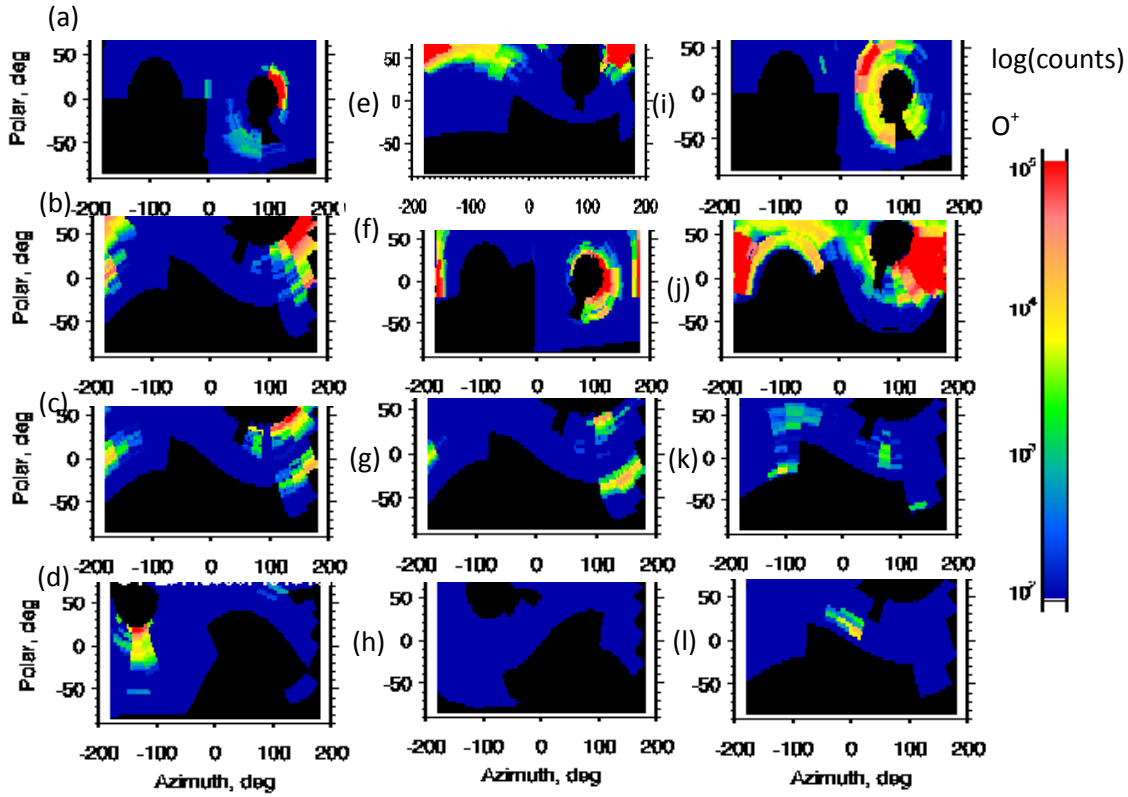

Figure 5.10: IMA O^+ detections plotted by the angle that they are entering the instrument (averaged over 3 minutes). In these plots, O^+ detected at an azimuth and polar angle of (0, 0) is due to ions that are coming from the sunward direction moving tailward. (180, 0) corresponds to ions coming from the opposite direction (moving toward the Sun). These plots correspond to the times labeled with the white arrows and letters in Figure 5.: a) Nov 3/07:01, b) Nov 3/07:18, c) Nov 3/07:40, d)

Nov 3/07:50, e) Nov 4/07:07, f) Nov 4/07:18, g) Nov 4/07:40, h) Nov 4/08:02, i) Nov 5/07:09, j) Nov 5/07:18, k) Nov 5/07:40, l) Nov 5/07:47.

In order to compare these measurements to average undisturbed conditions, we must consider the IMF direction. Statistical studies of ion escape, such as Fedorov et al. (2011) put the escaping ions into the VSE (Venus-Sun-Electrical) frame. In this reference frame, Z_{VSE} is parallel to the convection electric field, X_{VSE} is antiparallel to the solar wind velocity, and Y_{VSE} completes the system. From mid-2006 to 2007 the average O^+ escape flux in the region between Y_{VSE} -0.5 to 0.5 and Z_{VSE} -1.0 to 1.0 was ~5x10^6 $O^+cm^{-2}sec^{-1}$, while a few spatial bins were higher than 10^7 $O^+cm^{-2}sec^{-1}$ (see the left of Figure 5.11, which was from Fedorov et al., 2011). Outside of this region, the escape flux varied between 5x10^4 $O^+cm^{-2}sec^{-1}$ to 5x10^6 $O^+cm^{-2}sec^{-1}$. Fedorov et al. (2011) did not include measurements made sunward of -0.8 X_{VSE}, so we only compare our outbound measurements, which were from the wake. This escape flux of 2.5x10^8 $O^+cm^{-2}sec^{-1}$ is higher than any of the values from Fedorov et al. (2011). In addition, due to the IMF during this orbit, the measurements were made away from the region of highest flux in the VSE frame described above (see Figure 5.11). Because of this IMF affect, it is possible that the escape flux was even higher than 2.5x10^8 $O^+cm^{-2}sec^{-1}$ in the VSE locations that the spacecraft did not sample. The only way to confirm this is to wait for more large ICMEs with diverse VSE frame orbital sampling.

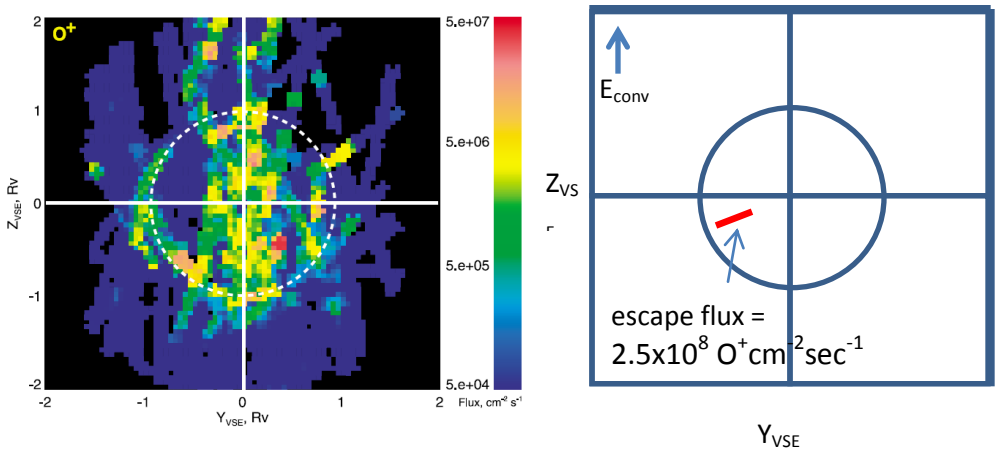

Figure 5.11: (left) Average escape flux in the VSE frame mid-2006-2007 (from Fedorov et al., 2011). (right) Location (in the VSE frame) of O^+ detections outbound on November 5, 2011.

5.6 Conclusions

An ICME impacted Venus on November 5, 2011 with timing unique for studying its effect on escaping oxygen ions - VEX was measuring planetary ions during the high dynamic pressure sheath region of the ICME. This timing is rare, because the high dynamic pressure sheath region of ICMEs typically only takes a few hours to pass, and the VEX spacecraft only measures planetary ions for a few hours out of each 24-hour orbit. This event was also unique, because it has a dynamic pressure of 17.6 nPa, which is significantly higher than the average dynamic pressure that VEX has measured (~1.5 nPa) and of other solar wind disturbances that VEX encountered (up to 4 nPa) (Edberg et al., 2011). In addition, the magnetic field near Venus reached 250 nT. This is the highest field yet measured in the mission. The location of Venus with respect to the twin STEREO spacecraft, allowed confirmation that the ICME came from the far side of the Sun (with respect to Earth) and had a speed of ~1000 km/sec.

During this event, on November 5, 2011, O^+ coming from the atmosphere of Venus was measured to have much higher energies than the previous 2 days (when the solar wind was undisturbed). Detailed study revealed that in fact, the majority of the O^+ detected on the undisturbed orbits was not escaping from the planet. Instead it was was turning back toward the planet or gravitationally bound in the wake. The one region within the Venus-solar wind interaction that had escaping O^+ on all three days was in the dayside magnetosheath in a thin layer near the ionopause. Within this region, the counts of escaping O^+ were enhanced by up to three orders of magnitude. O^+ was also detected at high energies in the wake during the ICME with an escape flux of 2.5×10^8 $O^+ cm^{-2} sec^{-1}$. Similar escaping ions were not detected during our case studies of undisturbed orbits. Therefore, we instead compared this flux to the average escape fluxes in the wake from Fedorov et al. (2011). This escape flux was higher than any of the average escape fluxes. In addition, the IMF during this ICME would have actually biased the orbital sampling to lower O^+ fluxes, which makes it possible that escape fluxes were even higher in different regions of the VSE frame that the spacecraft did not sample. However, there was also a region in the wake that had lower counts during the ICME than during the undisturbed days. Perhaps the gravitationally bound ions that were detected in the wake on Nov 3 and 4 were energized to escape velocity by the ICME on Nov 5.

Future studies can build a statistical picture in the VSE reference frame of the O^+ escape flux during large ICMEs. For now, we can only speculate that the escape flux that VEX measured during the November 5, 2011 ICME could be a lower bound. If this were true, the lower bound on the total escape flux escaping within a circle of radius 1 Rv during this large event would be $2.8x10^{26}$ O^+/sec. For an escape region of 1.5 Rv, the total escape would be $6.5x10^{27}$ O^+/sec. This is 3 orders of magnitude higher than the average escape rate measured by VEX of $2.7x10^{24}$ O^+/sec, which highlights that ICMEs may have a significant affect on the total escape over time. If the O^+ escape is enhanced to the level suggested by this study, it could have been even more important early in the solar system when the Sun was likely more active (with more frequent large ICMEs). In addition, although this ICME was the highest dynamic pressure encountered by VEX thus far (17.6 nPa), it still is much weaker than some of the largest ICMEs that impacted Venus during PVO (>80 nPa). As VEX continues to make measurements into solar maximum events of this size may enhance O^+ escape even further.

Chapter 6

Conclusion

6.1 Summary

In this dissertation, my goal was to contribute to understanding the global picture of oxygen ion escape from Venus to space, and how escape is influenced by extreme solar wind conditions in ICMEs. The work in this dissertation started chronologically with the study focused on high energy O^+ pick-up ions during ICMEs (Chapter 3). This first study did not include the lower energy O^+ ion population that is also measured by VEX, because these low energy ions were difficult to interpret. In particular, there was an open question of whether or not these ions were even escaping. The main result of this high energy pick-up ion study was that the O^+ pick-up ions reach higher energies at lower altitudes (compared to O^+ escaping when the solar wind was undisturbed), but the O^+ counts were not significantly affected. The result that the O^+ counts were not affected raised the following questions, which motivated the other studies in this dissertation: Is VEX measuring O^+ escape during external conditions that are representative of average solar minimum conditions? What happens to the low energy O^+ population during ICMEs? Is the O^+ escape rate different during large (fast) ICMEs that did not occur during the time period of the first study?

The following three studies completed for this dissertation addressed these questions. Comparison of the external conditions encountered by VEX to the conditions during Pioneer Venus (Chapter 2) highlighted that VEX is measuring

during a particularly weak solar minimum. Through 2009, VEX had not encountered the high dynamic pressures that PVO had (>20 nPa), which may be associated with enhanced ion escape. To study the low energy ion population, I compared VEX data to an MHD model in Chapter 4. This comparison showed that it was possible for the low energy ions measured by VEX to be gravitationally bound and not escaping, even though they appeared to have above escape velocity in the ion measurements. This study also pointed out that some ions measured by VEX may be heading back toward the planet, and therefore not escaping. This result was important to inform the last study of this dissertation, which studied O^+ escape at both low and high energies during a large ICME. The last study (Chapter 5), revealed that O^+ escape was enhanced in both the low and high energy ion populations during a large ICME.

6.2 Major scientific contributions

I have made new and interesting discoveries in understanding the external conditions at Venus, the geometry of oxygen ion escape, and how escape can be affected by ICMEs. Below is a list of major contributions of the work presented in this dissertation:

External conditions at Venus

- Venus Express has been making measurements of oxygen ion escape during a time of particularly weak solar wind dynamic pressure. In particular, through the end of 2009 VEX had not measured any dynamic pressures above 20 nPa, while PVO measured up to 80 nPa.

Geometry of oxygen ion escape at Venus

- There are high energy (~1-30 keV) pick-up oxygen ions within the Venus magnetosheath and during ICMEs they reach high energy at a lower altitude (smaller gyroradius) than at undisturbed times.
- Low energy (<100 eV) oxygen ions measured by VEX within the ionosphere and in the wake must be investigated in detail before interpretation. The measured energy of the O^+ is affected by the spacecraft relative velocity and potential. These effects can make gravitationally bound ions appear to be moving above escape velocity.

- Besides being gravitationally bound, some low energy ions measured by VEX in the wake are actually moving back toward the planet. Similar "return flows" are also seen in an MHD model.
- An MHD model is able to approximate the ion energies in the wake and is useful for putting case studies within a global picture.

Influence of ICMEs on oxygen escape from Venus

- ICMEs can accelerate high energy pick-up ions to higher energies at low altitudes, compared to undisturbed days. However, for the ICMEs in 2006-2007 with average velocity ~250 km/sec there was no change in the escape rate.
- Large (fast) ICMEs, with high dynamic pressure can enhance the oxygen escape rate.

6.3 Implications for future Venus ion escape studies

The statistics of the solar wind and IMF conditions that can affect ion escape (in Chapter 2) can be used to guide future comparisons of different time periods. I learned that the conditions that VEX has encountered are much less intense than what is possible. This should be kept in mind in interpreting the absolute escape rates that are measured by VEX, even at solar maximum (since this maximum may be weak).

The work comparing VEX data to an MHD model (Chapter 4) can be used in interpreting future total escape rate estimates. Investigators that work with VEX ion data should be aware of the return ion flows in case studies, such as my large ICME study. Without an awareness of the possibility of return flow, I may have misinterpreted the difference in ion escape during this ICME. In addition, this paper pointed out the importance of considering the spacecraft's relative velocity when studying ions near periapsis. Ions can appear to have above escape velocity even though they are actually gravitationally bound.

The results from the large ICME study (Chapter 5) highlight that the sheath of the ICME is of particular interest for future statistical studies. Instead of considering escape during the few days that the ICME lasts and then averaging the escape rate

over that time period, future studies should separate the effects of the sheath and ejecta portion.

6.4 Future work

Mars does not have a dynamo magnetic field, so its upper atmosphere interacts with the solar wind similar way to Venus. I plan to use what I have learned about Venus, and conduct similar studies at Mars on the effects of extreme solar wind on ion escape. An interesting difference between Mars and Venus is that Mars has remnant crustal magnetic fields. I am curious how the crustal magnetic fields change the ion escape processes. I would like to study what happens to the atmosphere and ion escape when there is magnetic reconnection between the crustal fields and the interplanetary magnetic fields. The Mars Express (MEX) spacecraft carries a sister instrument to the VEX IMA that produces similar ion data. MEX does not have a magnetometer, making it significantly more difficult to interpret the ion data. There was a period of overlap in the operation of MEX and the Mars Global Survey (MGS) mission, and MGS did have a magnetometer. It would be interesting to identify signatures of magnetic reconnection the MGS magnetometer data and then investigate if there was anything unusual in the MEX IMA data at those times.

Mars atmospheric escape science will become even more exciting within the next few years. A mission called MAVEN (Mars Atmosphere and Volatile EvolutioN) will be launched in late 2013. The main goal of this mission is to understand the history of volatiles on the planet, and part of the puzzle is to quantify ion escape rates and their dependence on extreme solar wind conditions. MAVEN will have multiple plasma instruments that will cover the full energy range that we expect for O^+ escape, and will have a magnetometer.

Bibliography

Barabash, S. et al. (2006), The Analyzer of Space Plasmas and Energetic Atoms (ASPERA-3) for the Mars Express Mission, *Space Science Reviews*, *126*, 113–164, doi:10.1007/s11214-006-9124-8.

Barabash, S. et al. (2007a), The Analyser of Space Plasmas and Energetic Atoms (ASPERA-4) for the Venus Express mission, *Planetary and Space Science*, *55*, 1772–1792, doi:10.1016/j.pss.2007.01.014.

Barabash, S. et al. (2007b), The loss of ions from Venus through the plasma wake, *Nature*, *450*, 650–653, doi:10.1038/nature06434.

Bauer, S. J., and H. A. Taylor (1981), Modulation of Venus ion densities associated with solar variations, *Geophysical Research Letters*, *8*, 840–842.

Brace, L. H., R. F. Theis, and W. R. Hoegy (1982), Plasma clouds above the ionopause of Venus and their implications, *Planetary and Space Science*, *30*, 29–37.

Brace, L. H., W. R. Hoegy, and R. F. Theis (1988), Solar EUV measurements at Venus based on photoelectron emission from the Pioneer Venus Langmuir probe, *Journal of Geophysical Research*, *93*, 7282–7296.

Brace, L. H., R. E. Hartle, and R. F. Theis (1995), The nightward ion flow scenario at Venus revisited, *Advances in Space Research*, *16*, 99.

Carlsson, E. et al. (2006), Mass composition of the escaping plasma at Mars, *Icarus*, *182*, 320–328, doi:10.1016/j.icarus.2005.09.020.

Chassefière, E., R. Wieler, B. Marty, and F. Leblanc (2012), The evolution of Venus: Present state of knowledge and future exploration, *Planetary and Space Science*, *63*, 15–23, doi:10.1016/j.pss.2011.04.007.

Cravens, T. E., S. L. Crawford, A. F. Nagy, and T. I. Gombosi (n.d.), A Two-Dimensional Model of the Ionosphere of Venus, *J. Geophys. Res.*, *88*(A7),

PP. 5595–5606, doi:198310.1029/JA088iA07p05595.

Donahue, T. M., J. H. Hoffman, R. R. Hodges, and A. J. Watson (1982), Venus was wet - A measurement of the ratio of deuterium to hydrogen, *Science*, *216*, 630–633, doi:10.1126/science.216.4546.630.

Dubinin, E. et al. (2006), Electric fields within the martian magnetosphere and ion extraction: ASPERA-3 observations, *Icarus*, *182*, 337–342, doi:10.1016/j.icarus.2005.05.022.

Edberg, N. J. T. et al. (2011), Atmospheric erosion of Venus during stormy space weather, *Journal of Geophysical Research (Space Physics)*, *116*, 09308.

Fang, X., M. W. Liemohn, A. F. Nagy, J. G. Luhmann, and Y. Ma (2010), On the effect of the martian crustal magnetic field on atmospheric erosion, *Icarus*, *206*, 130–138, doi:10.1016/j.icarus.2009.01.012.

Fedorov, A., S. Barabash, J.-A. Sauvaud, Y. Futaana, T. L. Zhang, R. Lundin, and C. Ferrier (2011), Measurements of the ion escape rates from Venus for solar minimum, *Journal of Geophysical Research (Space Physics)*, *116*, 07220.

Fegley, B. (1997), NOTE: Why Pyrite Is Unstable on the Surface of Venus, *Icarus*, *128*, 474–479, doi:10.1006/icar.1997.5744.

Fox, J. L., and K. Y. Sung (2001), Solar activity variations of the Venus thermosphere/ionosphere, *Journal of Geophysical Research*, *106*, 21305–21336.

Fränz, M., E. Dubinin, E. Nielsen, J. Woch, S. Barabash, R. Lundin, and A. Fedorov (2010), Transterminator ion flow in the Martian ionosphere, *Planetary and Space Science*, *58*, 1442–1454.

Futaana, Y. et al. (2008), Mars Express and Venus Express multi-point observations of geoeffective solar flare events in December 2006, *Planetary and Space Science*, *56*, 873–880.

Gosling, J. T., J. R. Asbridge, S. J. Bame, and W. C. Feldman (1978), Solar wind stream interfaces, *Journal of Geophysical Research*, *83*, 1401–1412.

Grebowsky, J. M., W. T. Kasprzak, R. E. Hartle, K. K. Mahajan, and T. C. G. Wagner (1993), Superthermal ions detected in Venus' dayside ionosheath, ionopause, and magnetic barrier regions, *Journal of Geophysical Research*,

98, 9055–9064.

Hartle, R. E., and J. M. Grebowsky (1990), Upward ion flow in ionospheric holes on Venus, *Journal of Geophysical Research*, *95*, 31–37.

Head, J. W., H. Hiesinger, M. A. Ivanov, M. A. Kreslavsky, S. Pratt, and B. J. Thomson (1999), Possible ancient oceans on Mars: evidence from Mars Orbiter Laser Altimeter data., *Science*, *286*, 2134–2137, doi:10.1126/science.286.5447.2134.

Ho, C. M., R. J. Strangeway, C. T. Russell, J. G. Luhmann, and L. H. Brace (1993), The nightside ionosphere of Venus under varying levels of solar EUV flux, *Geophysical Research Letters*, *20*, 2727–2730.

Hoeksema, J. T., J. M. Wilcox, and P. H. Scherrer (1983), The structure of the heliospheric current sheet - 1978-1982, *Journal of Geophysical Research*, *88*, 9910–9918.

Hoffman, J. H., R. R. Hodges, T. M. Donahue, and M. M. McElroy (1980), Composition of the Venus lower atmosphere from the Pioneer Venus mass spectrometer, *Journal of Geophysical Research*, *85*, 7882–7890, doi:10.1029/JA085iA13p07882.

Intriligator, D. S., J. H. Wolfe, and J. D. Mihalov (1980), The Pioneer Venus Orbiter plasma analyzer experiment, *IEEE Transactions on Geoscience and Remote Sensing*, *18*, 39–43.

Jarvinen, R., E. Kallio, P. Janhunen, S. Barabash, T. L. Zhang, V. Pohjola, and I. Sillanpää (2009), Oxygen ion escape from Venus in a global hybrid simulation: role of the ionospheric O+ ions, *Annales Geophysicae*, *27*, 4333–4348, doi:10.5194/angeo-27-4333-2009.

Jian, L., C. T. Russell, J. G. Luhmann, and R. M. Skoug (2006a), Properties of Interplanetary Coronal Mass Ejections at One AU During 1995 2004, *Solar Physics*, *239*, 393–436.

Jian, L., C. T. Russell, J. G. Luhmann, and R. M. Skoug (2006b), Properties of Interplanetary Coronal Mass Ejections at One AU During 1995 2004, *Solar Physics*, *239*, 393–436, doi:10.1007/s11207-006-0133-2.

Jian, L., C. T. Russell, J. G. Luhmann, and R. M. Skoug (2006c), Properties of Stream Interactions at One AU During 1995 2004, *Solar Physics*, *239*,

337–392.

Jian, L., C. T. Russell, J. G. Luhmann, and R. M. Skoug (2008a), Evolution of solar wind structures from 0.72 to 1 AU, *Advances in Space Research*, *41*, 259–266, doi:10.1016/j.asr.2007.03.023.

Jian, L. K., C. T. Russell, J. G. Luhmann, R. M. Skoug, and J. T. Steinberg (2008b), Stream Interactions and Interplanetary Coronal Mass Ejections at 0.72 AU, *Solar Physics*, *249*, 85–101.

Jian, L. K., C. T. Russell, and J. G. Luhmann (2011), Comparing Solar Minimum 23/24 with Historical Solar Wind Records at 1 AU, *Solar Physics*, *274*(1-2), 321–344, doi:10.1007/s11207-011-9737-2.

Johnson, N. M., and B. Fegley (2000), Water on Venus: New Insights from Tremolite Decomposition, *Icarus*, *146*, 301–306, doi:10.1006/icar.2000.6392.

Kasprzak, W. T., J. M. Grebowsky, H. B. Niemann, and L. H. Brace (1991), Superthermal over 36-eV ions observed in the near-tail region of Venus by the Pioneer Venus Orbiter neutral mass spectrometer, *Journal of Geophysical Research*, *96*, 11175.

Kasting, J. F., and J. B. Pollack (1983), Loss of water from Venus. I - Hydrodynamic escape of hydrogen, *Icarus*, *53*, 479–508, doi:10.1016/0019-1035(83)90212-9.

Knudsen, W. C., K. Spenner, and K. L. Miller (1981), Anti-solar acceleration of ionospheric plasma across the Venus terminator, *Geophysical Research Letters*, *8*, 241–244.

Lammer, H. S. J. (2003), Isotopic Fractionation by Gravitational Escape, *Space Science Reviews*, *106*, 281–291, doi:10.1023/A:1024602124097.

Lee, C. O., J. G. Luhmann, X. P. Zhao, Y. Liu, P. Riley, C. N. Arge, C. T. Russell, and I. de Pater (2009), Effects of the Weak Polar Fields of Solar Cycle 23: Investigation Using OMNI for the STEREO Mission Period, *Solar Physics*, *256*, 345–363.

Lewis, J. S., and F. A. Kreimendahl (1980), Oxidation state of the atmosphere and crust of Venus from Pioneer Venus results, *Icarus*, *42*, 330–337, doi:10.1016/0019-1035(80)90098-6.

Liu, K., E. Kallio, R. Jarvinen, H. Lammer, H. I. M. Lichtenegger, Y. N. Kulikov, N. Terada, T. L. Zhang, and P. Janhunen (2009), Hybrid simulations of the O+ ion escape from Venus: Influence of the solar wind density and the IMF x component, *Advances in Space Research*, *43*, 1436–1441.

Luhmann, J. G. (1986), The solar wind interaction with Venus, *Space Science Reviews*, *44*, 241–306.

Luhmann, J. G., and S. J. Bauer (1992), Solar wind effects on atmosphere evolution at Venus and Mars, *Washington DC American Geophysical Union Geophysical Monograph Series*, *66*, 417–430.

Luhmann, J. G., and T. E. Cravens (1991), Magnetic fields in the ionosphere of Venus, *Space Science Reviews*, *55*, 201–274.

Luhmann, J. G., T.-L. Zhang, S. M. Petrinec, C. T. Russell, P. Gazis, and A. Barnes (1993), Solar cycle 21 effects on the Interplanetary Magnetic Field and related parameters at 0.7 and 1.0 AU, *Journal of Geophysical Research*, *98*, 5559–5572.

Luhmann, J. G., S. M. Petrinec, and C. T. Russell (1994), Long Term Variations in the Solar Wind of Importance to ULF Phenomena, p. 67. [online] Available from: http://adsabs.harvard.edu/abs/1994swsm.conf...67L (Accessed 2 February 2012)

Luhmann, J. G., S. A. Ledvina, J. G. Lyon, and C. T. Russell (2006), Venus O+ pickup ions: Collected PVO results and expectations for Venus Express, *Planetary and Space Science*, *54*, 1457–1471.

Luhmann, J. G., W. T. Kasprzak, and C. T. Russell (2007), Space weather at Venus and its potential consequences for atmosphere evolution, *Journal of Geophysical Research (Planets)*, *112*. [online] Available from: http://adsabs.harvard.edu/abs/2007JGRE..11204S10L (Accessed 2 February 2012)

Luhmann, J. G., A. Fedorov, S. Barabash, E. Carlsson, Y. Futaana, T. L. Zhang, C. T. Russell, J. G. Lyon, S. A. Ledvina, and D. A. Brain (2008), Venus Express observations of atmospheric oxygen escape during the passage of several coronal mass ejections, *Journal of Geophysical Research (Planets)*, *113*. [online] Available from:

http://adsabs.harvard.edu/abs/2008JGRE..11300B04L (Accessed 2 February 2012)

Lundin, R., S. Barabash, Y. Futaana, J.-A. Sauvaud, A. Fedorov, and H. Perez-de-Tejada (2011), Ion flow and momentum transfer in the Venus plasma environment, *Icarus*, *215*, 751–758.

Ma, Y., A. F. Nagy, I. V. Sokolov, and K. C. Hansen (2004a), Three-dimensional, multispecies, high spatial resolution MHD studies of the solar wind interaction with Mars, *Journal of Geophysical Research (Space Physics)*, *109*, 07211.

Ma, Y.-J., and A. F. Nagy (2007), Ion escape fluxes from Mars, *Geophysical Research Letters*, *34*, 08201.

Ma, Y.-J., A. F. Nagy, T. E. Cravens, I. V. Sokolov, J. Clark, and K. C. Hansen (2004b), 3-D global MHD model prediction for the first close flyby of Titan by Cassini, *Geophysical Research Letters*, *31*, 22803.

Masunaga, K., Y. Futaana, M. Yamauchi, S. Barabash, T. L. Zhang, A. O. Fedorov, N. Terada, and S. Okano (2011), O+ outflow channels around Venus controlled by directions of the interplanetary magnetic field: Observations of high energy O+ ions around the terminator, *Journal of Geophysical Research (Space Physics)*, *116*, 09326.

McComas, D. J., R. W. Ebert, H. A. Elliott, B. E. Goldstein, J. T. Gosling, N. A. Schwadron, and R. M. Skoug (2008), Weaker solar wind from the polar coronal holes and the whole Sun, *Geophysical Research Letters*, *35*, 18103.

McElroy, M. B., M. J. Prather, and J. M. Rodriguez (1982), Escape of hydrogen from Venus, *Science*, *215*, 1614, doi:10.1126/science.215.4540.1614.

McEnulty, T. R., J. G. Luhmann, I. de Pater, D. A. Brain, A. Fedorov, T. L. Zhang, and E. Dubinin (2010), Interplanetary coronal mass ejection influence on high energy pick-up ions at Venus, *Planetary and Space Science*, *58*, 1784–1791.

Miller, K. L., and R. C. Whitten (1991), Ion dynamics in the Venus ionosphere, *Space Science Reviews*, *55*, 165–199.

Moore, K. R., D. J. McComas, C. T. Russell, and J. D. Mihalov (1990), A statistical study of ions and magnetic fields in the Venus magnetotail, *Journal of Geophysical Research*, *95*, 12005–12018.

Nagy, A. F., T. E. Cravens, J.-H. Yee, and A. I. F. Stewart (1981), Hot oxygen

atoms in the upper atmosphere of Venus, *Geophysical Research Letters*, *8*, 629–632, doi:10.1029/GL008i006p00629.

Niedner, M. B., and J. C. Brandt (1978), Interplanetary gas. XXII - Plasma tail disconnection events in comets - Evidence for magnetic field line reconnection at interplanetary sector boundaries, *The Astrophysical Journal*, *223*, 655–670.

Niedner, M. B., E. D. Rothe, and J. C. Brandt (1978), Interplanetary gas. XXII - Interaction of comet Kohoutek's ion tail with the compression region of a solar-wind corotating stream, *The Astrophysical Journal*, *221*, 1014–1025.

Ong, M., J. G. Luhmann, C. T. Russell, R. J. Strangeway, and L. H. Brace (1991), Venus ionospheric "clouds" - Relationship to the magnetosheath field geometry, *Journal of Geophysical Research*, *96*, 11133.

Parker, E. N. (1963), *Interplanetary dynamical processes.* [online] Available from: http://adsabs.harvard.edu/abs/1963QB505.P3..... (Accessed 2 February 2012)

Phillips, J. L., J. G. Luhmann, and C. T. Russell (1984), Growth and maintenance of large-scale magnetic fields in the dayside Venus ionosphere, *Journal of Geophysical Research*, *89*, 10676–10684.

Phillips, J. L., J. G. Luhmann, and C. T. Russell (1985), Dependence of Venus ionopause altitude and ionospheric magnetic field on solar wind dynamic pressure, *Advances in Space Research*, *5*, 173–176, doi:10.1016/0273-1177(85)90286-8.

Pizzo, V. (1978), A three-dimensional model of corotating streams in the solar wind. I - Theoretical foundations, *Journal of Geophysical Research*, *83*, 5563–5572.

Powell, K. G., P. L. Roe, T. J. Linde, T. I. Gombosi, and D. L. de Zeeuw (1999), A Solution-Adaptive Upwind Scheme for Ideal Magnetohydrodynamics, *Journal of Computational Physics*, *154*, 284–309.

Riley, P., and J. T. Gosling (2007), On the origin of near-radial magnetic fields in the heliosphere: Numerical simulations, *Journal of Geophysical Research (Space Physics)*, *112*, 06115.

Russell, C. T. (n.d.), Venus upper atmosphere and plasma environment: Critical

issues for future exploration, *Geophysical Monograph Series*, *176*, PP. 139–156.

Russell, C. T., R. C. Snare, J. D. Means, and R. C. Elphic (1980), Pioneer Venus Orbiter fluxgate magnetometer, *IEEE Transactions on Geoscience and Remote Sensing*, *18*, 32–35.

Russell, C. T., J. G. Luhmann, R. C. Elphic, F. L. Scarf, and L. H. Brace (1982), Magnetic field and plasma wave observations in a plasma cloud at Venus, *Geophysical Research Letters*, *9*, 45–48.

Russell, C. T., J. G. Luhmann, and R. J. Strangeway (2006), The solar wind interaction with Venus through the eyes of the Pioneer Venus Orbiter, *Planetary and Space Science*, *54*, 1482–1495.

Schulz, M. (1973), Interplanetary sector structure and the helliomagnetic equator, *Astrophysics and Space Science*, *24*, 371–383.

Schunk, R. W., and A. F. Nagy (2000), *Ionospheres: Physics, Plasma Physics, and Chemistry*, Cambridge University Press.

Shinagawa, H. (1996a), A two-dimensional model of the Venus ionosphere 1. Unmagnetized ionosphere, *Journal of Geophysical Research*, *101*, 26911–26920.

Shinagawa, H. (1996b), A two-dimensional model of the Venus ionosphere 2. Magnetized ionosphere, *Journal of Geophysical Research*, *101*, 26921–26930.

Squyres, S. W. et al. (2004), In Situ Evidence for an Ancient Aqueous Environment at Meridiani Planum, Mars, *Science*, *306*, 1709–1714, doi:10.1126/science.1104559.

Tanaka, T. (1998), Effects of decreasing ionospheric pressure on the solar wind interaction with non-magnetized planets, *Earth, Planets, and Space*, *50*, 259–287.

Terada, N., S. Machida, and H. Shinagawa (2002), Global hybrid simulation of the Kelvin-Helmholtz instability at the Venus ionopause, *Journal of Geophysical Research (Space Physics)*, *107*, 1471, doi:10.1029/2001JA009224.

Vaisberg, O., A. Fedorov, F. Dunjushkin, A. Kozhukhovsky, V. Smirnov, L. Avanov, C. T. Russell, and J. G. Luhmann (1995), Ion populations in the tail of Venus, *Advances in Space Research*, *16*, 105.

Zahnle, K. J., and J. C. G. Walker (1982), The evolution of solar ultraviolet luminosity, *Reviews of Geophysics and Space Physics*, *20*, 280–292, doi:10.1029/RG020i002p00280.

Zhang, T. L., J. G. Luhmann, and C. T. Russell (1991), The magnetic barrier at Venus, *Journal of Geophysical Research*, *96*, 11145.

Zhang, T. L. et al. (2006), Magnetic field investigation of the Venus plasma environment: Expected new results from Venus Express, *Planetary and Space Science*, *54*, 1336–1343.

Zhang, T. L. et al. (2007), Little or no solar wind enters Venus' atmosphere at solar minimum, *Nature*, *450*, 654–656.

Zhang, T. L. et al. (2008), Initial Venus Express magnetic field observations of the Venus bow shock location at solar minimum, *Planetary and Space Science*, *56*, 785–789.

Zhang, T. L., J. Du, Y. J. Ma, H. Lammer, W. Baumjohann, C. Wang, and C. T. Russell (2009), Disappearing induced magnetosphere at Venus: Implications for close-in exoplanets, *Geophysical Research Letters*, *36*, 20203.